Ida Andersskog

Modelling and control of a Heat-to-Power cycle

Master's thesis in Chemical Engineering and Biotechnology
Supervisor: Sigurd Skogestad
Co-supervisor: Cristina Zotica

June 2019

Master's thesis

NTNU
Norwegian University of
Science and Technology

Ida Andersskog

Modelling and control of a Heat-to-Power cycle

NTNU
Kunnskap for en bedre verden

Summary

The Heat-to-Power cycle is commonly utilized in the power industry to convert thermal energy sources into electrical energy. It can be divided into three main processes: combustion, water/steam, and generator, assuming water as a working fluid. The cycle contains many interactive states such as temperature and pressure, making it a difficult process to control with Single-Input-Single-Output (SISO) PID-controllers. Currently, most research of power plant control is with regards to multivariable controllers, even if the most common controllers in the process industry are SISO PI/PID-controllers.

The first aim of the thesis is to model the Heat-to-Power cycle in the simulation environment Simulink in MATLAB. The combustion side of the cycle is not considered during the simulation, only the steam side of the Heat-to-Power cycle. The cycle was modelled using the pressure-flow network model creating a stiff model with small and fast dynamics by alternating dynamic and static components in the system. Modelling a stiff system requires a *ode15s* solver for the integration of the differential equations.

The second aim is to obtain a decentralized control structure for the Heat-to-Power cycle with good performance. This is accomplished through the application of the plantwide procedure on the modelled Heat-to-Power cycle. The plantwide control procedure is an eight-step method that can be utilized to design optimal control structure design for chemical plants. The Heat-to-Power cycle modelled is in this case required to supply power to the electric grid, causing the power setpoint to become the throughput manipulator of the system. The flue gas flow and valve position before the turbine were paired through five different control structures and compared based on their ability to control the power output. The first three control structures: boiler-driven, turbine-driven, and floating pressure were tuned through three different tuning strategies: independent, τ_1- and τ_c-sequential.

The turbine-driven control structure was the only control structure to give good control performance from the decentralized independent controller tuning, indicating a lower coupling between the control loops in this control structure. The τ_1-sequential controller tuning procedure was determined from the open loop time constants found for each control structure in the independent control tuning and resulted in good power control performance for the turbine-driven and floating pressure control structure. The τ_c-sequence was obtained from the closed loop time constants for each control structure in the independent tuning. The boiler-driven control structure was the only control structure to benefit from the τ_c-sequential procedure and improved with regards to settling time and response curve in the power output. A strong coupling between the flue gas flow and the condenser temperature was identified for the control structures.

The fourth control structure, the parallel power controller, was found to give smooth power control, on the trade-off of a long settling time for the power output. The fifth control structure, the valve position controller, improved the turbine-driven control structure with regards to valve saturation while maintaining fast power control. However, the power output experienced an overshoot possibly caused by the coupling between the power and valve position control loops, reducing the overall control performance.

The aim of designing a decentralized control structure for a Heat-to-Power cycle was accom-

plished, but with a trade-off for each control structure. Accepting the overshoot from the valve position control structure leads to a conclusion of a decentralized τ_1-sequential tuned turbine-driven control structure, with an added valve position with clamping anti-windup as the optimal control structure for fast and tight power control.

Sammendrag

En Varme-til-Kraft syklus er ofte benyttet i kraftindustrien for å konvertere termisk energi til elektrisk energi. Syklusen kan deles inn i tre hovedprosesser: forbrenning, vann/damp og generator, under antagelse om at vann er utnyttet som arbeidsmedium. Syklusen har mange interaktive tilstander slik som temperatur og trykk som kan gjøre den vanskelig å regulere med enkel-in-enkel-ut (SISO) PID-regulatorer. I dag er det meste av forskningen innenfor Varme-til-Kraft regulering innenfor fler variabel regulering selv om de vanligste regulatorene innenfor prosessindustrien er SISO PI/PID-regulatorer.

Det første målet med denne masteren er å modellere Varme-til-Kraft syklusen i simuleringsverktøyet Simulink i MATLAB. Forbrenningssiden av syklusen er ikke medregnet i simuleringen, kun vann-/damp-siden. Syklusen var modellert ved å bruke trykk-strøm nettverksmodellen som lager en stiv modell med kort og rask dynamikk. Dette gjøres ved å posisjonere dynamiske og statiske komponenter annethvert i systemet. Når man modellerer et stivt system i Simulink kreves *ode15s*-løseren for integrering av differensielle likninger.

Det andre målet er å lage en desentralisert kontrollstruktur for Varme-til-Kraft syklusen med god ytelse. Dette kan gjøres ved å anvende "the plantwide procedure" på den modellerte Varme-til-Kraft syklusen. "The plantwide control procedure" er en åtte stegs metode for å konstruere en optimal kontrollstruktur for kjemiske anlegg. Varme-til-Kraft syklusen er i dette tilfelle påkrevd å levere kraft til det elektriske rutenettet, som gjør at innstillingspunktet til kraften blir gjennomstrømningsmanipulatoren (TPM) til systemet. Røykgass strømmen og ventilstillingen før turbinen ble koblet igjennom fem kontrollstrukturer. De tre første: kjel-drevet, turbin-drevet og flytende trykk, ble innstilt ved hjelp av tre forskjellige innstillingsstrategier: selvstendig, τ_1- og τ_c-sekvensielt.

Den turbin-drevne kontrollstrukturen var den eneste kontrollstrukturen til å gi god ytelse fra den desentraliserte selvstendige regulatorinnstillingen, noe som indikerer en lavere kopling mellom regulerings sløyfer i denne kontrollstrukturen. Den τ_1-sekvensielle regulatorinnstillingen ble bestemt ut i fra åpen sløyfe konstantene for hver kontroll struktur i den selvstendige regulatorinnstillingen og gav gode resultater for de turbin-drevne og flytende trykk reguleringsstrukturene. τ_c-sekvensen ble funnet fra de lukkede sløyfe konstantene fra hver kontrollstruktur i den selvstendige regulatorinnstillingen. Det var kun den kjel-drevne kontrollstrukturen som fikk bedre ytelse av denne sekvensmetoden og ble forbedret med hensyn på tid brukt på å nå innstillingspunkt og responskurve i kraftproduksjonen. En sterk kopling ble funnet mellom røykgasstrømmen og kondensator temperaturen for kontrollstrukturene.

Den fjerde kontrollstrukturen som ble implementert var parallell kraftregulering. Parallell kraftregulering ble funnet til å gi jevn kraftregulering, men på bekostning av tid det tok for kraften å nå innstillingspunkt. Den femte kontrollstrukturen som ble implementert var ventilposisjonskontroll. Ventilposisjonskontrolleren forbedret den turbin-drevne kontrollstrukturen med hensyn på ventilmetning samtidig som den opprettholdte rask kraftregulering. Den totale ytelsen av kontrollstrukturen ble redusert av at kraftproduksjonen opplevde overskridelse av innstillingspunkt, noe som mest sannsynligvis ble forårsaket av koplingen mellom kraft og ventilinnstillings sløyfene.

Målet med å utforme en desentralisert kontrollstruktur for en Varme-til-Kraft syklus ble fullført, men på en bekostning hos hver enkelt kontrollstruktur. Ved å godta en liten overskridelse av innstillingspunkt fra ventilinnstillingskontrolleren fører til en konklusjon med en desentralisert τ_1-sekvensiell kontrollinnstilling av en turbin-dreven kontrollstruktur, med ventilinnstillingskontroll med "clamping" som type integral-oppvikling som den optimale kontrollstrukturen for rask og fast kraftregulering.

Preface

This master thesis is submitted for the chemical engineering department at the Norwegian University of Science and Technology during the spring of 2019. I would like to thank my supervisor Prof. Sigurd Skogestad and co-supervisor Cristina Zotica for their support, curiosity and engagement throughout the project. In addition, I would like to thank my parents, sisters and close friends for their continuous support and encouragement.

Declaration of Compliance

I, Ida Andersskog, hereby declare that this is an independent work according to the exam regulations of the Norwegian University of Science and Technology.

Ida Andersskog
Trondheim
June 20, 2019

Table of Contents

List of Tables

List of Figures

Abbreviations

The next table lists several abbreviations that will be later used within the body of the document.

Abbreviation	Definition
AE	Algebraic equation
BD	Boiler-driven
CV	Controlled variable
DAE	Differiental algebraic equations
DOF	Degrees of freedom
DV	Disturbance variable
FP	Floating pressure
HEX	Heat exchanger
HP	High pressure
LP	Low pressure
MC	Holdup (mass) controller
MPC	Model Predictive Control
MV	Manipulated variable
ODE	Ordinary differential equations
PC	Pressure controller
PID	Proportional-Integrating-Derivative
SIMC	Simplified-Internal-Model-Control
TC	Temperature controller
TD	Turbine-driven
UA	Heat transfer coefficient multiplied with the surface area where the heat transfer takes place
VPC	Valve Position Controller
WC	Power controller

Chapter 1

Introduction

1.1 Background

A Heat-to-Power cycle is a process that converts the thermal energy stored in an energy carrier medium into mechanical energy and electrical energy. Since most forms of energy can be converted to heat, the Heat-to-Power cycle is commonly utilized in converting chemical energy sources into power. The chemical energy can be transformed into thermal energy through combustion, creating a high-temperature gas. The energy stored in the gas is exchanged with liquid, commonly water, in a boiler to produce high pressure and high-temperature steam. The steam is sent through a turbine in which the pressure drop across the turbine rotates the turbine blades. The mechanical energy from these turbine blades drives a generator to convert the mechanical energy into electrical energy. The low-pressure outlet steam from the turbine is condensed and pumped back into the cycle. A simple representation of the Heat-to-Power cycle is shown in Figure 1.1 where the arrow lines represent the flow of the water in its liquid (blue) and vapour (red) phase form.
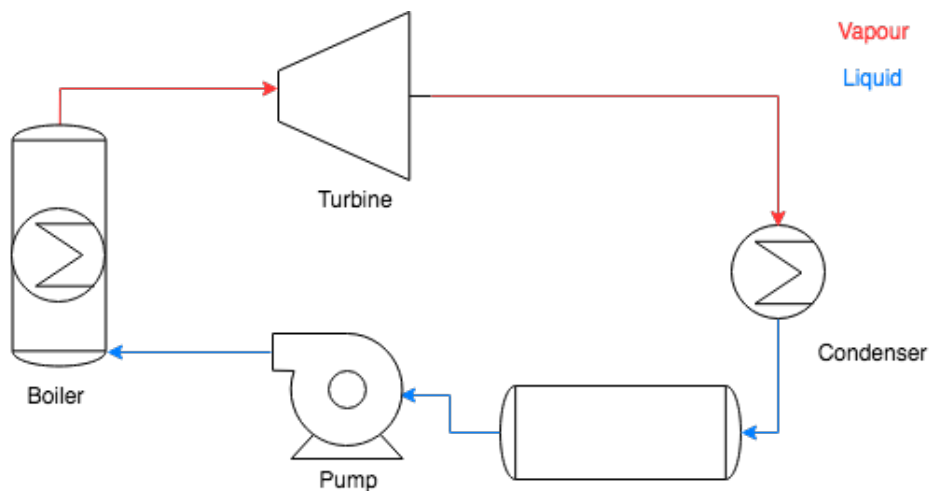
Figure 1.1: A simple process flow diagram representation of a Heat-to-Power cycle

The main objectives in a Heat-to-Power cycle are either to regulate the power output, subject to the demand and constraints in the electric grid or to maximize the energy efficiency by utilizing as much fuel as possible. Whilst doing this it is also necessary to maintain safe operation of the plant [Wu et al., 2015]. In order to complete this task, variables such as the steam temperature, pressure and boiler drum level are regulated. The Heat-to-Power cycle is a highly coupled system, making it difficult to control with simple controllers. Besides that, additional operational requirements have arisen over the last few decades with regards to variable fuel load and electricity demand. This causes a need for more complex control methods where the PID controllers alone cannot deliver on these criterion's sufficiently.

From the study of fossil-fuelled power plant (FFPP) configurations, design and control technology in [Wu et al., 2015] five specific issues are mentioned that are required to be studied further. One issue underlines the need for broadening the control objective from dynamic control optimality to a case of multiple objectives solved simultaneously such as plant economic operation, emission, and dynamic control performance. Another important issue mentioned is the increased focus on FFPP modelling. As the Heat-to-Power cycle contains coupled variables and nonlinear interactions, obtaining a realistic model of the cycle itself is just as important as implementing a proper control structure.

The first objective of this master thesis is to model a simple heat-to-power cycle in Simulink. The simulation is a continuation from a model built in the specialization project [Andersskog, 2018] and consists of an economizer, mixer, drum, superheater, attemperator (cooling water spray), high-pressure turbine, reheater, low-pressure turbine, condenser, and pump. The process is modelled as a pressure-flow network with alternating dynamic and static components, creating a stiff system requiring the utilized *ode15s* solver in Simulink for the differential equations.

The second objective is to apply the plantwide procedure on the cycle to design a control structure with good performance for a highly coupled system. Specifically, decentralized control of a heat-to-power cycle is studied in order to see what recommendations should be made for stable internal control and fast power control. Five control structures are compared with regards to their overall control performance and their ability to control the power to its desired setpoint. The five control structures studied are

- Boiler-driven control

- Turbine-driven control

- Floating pressure control

- Parallel power control

- Valve position control

1.2 Previous work

The Heat-to-Power cycle has been widely utilized in the power industry over the last hundred years[Wu et al., 2015]. The idea of converting thermal energy to mechanical energy can even be traced back as far as 130 BC, where the "Aeolipile" was designed by Heron of Alexandria[Scaife, 1985, p.132]. In 1884 Charles Parsons' patented multistage turbine was invented which in this case was connected to a generator, allowing for the last step of conversion from mechanical to electrical energy to take place. Charles Parsons already at that time saw the need for improving the efficiency of the steam turbine by expanding the steam over several steps[Scaife, 1985]. Today, most Heat-to-Power cycles have multistage turbine systems, with added super and - reheating for high thermal efficiency. The heating in the boiler is done over several steps to obtain as high as possible temperature and pressure in the steam. The current limitations are now with regards to reliability, technical risks and material properties of the cycle components [Wu et al., 2015][Breeze, 2012]. Another important aspect of the current Heat-to-Power cycle is the coupling of the variables such as mass flow, pressure and temperature, leading to increased research in this area. Not just have the control objectives of the cycle been broadened, but now also a focus is on controlling internal and external variations sufficiently for stable operation [Wu et al., 2015].

In [Welfonder, 1999] the dynamic interaction of power plant and power systems have been studied to see how and if model-based power control concepts can handle internal and external disturbances. In this paper, Welfonder describes the importance of model-based block control and regulation concepts in order to use feedback control on the main regulation variables (CVs): the generator power and the live steam pressure. These two CVs can be controlled with the two main actuator variables: the thermal power and the turbine valve setting. He proposes three operating modes for regulating the CVs: steam generator-driven, block-driven and turbine-driven. The fuel load and power production pairing in the steam generator-driven control structure has an advantage when it comes to direct load effect on power production. A disadvantage is the long controller pairing distances and thus slow response time can be expected. In the turbine-driven control structure, the valve position is paired close to the power production resulting in fast power control. Block-driven control structure releases the valve position from controlling the pressure to being utilized for other controlled variables. This control structure can be expected to have low throughput variability as the valve position is fixed.

Oscillations in the Heat-to-Power cycle has been a continuous obstacle in Heat-to-Power control. In [Blaazer, 2010] multivariable advanced process control (MIMO APC) is confirmed to reduce the oscillations as well as improving internal and overall plant performance. Blaazer uses H_∞-control that minimizes a performance objective matrix, N, to compute the H_∞-controllers. The main advantage of MIMO APC is that these controllers automatically deal with coupling within the system, which in the case of Heat-to-Power control is of great importance. The disadvantage of MIMO systems is the model uncertainty with regards to plant direction [Skogestad, 2004, p.230]. As well as mentioned in [Wu et al., 2015] the H_∞-control relies on a linear plant model. Thus, for a nonlinear process such as the Heat-to-Power cycle, H_∞-control trades off performance for robustness as it cannot deal with the input constraints effectively.

A possible improvement to the H_∞-control in [Blaazer, 2010], is model predictive control (MPC). MPC effectively handles multivariable systems, input constraints and pushes the oper-

ation towards the constraint limits. It is thus often used to improve economic profit in industrial processes and response time. For such an interactive and nonlinear system as the Heat-to-Power cycle, a Nonlinear MPC should be used in order to obtain realistic results. The main issues with NMPC are the computational requirements, lack in robustness and difficulties in building of a satisfactory nonlinear dynamic model [Wu et al., 2015].

From the thorough research of FFPP configuration, design and control in [Wu et al., 2015] advanced multivariable control is recommended for a Heat-to-Power cycle. Especially as decentralized control is not really suited for highly interactive processes and suffers from performance loss. Multivariable control can handle these problems effectively but still requires a satisfactory multivariable dynamic model. It also becomes very sensitive to uncertainty, changes in plant operation and can be difficult to tune. The transparency of decentralized control is an advantage multivariable control lacks. In cases where it is desired to understand and visualize the process that is controlled, decentralized control meets these criterion's better.

Most of the current research of the Heat-to-Power cycle control is with regards to Advanced MIMO control, even if the majority of the controllers in the process industry are PI/PID-controllers[Gustavsson and Rönnberg, 2016][Halevi et al., 1997]. This is because PID-controllers are easy to implement and understand, such that people without any background knowledge within process control can still utilize them [Skogestad and Morari, 1989] [Hovd and Skogestad, 1993]. It is therefore desired to further investigate the possibilities of decentralized PID-control of a Heat-to-Power cycle. The three operating modes mentioned in [Welfonder, 1999], boiler-driven, turbine-driven and floating pressure, are compared and tested. Three different tuning designs, independent, τ_1- and τ_c-sequential, are used to tune the boiler-driven, turbine-driven and floating pressure control structure to compare which method or sequence obtains the best controller tunings for each control structure. Two advanced control structures are implemented in addition, parallel power control and valve position control, and compared with the three operating modes with regards to control performance and improvements of valve saturation.

1.3   Thesis structure

- Chapter 2 introduces the most important theory with regards to Heat-to-Power cycles, pressure-flow network modeling and Simulink as a simulation tool.

- Chapter 3 explains the plantwide control structure design procedure, PID-control, as well as different Heat-to-Power cycle control structures.

- In Chapter 4 the model assumptions, equations and strategies are explained.

- In Chapter 5 the plantwide control procedure is applied to the Heat-to-Power cycle and the designs of the control structures of the cycle are presented.

- In Chapter 6 the simulation results are presented.

- In Chapter 7 the results from Chapter 6 are discussed.

- In Chapter 8 and 9 conclusions of the discussion are made and future recommendations presented, respectively.

Chapter 2

Model theory

In this chapter, the model theory with regards to the Heat-to-Power cycle, pressure node-flow element method and Simulink is presented.

2.1 Heat-to-Power cycle

In the power industry, there exist three common classifications of power plants: electrical-, thermal-, and co-energy production power plants. The most common classification is the co-energy power plants that produce both electrical power and thermal energy in the form of district heating and steam production. There exist several energy carriers in the cycle. The primary energy carriers of the cycle are the heating sources such as fossil fuels, nuclear, waste and biomass. The secondary energy carrier of the cycle is the medium in which the energy is transferred to, commonly water[Kovacs, 2004]. For simplicity, only electrical production will be considered in this thesis, also known as a Heat-to-Power cycle, where water is the medium of choice.

A Heat-to-Power cycle can be divided into 3 subsystems: combustion, water/steam and generator. The combustion subsystem, also called the fire-side, consists of combusting the fuel, creating a high-temperature gas in which can be exchanged with the water side to produce superheated steam[Wu et al., 2015]. In the water/steam subsystem, the water is heated to generate high pressure and high-temperature steam, which is expanded through a turbine, condensed and pressurized through a pump before it is recycled back into the cycle. In the generator subsystem, the mechanical energy obtained from the rotating turbine blades is converted to electric energy through a generator connected to the electric grid. The combustion and generator subsystem will not be considered in this thesis.

A Heat-to-Power cycle utilizing water as its working fluid is also called a steam cycle, where the steam subsystem can be divided into six individual stages shown in the list below [Øverli, 1981, p.9]:

1. Boosting the pressure of the water through a pump

2. Heating of water to saturation

3. Evaporation

---

4. Superheating

5. Isentropic expansion of the steam through a turbine

    5.1 Reheating of the steam

    5.2 Isentropic expansion of the steam through a turbine

6. Condensation

The combined stages 2-4 all have the purpose of heating the water and are also known as the boiler. There exist two different configuration types of how the boiler is implemented in Heat-to-Power cycles. The first heats the water and steam through individual stages, with individual heat exchangers. The second configuration utilizes only one heat exchanger for all three heat transfer regimes, called a once-through boiler [Kovacs, 2004, p.43-56]. If an additional turbine is added in step 5, the steam is heated again, similar to the superheating in stage 4, before the steam is expanded once more through a low-pressure turbine.

The steps of the cycle are shown in a T-s diagram in Figure 2.1. The T-s diagram illustrates the benefits of adding the reheater in Step 5.1 after the high-pressure turbine, as more heat is recovered from the cycle by Step 5.2 compared to Step 5.
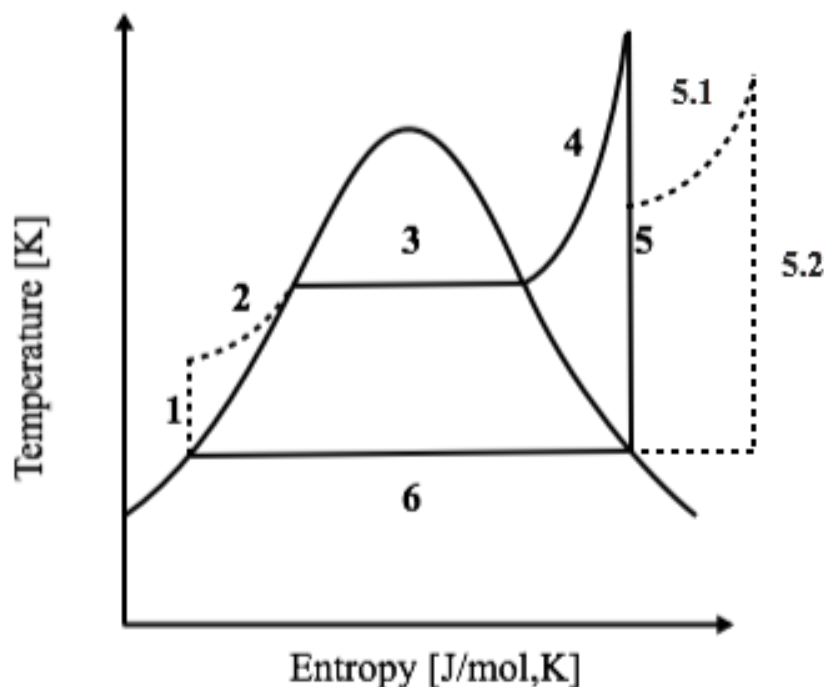
Figure 2.1: T-s diagram of the Heat-to-Power cycle [Kovacs, 2004, p.89].

A figure representing the Heat-to-Power cycle with its six individual stages is illustrated in Figure 2.2 by a process flow diagram [Tanuma, 2017, p.12-14]. The individual stages will be described in detail in the succeeding subsections.
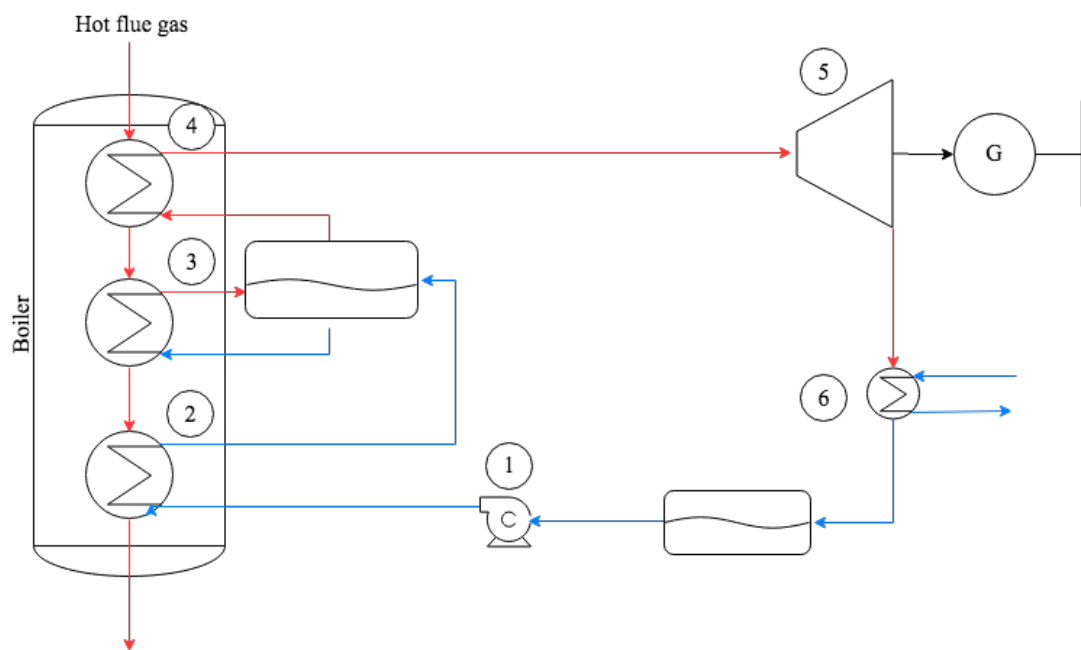
Figure 2.2: Illustration of the six stages of the Heat-to-Power cycle

2.1.1 Stage 1: Pump

The purpose of the pump is to increase the pressure such that the water is pumped from the condenser into the boiler, as well as obtaining high enough pressure necessary to produce high-pressure steam in the drum. The pressure of the water needs to exceed the pressure in the economizer and drum to ensure the required flow rate for the drum. The pump component has fast dynamics leading to negligible mass accumulation and is considered a pure static component [van Putten and Colonna, 2007]. The most common type of feedwater pump in Heat-to-Power plants is centrifugal pumps where the rotational energy from the pump is converted to kinetic energy in the fluid[Oryds et al., 1994, p.183].

2.1.2 Stage 2: Economizer

The economizer stage heats the liquid water up to its boiling point. The water remains a liquid as it is sent to the drum. The reason for separating the heating of the water in this manner is for energy economic reasons. The stream from or to the economizer can be separated into a main and a bypass stream, where the bypass stream adds a degree of freedom to be used for additional purposes such as temperature control. The liquid bypass stream improves the efficiency of the cycle by recovering more enthalpy compared to using bypass flows consisting of steam. Another advantage is that the economizer utilizes the excess heat from the flue gas through the heat exchanger in the heating of the water and thus saves fuel consumption.

2.1.3 Stage 3: Drum

In the drum, the water from the economizer is heated through a heat exchanger past its boiling point in which it evaporates [Kovacs, 2004][Wu et al., 2015]. What is produced is high pressure saturated steam. The point of evaporation and thus the heat of vaporization required for the steam depends on the pressure and boiling temperature. The heat of vaporization can be obtained from a pressure-enthalpy diagram illustrated in Figure 2.3.

2.1.3.1 Saturated pressure

For saturated steam at its critical point between the liquid and gaseous phase, the Antoine Equation is used to compute the saturation pressure, represented in Equation 2.1. The Antoine equation describes a semi-empirical correlation between saturated pressure and temperature for pure components by the use of three constants: A, B and C [Skogestad, 2009, p.342].

$$log_p = A - \frac{B + T}{C} \tag{2.1}$$

where T is the temperature. The Antoine constants for calculation of the saturation pressure of water in bar from temperature in Kelvin is rendered in Table 2.1 below.

Table 2.1: Antoine constants for saturated steam

Constant	Value
A	11.6834
B	3816.44
C	-46.13
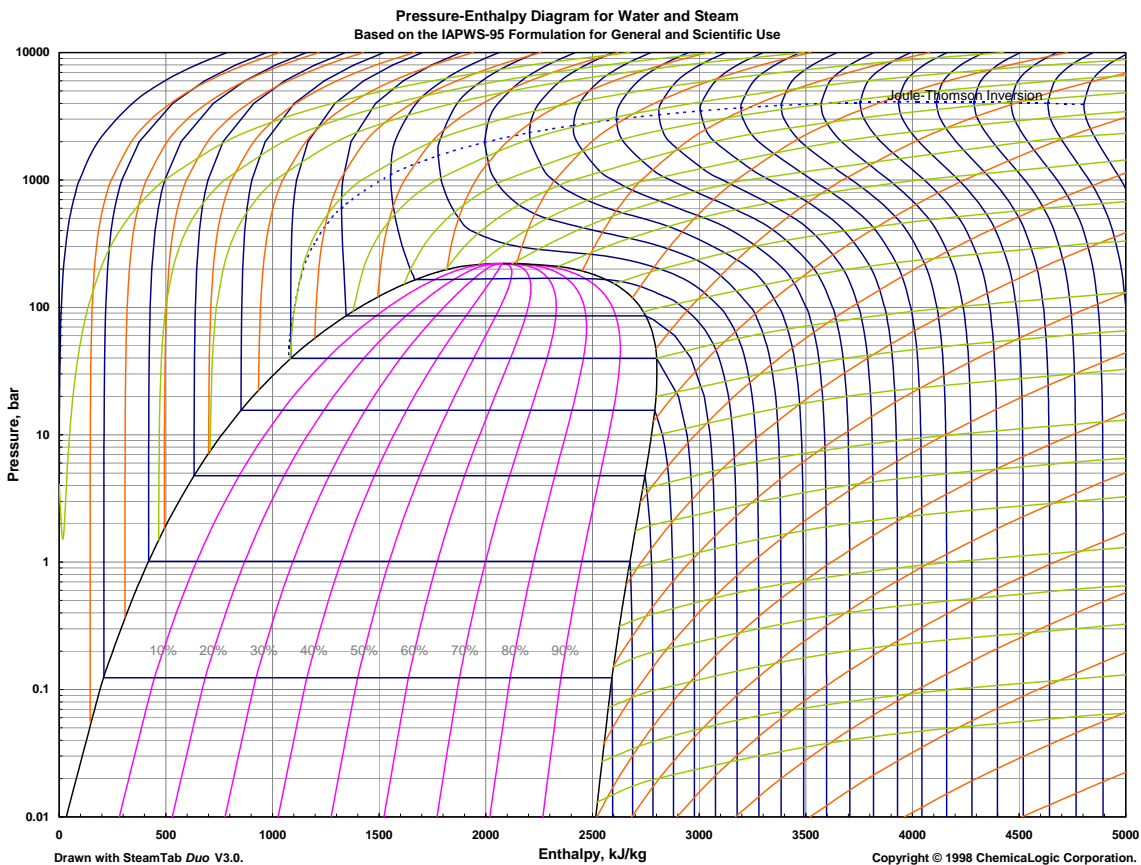
Figure 2.3: Pressure-Enthalpy diagram for water and steam [ChemicaLogic Corporation, 1998].

2.1.4 Stage 4 and 5.1: Superheater and reheater

In the superheater, the steam from the drum is heated through a heat exchanger to increase the kinetic energy of the steam and thus increasing the power produced. This results in a higher thermal efficiency of the steam cycle as well as a lower risk of condensation of the steam through the turbine [Kovacs, 2004, p. 59]. The liquid in the turbine causes damages such as corrosion and must be avoided [Skogestad, 2009, p. 194]. In steam cycles with multistage turbines, a reheater should be placed in between the turbines for the same reasons as the superheater [Wu et al., 2015].

Limitations on the maximum temperature of the steam still exist with regards to the turbine blade material properties. At a certain point, the thermal strength of the turbine blades are exceeded and the blades start to melt. The current maximum steam temperature turbine blades are able to withstand today is around 620 °C[Breeze, 2012].

2.1.4.1 Attemperator

An attemperator spray is often added after the superheater in order to regulate the steam temperature. The cold water is extracted from the feedwater out of the pump in Stage 1, where the total mass flow rate can be adjusted after the mixing of the steam and water through a valve[Alobaid et al., 2017, p.97].

2.1.5 Stage 5: Turbine

A steam turbine is a component that converts the kinetic energy in the high-pressure steam to mechanical energy by the use of rotor blades. The mechanical energy from the axial rotation of these blades is then converted to electrical energy through a generator[Alobaid et al., 2017]. The expansion of the steam through the turbine system can be controlled by the addition of valves and extraction points between the turbines. Uncontrolled expansions are turbines where the in and outlet pressure or flow is not regulated resulting in the pressure ratio over the turbine to vary, such as in the simple Heat-to-Power cycle modelled in this thesis illustrated in Figure 2.4 with a single turbine[Cooke, 1985].
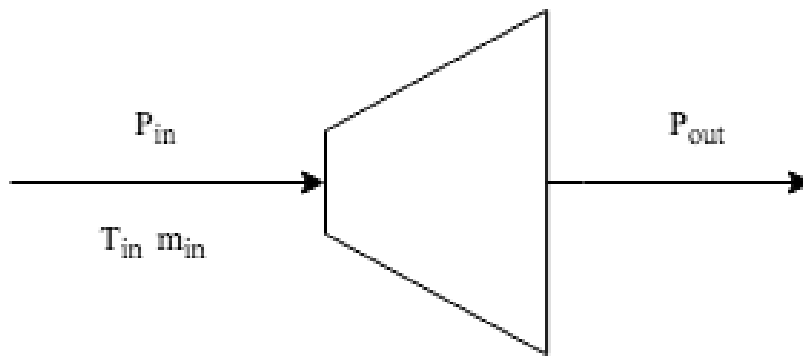
Figure 2.4: Simple turbine process flow diagram

2.1.5.1 Constant volumetric flow

Constant volumetric flow rate is usually assumed in cases for uncontrolled expansions to high vacuum. Assuming that the steam is an ideal gas, the relation that is shown in Equation 2.2 can be used when computing the mass flow through the turbine [Cooke, 1985, p.598].

$$\dot{m}_{in} = q_s \frac{M_{m,water} P_{in}}{R T_{in}} \tag{2.2}$$

where $M_{m,water}$ is the molar mass of water, R is the universal gas constant, P_{in} is the inlet pressure, T_{in} is the inlet temperature and q_s is the volumetric flow constant. The volumetric flow constant, q_s, is computed at design conditions for the flow, $\dot{m}_{in,nom}$, inlet temperature, T_{in}^* and inlet pressure, P_{in}^*.

$$q_s = \frac{\dot{m}_{in,nom} R T_{in}^*}{M_{m,water} P_{in}^*} \tag{2.3}$$

2.1.5.2 Stodola Equation

As the mass flow rate and the pressure may vary during operation, a constant volumetric flow might not predict the flow through the turbine accurately at off-design conditions[Cooke, 1985, p.598-599]. Hence, the Stodola Equation is introduced to determine the performance of the turbine as shown in Equation 2.4 [Cooke, 1985] [Mazzi et al., 2015].

$$\dot{m}_{in} = K_t \sqrt{\rho_{in} P_{in} \left[1 - \left(PR \right)^2 \right]} \tag{2.4}$$

$$PR = \frac{P_{out}}{P_{in}} \tag{2.5}$$

$$\rho_{in} = \frac{M_{m,water} P_{in}}{R T_{in}} \tag{2.6}$$

where ρ_{in} is the inlet steam density, where $M_{m,water}$ is the molar mass of water, R is the universal gas constant, T_{in} is the inlet temperature, P_{in} and P_{out} are the inlet and outlet pressures, respectively. PR is the pressure or expansion ration and K_t is the Stodola coefficient found from nominal and steady state data in Equation 2.7.

$$K_t = \frac{\dot{m}_{in,nom}}{\sqrt{\rho_{in,nom} P_{in,nom} \left[1 - \left(\frac{P_{out,nom}}{P_{in,nom}} \right)^2 \right]}} \tag{2.7}$$

The Stodola Equation should only be applied to single staged turbines if the expansion ratio and rotation are constant[Cooke, 1985]. For expansions with large pressure variations and an outlet pressure close to vacuum more stages are required[Sinnott and Towler, 2009, p. 121].

2.1.5.3 Turbine map and valve saturation

In [Andersskog, 2018] it was established that the Stodola approximation modelled the mass flow rate better with regards to its response to a setpoint change in the valve position compared to the constant volumetric flow. The increased valve position resulted in a decrease in the pressure before the valve and increased pressure into the turbine. The results are further an increased mass flow through the turbine and power production. This classifies the process as an uncontrolled expansion where the only set variables are the outlet pressures of the turbines.
In [Øverli, 1981, p.187-188], turbine characteristics are studied with regards to the relationship between pressure ratio and the ratio of mass flow, temperature and inlet pressure (MTP) through the turbine, presented in Equation 2.8.

$$\frac{P_{out}}{P_{in}} = f \left\{ \dot{m} \frac{\sqrt{T_{in}}}{P_{in}}, \frac{n}{\sqrt{T_{in}}} \right\} \tag{2.8}$$

where n is the rotational speed of the turbine [$rmin^{-1}$].

By plotting the first relation, $\dot{m} \frac{\sqrt{T_{in}}}{P_{in}}$, from Equation 2.8 over a large range of inlet pressures, P_{in}, for both the Stodola and constant volumetric flow approximation of the flow, Figure 2.5 is obtained.
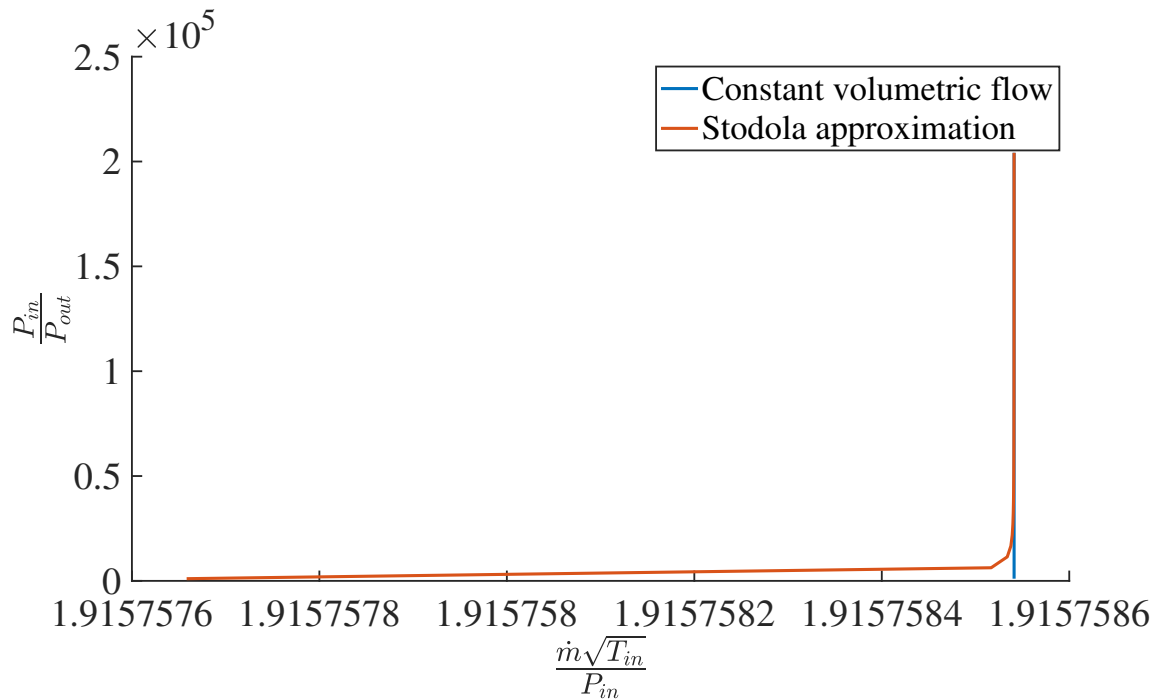
Figure 2.5: The performance of a turbine at different pressure ratios

In Figure 2.5, it can be seen that the performance of a turbine is limited at a certain MTP ratio. At this point choking, or saturation, of the valve occurs and the increase in the pressure ratio does not increase the mass flow any more [Øverli, 1981, p.188]. In this case, the approximation of the mass flow through the Stodola equation becomes similar to assuming constant volumetric flow as the fluid velocity becomes limited.

In [Cooke, 1985, p. 601-602] the increased pressure ratios for uncontrolled expansions are visualized for multistaged turbines and show the same effect.

2.1.6 Stage 6: Condenser

The purpose of the condenser is to condense the saturated steam from the turbine to water by the means of a coolant[Tanuma, 2017, p.12]. The process occurs similarly to the evaporation in stage 3 but in the opposite manner. To obtain high thermal efficiency of the Heat-to-Power cycle, the outlet pressure of the turbine should be close to a vacuum. Considering the pressure-enthalpy diagram in Figure 2.3, the temperature at this point is limited with regards to maintaining the water to be in the gaseous phase. Accordingly, the temperature of the condenser affects the exhaust pressure of the turbine. The condenser is, therefore, an important mean to regulate the exhaust pressure of the turbine[Tanuma, 2017, p.17].

2.2 Dynamic conservation balances

The dynamic conservation of mass under the assumption of no chemical reactions in a system is represented by Equation 2.9[Himmelblau and Riggs, 2012].

$$\frac{dM}{dt} = \dot{m}_{in} - \dot{m}_{out} \tag{2.9}$$

where M is the mass holdup and $\dot{m}_{in}$ and $\dot{m}_{out}$ represents the inlet and outlet flows, respectively. Assuming constant heat capacity, C_p, the dynamic energy balance is represented with enthalpy as the dynamic state in Equation 2.10[Himmelblau and Riggs, 2012].

$$\frac{dH}{dt} = \dot{m}_{in}h_{in} - \dot{m}_{out}h_{out} + Q \tag{2.10}$$

where H is the enthalpy, Q is the heat transferred and h_{in} and h_{out} are the specific enthalpies of the in and outlet streams computed through Equation 2.11.

$$h = C_p(T - T_{ref}) + \Delta H_{phase} \tag{2.11}$$

where T is the temperature in of the system, T_{ref} is the reference temperature and ΔH_{phase} is the heat of phase change.
$\frac{dH}{dt}$ can be simplified to $\frac{dT}{dt}$ using the relation represented in Equation 2.12, assuming constant heat capacity, C_p.

$$\frac{dH}{dt} = C_p\Big(M\frac{dT}{dt} + T\frac{dM}{dt}\Big) \tag{2.12}$$

2.3 Pressure Node-Flow Element method

The Heat-to-Power cycle consists of several components such as the economizer, evaporator and condenser that contains dynamical holdups. The mass or energy stored in the holdups can be considered buffer capacities and smooths the dynamics of the system. Furthermore, static components such as the superheater, turbine and pump alternate with the dynamical components. In these components, the dynamics occur quickly leading to steady state like conditions. This is because the speed of the processes occur too fast for any significant accumulation to take place. Accordingly, the fast dynamics of the static components become embedded into the dynamical components and have to be considered during the modelling of the Heat-to-Power cycle [Celis et al., 2017, p.596] [Mazzi et al., 2015, p.543-544].

The approach of modelling alternating dynamic capacities and static components is called the pressure-flow network model or pressure node - flow element method[Batalov, 2011]. The pressure-flow network model creates a meshed like model of the system with each capacity as its node. The inputs of the pressure node are the current and succeeding mass flows of the node, in which the accumulation or loss of mass flow is integrated to obtain the capacity of the node. The pressure of the node is computed utilizing the capacity as input, causing the dynamics of the holdup to directly be coupled to the pressure. The computed pressure and the pressure obtained from the succeeding pressure node becomes input for the flow element, which computes the current mass flow through its relation to the pressure difference over the valve[Rua Pazoz, 2017].

2.3.1 Gas flow through a pipe

In order to present the pressure-flow network model more clearly a common example seen in the industry is explained: gas flow through a pipe, [Gustavsson and Rönnberg, 2016]. In this case, the pipe itself acts as a capacity and is modelled by the pressure node approach. The mass flows through the valves occur fast compared to the flow through the pipe and are modelled as flow elements. In the Heat-to-Power cycle, the pressure nodes are located at the holdups as they will slow down the dynamics more than the pipelines themselves, thus, including the main dynamics of the cycle. The flow elements are still considered to be the mass flows.

An illustration of the process flow diagram of gas flow through a pipe is shown in Figure 2.6, while its respected pressure-flow network model is presented in Figure 2.7.
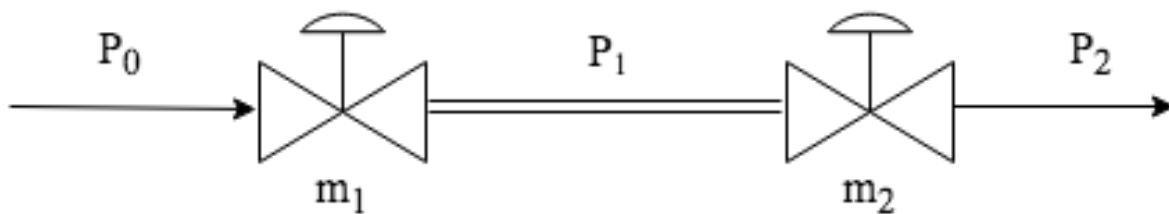
Figure 2.6: Process flow diagram for gas flow through a pipe
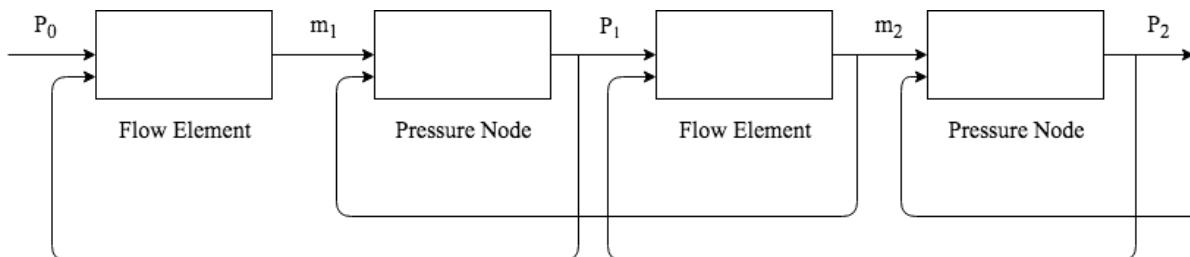
Figure 2.7: Pressure Nodes and Flow Elements for gas flow through a pipe [Batalov, 2011, p.4].

2.4 Simulink

The programming language MATLAB offers a connected simulation environment called, Simulink, which can be used to design simulations with both a graphical user interface (Simulink) integrated with back-end text coding (MATLAB). Simulink provides multiple system blocks that lower the amount of hand-written code, as well as allowing for a meshed-like separation of the simulation through the subsystem blocks[The MathWorks Inc, 2018]. The utilization of the subsystem blocks gives the user the opportunity to separate the process into its corresponding components, creating a front-end point of view similar to a process flow diagram. The user can from there on click into each subsystem to see the modelling of the respected components.

2.4.1 ODE

An ODE is a set of ordinary differential equations, where the dynamic states are solved through integration of the states on their differential form. An example of a differential equation is shown in Equation 2.13.

$$\frac{dx}{dt} = f_1(x, z, u) \tag{2.13}$$

where x is a vector of the dynamic states, z is a vector of the algebraic states, u are the inputs and $\frac{dx}{dt}$ is the change in the dynamic state with regards to time.

2.4.2 AE

If a state is assumed to not change with regards to time it is solved through an algebraic equation. Implicit algebraic functions solve a function equal to zero containing the algebraic state through iteration until the function converges. Explicit algebraic functions solve an algebraic function directly to obtain the algebraic state. Examples of implicit and explicit algebraic equations as are shown in Equation 2.14 and 2.15, respectively.

$$0 = f_2(x, z, u) \tag{2.14}$$

$$z = f_2(x, u) \tag{2.15}$$

where x is a vector of the dynamic states, z is a vector of the algebraic states and u are the inputs.

2.4.3 DAE

A system where dynamic and algebraic (static) equations are solved together are also called differential algebraic equations (DAE). An example of a semi-explicit DAE is illustrated in Equation 2.16.

$$\frac{dx}{dt} = f_1(x, z, u) \tag{2.16}$$

$$0 = f_2(x, z, u) \tag{2.17}$$

where u are the inputs and x and z are vectors of the dynamic and algebraic states, respectively.

In Simulink a DAE set can be represented with a single MATLAB function block, where the dynamic and static states are separated through a gain block containing a selection matrix, K. K is on the size $[N_d \times N_{eq}]$ and $[N_a \times N_{eq}]$ for the dynamic and algebraic selection matrices, respectively. N_d is the number of differential equations, N_a is the number of algebraic equations and N_{eq} are the total number of equations in the DAE set. The selection matrices contain 1 on the diagonal elements corresponding to the state to be solved and 0 for the rest of the matrix elements. Once separated the differential equations are solved by integration and the algebraic equations by iteration until convergence. An illustration of a DAE system in Simulink is shown in Figure 2.8.
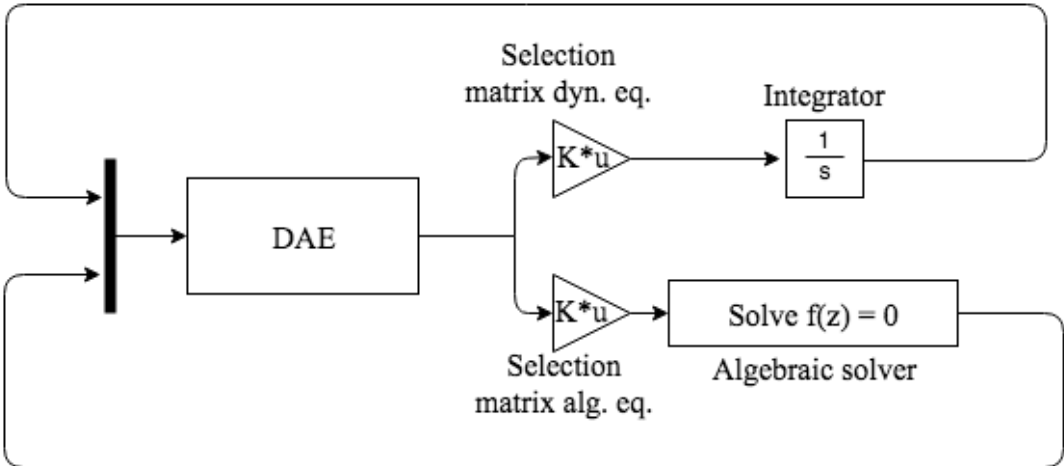
Figure 2.8: DAE system model in Simulink

Chapter 3

Control theory

This chapter describes the eight steps of the plantwide procedure, PID-control, SIMC tuning and common control structures seen in Heat-to-Power cycles.

3.1 Plantwide control structure design procedure

The control structure design for chemical plants presented in [Skogestad, 2004] consists of eight steps in order to establish what is the optimal operation of a given plant. The first four steps are called the "top-down" analysis in which the operational objectives and the degrees of freedom of the plant are determined. In the last four steps in the "bottom-up" design, the respective control layers are designed in order to obtain a stable, safe and optimal control system[Skogestad, 2004, p.220].

3.1.1 Top-down

3.1.1.1 Step S1: Definition of operational objectives

The first step of the plantwide procedure is to define the operational objectives of the plant. Usually, this objective is presented in the form of a cost function, J, which is minimized as a criterion for optimal operation[Skogestad, 2004, p.222]. In a typical plant, the cost function is the negative of the profit, P, as shown in Equation 3.1.

$$J = -P = \text{cost feed} + \text{cost energy} - \text{value products} \tag{3.1}$$

The optimal operation objective presented in Equation 3.1 can be interpreted differently with regards to factors such as varying market conditions. If the energy prices are cheap, the main cost function variables are with regards to the products and the production rate of the plan should be run at its maximum. In this case, the constraints are tightly controlled at their bottleneck. For circumstances where the price of energy is not cheap the aim will be to maximize the energy efficiency and it becomes less clear on what to control.

The system contains certain constraints that need to be satisfied during the optimization of the objective function. These limitations are classified as equality, inequality or integer constraints and can be combined with the objective function to form a programming problem, represented in Equation 3.2 on its canonical form.

$$\begin{aligned} \text{Minimize} \quad & J & (3.2) \\ \text{Subject to} \quad & Ax \leq b \\ & A_{eq}x = b_{eq} \\ & x \geq 0 \end{aligned}$$

where x is a vector of variables such as the system states, inputs and disturbances, A and A_{eq} are coefficient matrices, b and b_{eq} are the known limitation values for the inequality and equality constraints, respectively.

3.1.1.2 Step S2: Manipulated variables and degrees of freedom

In order to design a control structure for the plant, the steady-state degrees of freedom, N_{ss} needs to be determined. N_{ss} gives an indication if the number of available manipulated variables, MVs, are able to meet the operational objectives. In cases where N_{ss} is not sufficient, equipment such as bypass streams and storage tanks can be added to the process to increase the degrees of freedom [Skogestad, 2004].
N_{ss} can be computed from Equation 3.3.

$$N_{ss} = N_m - (N_{0m} + N_{0y}) \qquad (3.3)$$

where N_m is the number of dynamic degrees of freedom (MVs), N_{0m} is the number of MVs with no steady-state effect and N_{0y} is the number of controlled variables, CVs, with no steady-state effect.

3.1.1.3 Step S3: Primary controlled variables

The primary controlled variables are the variables that need to be controlled for optimal economic operation. The selection of the primary controlled variables starts with the CVs with active constraints. These CVs have been determined to reach their inequality value, b, at optimal operation and the inequality becomes an equality, also referred to as an active constraint.

For the remaining unconstrained (nonactive) CVs, the selection of a good candidate controlled variable can be determined under several requirements as explained by Skogestad in [Skogestad, 2004]:

- The CV has satisfactory disturbance rejection.

- The CV has to be easily measured and controlled.

- The CV should be able to affect the MVs easily.

- If the system contains several nonactive CVs, the candidate CVs should be independent.

3.1.1.4   Step S4: Production rate

The position of the production rate or the throughput manipulator, TPM, of a plant can determine the entire systems' control structure. Traditionally it is set as the flow rate at the feed of the process. A more general rule is to set the TPM at the bottleneck of the process. The bottleneck in a chemical plant is the MV that determines the maximum throughput of the process[Skogestad, 2004, p.225].

3.1.2   Bottom-up

3.1.2.1   Step S5: Regulatory control layer

The regulatory layer primarily consists of single-input-single-output (SISO) PID-control loops, creating a low complexity structure with a main objective of rejecting disturbances and stabilizing the plant[Skogestad, 2004, p.226].

3.1.2.2   Step S6: Supervisory control layer

In the supervisory control layer, the optimal setpoints are computed for the controllers in the regulatory layer. When designing the supervisory layer the first important step is to choose if single-loop decentralized control or multivariable control is going to be used.

Decentralized control is recommended for non-interactive processes where the active constraints remain constant. The control scheme consists of independent controllers where each MV is coupled with a single CV[Gustavsson and Rönnberg, 2016, p.5]. This means that each MV-CV pairing needs to be selectively determined, which might lead to performance loss at off-design conditions. As well, in the cases where the active constraints move, the logic required for reconfiguration of the control system can become complicated. The advantage of decentralized control, on the other hand, is the transparency and simplicity of the control structure. There are few model requirements and the opportunity to fix and change the controllers and tunings are easily available [Skogestad and Morari, 1989] [Skogestad, 2004, p.229].

There exist two ways of designing a decentralized control structure: independent design and sequential loop-closing design. In the independent design, each control loop is designed individually, while in the sequential design each loop that is designed is closed before tuning the succeeding loop, where usually the fastest loop is tuned first. The advantage of tuning sequentially only occurs if there exists interaction within the control loops, which can be tuned away as the loops are designed. The disadvantage is that the design does not guarantee failure tolerance or a robust tolerance of the system. As well, the sequential design causes the controllers last in the sequence to become slow, such that the order of the sequence needs to account for the proper or desired dynamics, which might lead to a trial-and-error way of tuning and overall slow control performance[Skogestad and Postlethwaite, 2005, p.430] [Skogestad and Morari, 1989].

Multivariable control consists of multiple-input-multiple-output (MIMO) controllers and is recommended for interacting processes. If the process also suffers from changes in active constraints an explicit constraint handling control can be added to the multivariable controller re-

sulting in a multivariable constraint controller [Skogestad, 2004, p.229]. A common example of this type of controller is the model predictive controller (MPC) that predicts the future response of the plant and computes the controller setpoints by utilizing an explicit process model [Wu et al., 2015]. The process model required is a multivariable dynamic model, often lacking transparency. The advantage with the MPC controller is that it handles a shift in active constraints and interactive processes effectively, with little required logic [Skogestad, 2004].

3.1.2.3 Step S7: Optimization layer

In step 7 the process is reoptimized on a larger time scale such as hourly or daily to obtain updated active constraints and optimal setpoints for the supervisory control layer. The optimization layer determines if the process is self-optimizing or requires real-time optimization (RTO)[Skogestad, 2004, p.230].

3.1.2.4 Step S8: Validation

The structure is validated in step 8. This is usually done by selectively simulating significant parts of the process[Skogestad, 2004, p.230].

3.2 PID - control

The purpose of process control is to counteract disturbances that may occur in the system. The most common way of counteracting disturbances is through feedback control, where the output of the controlled variable, CV, is measured in order to compute the setpoint error. The output error is used as a measure to adjust the manipulated variable, MV[Skogestad and Grimholt, 2012].

The PID-controller is a widely used feedback controller that is constructed from three terms. The first term is the proportional, P, control that handles the change in the output as a linear response and accordingly rejects the disturbance proportionally to its error. The integral, I, control term integrates the error such that the controller quickly rejects the disturbance until the desired setpoint is reached. The I term of the PID-controller is therefore necessary if it is important not just to stabilize the effect of the disturbance, but to keep the output at its desired setpoint at steady state. The third term, is the derivative, D, control action that computes the derivative of the error. D-control should be applied in cases of higher order response, where the response in the output contains a second order time lag larger than the delay[Skogestad and Grimholt, 2012].

The series (cascade) from of the PID-controller is presented in Equation 3.4 and 3.5 in time and transfer domain, respectively.

$$u(t) = u_0 + K_c \Big[e(t) + \frac{1}{\tau_I} \int_0^t e(t)dt + \tau_D \frac{de(t)}{dt} \Big] \tag{3.4}$$
$$e(t) = y(t) - y_s(t)$$

$$c(s) = K_c\Big(\frac{\tau_1 s + 1}{\tau_1 s}\Big)(\tau_D s + 1) \qquad (3.5)$$

where K_c is the controller gain, τ_I is the integral time constant, τ_D is the derivative time constant, $c(s)$ is the controller input, $u(t)$ is the input (MV) and e(t) is the error in the measured output, $y(t)$, from its desired setpoint, $y_s(t)$ [Skogestad, 2003]. The parameters for the PID-controller can be obtained using the SIMC-tuning rules, defined in Section 3.2.1.

3.2.1 SIMC - tuning

Two methods of obtaining the PID-controller tunings are through the Ziegler-Nichols IMC (Internal-Model-Control) method and the SIMC (Simple-Internal-Model-Control)-tuning method.

The SIMC - tuning rules were presented by Sigurd Skogestad in 2002 and are a result of improving the heuristic Ziegler-Nichols IMC tuning method from 1942. The IMC method contains multiple terms and has been found to give an aggressive response for steady state responses. The SIMC tuning rules account for both integrating, first and higher order steady state responses and is therefore recommended for process control applications[Skogestad, 2003][Ziegler and Nichols, 1993].

The SIMC-tuning procedure is divided into two main steps:

- Approximation of a first- or second- order plus time delay model (process transfer function)

- Derivation of the controller settings

The second order plus time delay model (SOPTD) is represented in Equation 3.6, where the first order plus timedelay model (FOPTD) has $\tau_2 = 0$ [Skogestad, 2003]. A Figure illustrating the curve of a first order open loop response is shown in Figure 3.1.
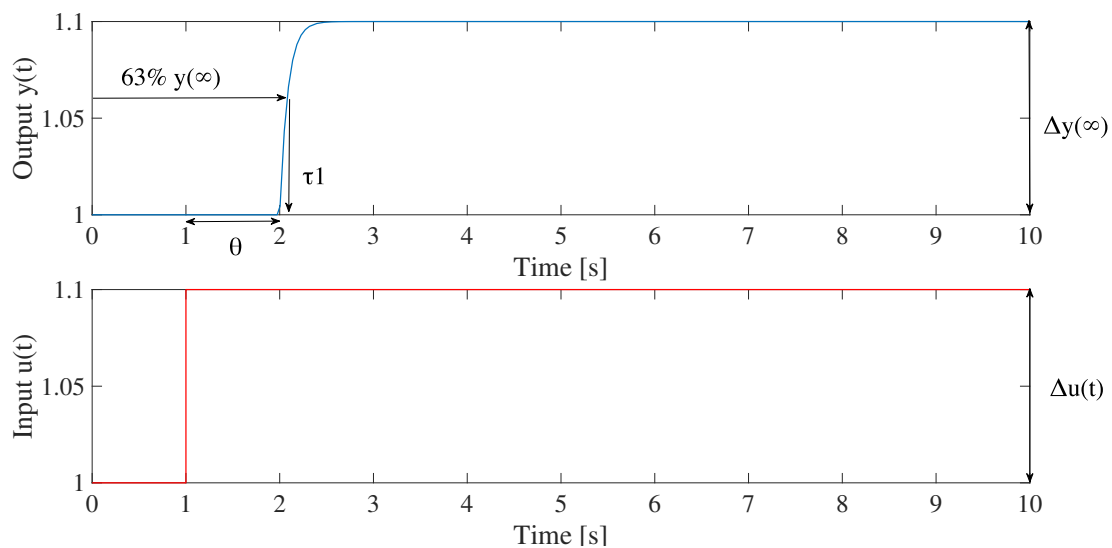
Figure 3.1: Example plot of a first order open loop steady state step response

$$g(s) = \frac{y(s)}{u(s)} = \frac{k}{(\tau_1 s + 1)(\tau_2 s + 1)} e^{-\theta s} \tag{3.6}$$

A pure gain process is a type of process with an infinitely small time constant, where a step in the input results in a quick change, or step, in the output. This can easily be seen from the pure gain process transfer function, presented in Equation 3.7.

$$g(s) = k e^{-\theta s} \tag{3.7}$$

An illustration of an open loop step response that can be considered pure gain at steady state is shown in Figure 3.2.
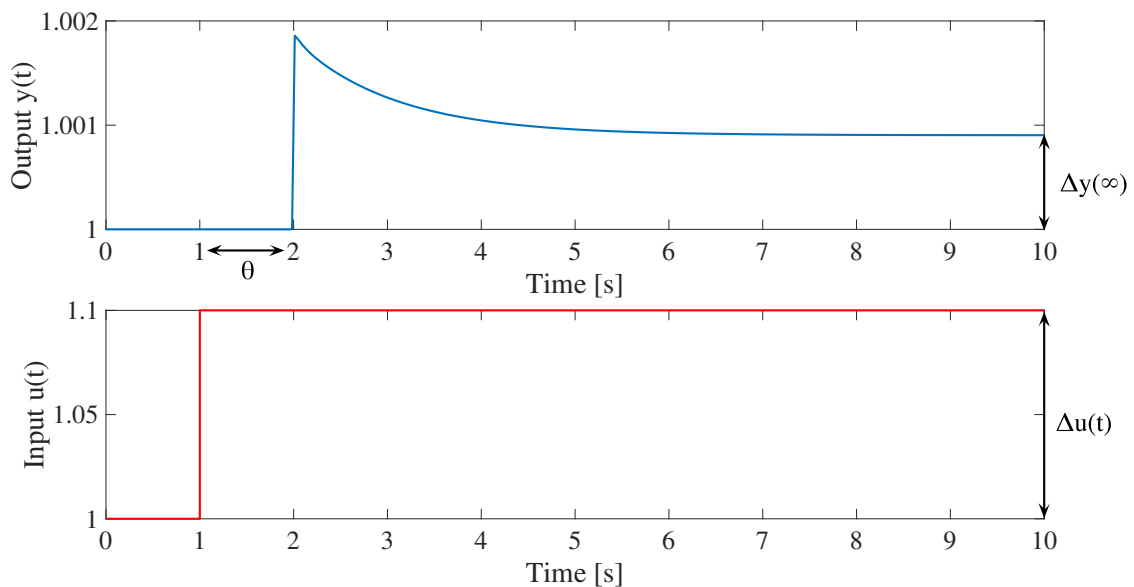
Figure 3.2: Example plot of a pure gain open loop step response

An integrating response is characterized by a response in output after an open loop step in input that does not reach steady state. The obtained τ_1 is large and $\tau_2 = 0$ leading to the simplification of Equation 3.6 shown in Equation 3.8. An example plot of an integrating response is illustrated in Figure 3.3.
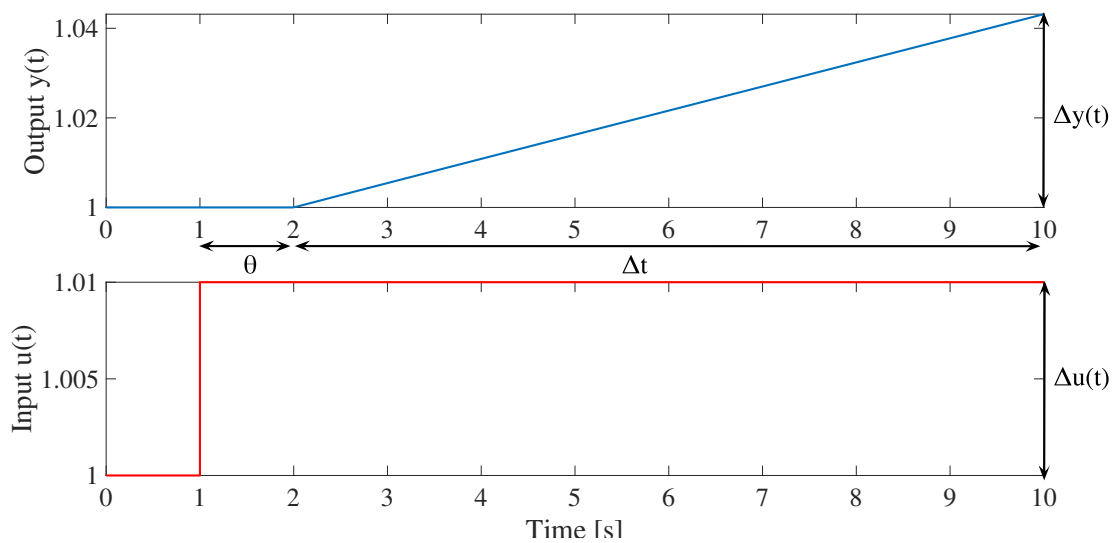
Figure 3.3: Example plot of an integrating open loop step response.

$$g(s) = \frac{k}{(\tau_1 s + 1)} e^{-\theta s} \tag{3.8}$$

$$g(s) = \frac{\frac{k}{\tau_1}}{\left(s + \frac{1}{\tau_1}\right)} e^{-\theta s} \tag{3.9}$$

$$g(s) \approx \frac{k}{\tau_1 s} e^{-\theta s} \tag{3.10}$$

$$g(s) = \frac{k'}{s} e^{-\theta s} \tag{3.11}$$

The SIMC tunings for the controller pairing can be determined directly from the process transfer function in cases of non-interactive processes or by performing an open loop input step response from the system itself. The open loop input step response is done by stepping on the input variable, u, and plotting the response of the output, y. Input step responses are shown for steady state, pure gain and integrating responses in Figure 3.1, 3.2 and Figure 3.3, respectively, where the succeeding parameters are noted and inserted into the SIMC tunings listed in Table 3.1.

- k, process gain $\frac{\Delta y(\infty)}{\Delta u}$

- k', integrating process gain $\frac{k}{\Delta t}$

- θ, effective time delay

- τ_1, dominant lag time constant found as the time the output uses to reach 63% of the steady state output value.

- τ_2, second-order lag time constant

- τ_c, closed loop time constant

Table 3.1: SIMC controller tunings for PID-control

Process	K_c	τ_I	τ_D
Integrating	$\frac{1}{k'}\frac{1}{\tau_c+\theta}$	$4(\tau_c+\theta)$	τ_2
FOPTD	$\frac{1}{k}\frac{\tau_1}{\tau_c+\theta}$	$\min\{\tau_1, 4(\tau_c+\theta)\}$	τ_2

From the input step response for a pure gain process, it is clear that the open loop time constant, τ_1, is approximately zero. Inserting the steady state SIMC controller tunings from Table 3.1 into Equation 3.5, the controller tunings derived in Equation 3.12 for the pure gain process simplifies to an I-controller.

$$
\begin{aligned}
c(s) &= \lim_{\tau_1 \to 0} K_c \Big(\frac{\tau_1 s + 1}{\tau_1 s} \Big) \\
c(s) &= \lim_{\tau_1 \to 0} \frac{1}{k}\frac{\tau_1}{\tau_c+\theta} \Big(\frac{\tau_1 s + 1}{\tau_1 s} \Big) \\
c(s) &= \frac{1}{k}\frac{1}{\tau_c+\theta}\frac{1}{s} \\
c(t) &= \frac{1}{k}\frac{1}{\tau_c+\theta}
\end{aligned}
\tag{3.12}
$$

3.2.2 Inverse responses

An inverse response is seen when the initial response in the output is in the opposite direction of its setpoint, also referred to as an undershoot. This occurs as a result of right-hand-plane(RHP)-zeros. RHP-zeros are also called unstable zeros, as they are located in the right-half plane of the complex plane. If the effect of the inverse response is not considered, the system can go unstable.

A system containing RHP-zeros add time lag to the process, similar to a delay to the system, leading to a tradeoff between inverse response in output and long settling time[Skogestad and Postlethwaite, 2005, p. 11, 19, 184]. When designing a controller for a process with an inverse response, the period of opposite response can be added as a delay.

3.2.3 Integral-windup

In cases where the manipulated variable reaches its input limitation, it is said to saturate. For PID-controllers with integrating action, I-control, the error will accumulate in the controller, leading to integral windup. Integral windup causes the I-control to become large and will require the system to produce an opposite sign error during a long time for the system to return to normal. In these cases, anti-windup should be applied to the controller. Anti-windup reduces or resets the integral action such that the actuator output is set at the actuator limit as well as limiting the integral windup in the controller[Åström, 2002, p.226-230].

To methods of anti-windup offered by MATLAB are clamping and back-calculation. Clamping or conditional integration switches off the integrating action once the actuator is saturated and will become constant as long as the controller output is not satisfying its limitations. The back-calculation anti-windup recomputes the integral during saturation of the actuator and resets

the integrator back to normal in a dynamic way. This method utilizes the error between the actuator output and controller output as well as the integral action in the PID-controller to drive the integral error towards zero in a feedback manner. The back-calculation method has thus the advantage of being tuned to the desired speed with a time constant, T_t, allowing for better dynamics than the clamping method, but also the disadvantage of performing equal or worse than the clamping method if a proper value for the back-calculation coefficient is not computed[The MathWorks Inc, 2019a] [Åström, 2002].

3.3 Heat-to-Power control structures

In [Welfonder, 1999, p.28] Welfonder depicts three operating modes for a power plant: steam generator-driven, block-driven and turbine-driven. For cases with decentralized control, these modes each represent different regulation concepts that should be selected with regards to the desired control objective of the plant. The three different control structures are illustrated in a simplified process diagram in Figure 3.4.

(a) Steam generator driven control structure   **(b)** Turbine-driven control structure   **(c)** Block-driven control structure
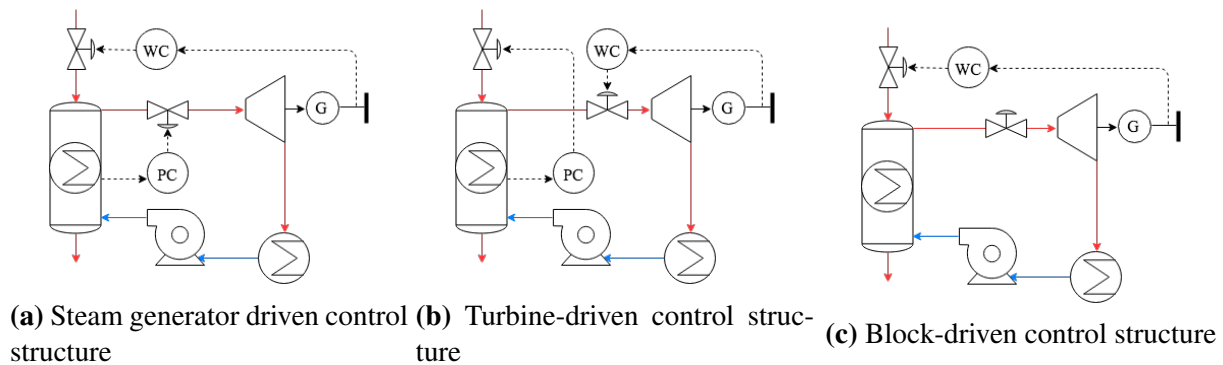
Figure 3.4: Control structures

3.3.1 Boiler-driven control structure

The boiler-driven (steam generator-driven) control structure manipulates the fuel flow and the turbine valve in order to regulate the power output and steam pressure, respectively. This leads to direct linking between the power output and fuel flow which can be desired if the objective is to achieve fast load changes in the cycle. The disadvantage with this structure is with regards to the distance between the fuel flow and power produced, leading to slow response time for the power controller[Welfonder, 1999]. As well the distance between the power and pressure control is expected to uncouple the controllers, which leads to a loss in coordination between the controllers with regards to their interaction[Kovacs, 2004, p.74].

3.3.2 Floating pressure control structure

The floating pressure (block-driven) control structure is similar to that of the boiler-driven control structure, where the steam pressure is left uncontrolled and the turbine valve position is manipulated to control other output such as for example the steam turbine speed[Welfonder, 1999].

3.3.3   Turbine-driven control structure

The turbine-driven control structure has its pairings opposite of the boiler-driven control structure, such that the power output is paired with the turbine valve position and the steam pressure with the fuel flow. An advantage with the turbine-driven control structure is the expected quick response in the power controller since the turbine valve position is close to where the power output is measured, leading to low time constants. The same can be experienced in the steam pressure as the fuel flow directly affects the boiler system [Welfonder, 1999] [Kovacs, 2004]. The disadvantage is the loss of direct load effect on the power output, thus removing the ability to utilize the boiler storage.

3.3.4   Sliding pressure

A more advanced version of the turbine-driven control structure is called sliding pressure control, where the setpoint of the pressure controller is adjusted according to the power controller to account for grid-frequency regulation or valve saturation [Welfonder, 1999]. The adjustment of the setpoint requires a supervisory controller such as for example a valve position controller or MID selector.

3.4   Advanced control structures

3.4.1   Valve position control

The valve position controller (VPC), also known as input resetting controller or midrange controller, is an advanced type of control that shifts a manipulated variable to its nominal input value after the regulation of its controlled variable has taken place. This is done by manipulating a second variable with a larger region to account for the same controller output. Valve position control can, therefore, be utilized in situations with extra manipulated variables to maximize the throughput and thus plant profitability [Jha and Kaistha, 2007]. A block diagram of a typical valve position controller is shown in Figure 3.5 [Skogestad and Postlethwaite, 2005, p. 422].
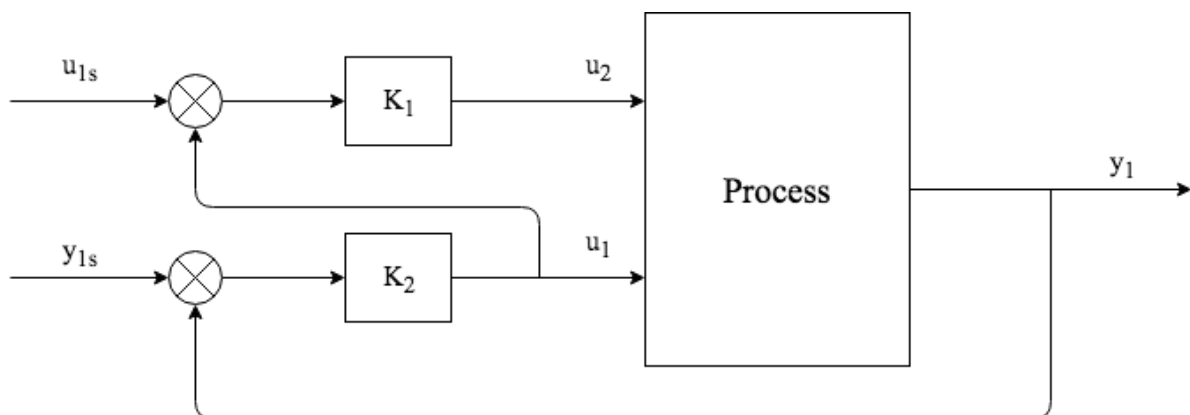
Figure 3.5: Block diagram of a valve position controller

The VPC can be considered a type of cascade controller, where the inner loop consists of fast control of the CV, acting as a slave controller. The outer loop is being used to set the inner loop

MV back to its desired setpoint, allowing it to be a slow, decoupled controller. The decoupling of the controllers should allow for integrating action to be present in both controllers without causing negative effects from correlation [Skogestad and Postlethwaite, 2005, p.426].

3.4.2 Parallel Control

A parallel controller also utilizes two manipulated variables, but now with the sole purpose of controlling one output. In the case of the valve position being one of the manipulated variables, the parallel controller can indirectly minimize the risk of valve saturation, if implemented correctly. During the tuning of the parallel controller, the fast and slow controllers have to be tuned in parallel from their respected open loop responses. Only one of the parallel controllers can have integral action, which should be selected to be for the slow controller [Åström, 2002, p. 245-247]. Implementing the PI-control to be executed by the slow, large range manipulated variable allows for offset removal in the fast, small range controller even if it only contains P-control.
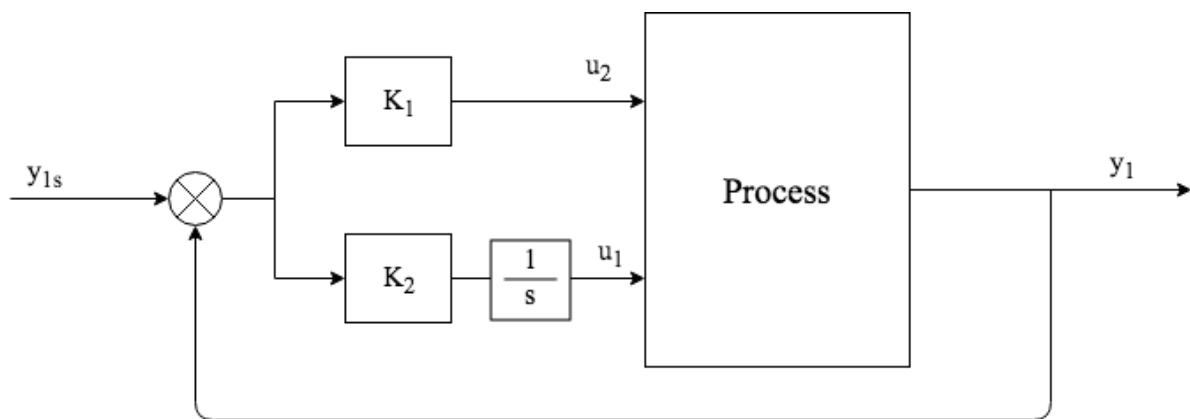
Figure 3.6: Block diagram of a parallel controller [Åström, 2002, p.246].

Chapter 4

Model description

In this chapter, the focus is on presenting the Heat-to-Power cycle that is modelled in Simulink. The model used is a continuation of the model built from the process control specialization project [Andersskog, 2018].

4.1 Model

The general decomposition of a heat-to-power cycle is into three main subsystems: water cycle, fireside and generator [Wu et al., 2015]. The main focus of the simulated model, in this case, is with regards to the water cycle, thus the modelling of the combustion and generator is simplified and implemented into the corresponding water cycle components. The flue gas is assumed to be a product of the combustion of natural gas and consists of 13% CO_2, 7% H_2O, 5 % O_2 and 75% N_2 in volume percent.

The steam cycle model consists of several main components as described in Section 2.1. The components are modelled separately into their own respected subsystems: Economizer, mixer, drum, superheater, attemperator, turbine inlet valve, high pressure (HP) turbine, reheater, low pressure (LP) turbine, condenser and pump. The boiler subsystem is modelled as a once-through boiler.

By modelling the components separately, the implementation of the pressure node-flow element method becomes more convenient. The pressure node-flow element method consists of alternating dynamic and static subsystems as mentioned in Section 2.3. This is to discretize the signals in Simulink as well as maintaining the different dynamics of the cycle. The dynamic subsystems are the drum, attemperator, holdup before the turbine and the condenser. The static subsystems are the mixing of the streams after the economizer, superheater, turbine and pump. The economizer subsystem was modelled both as a static and dynamic subsystem. This is because the holdup was assumed constant, while the temperature was modelled through dynamic energy conservation.

Most of the states of the simulation were scaled for higher computational efficiency and numerical purposes. Initial guesses and scalings for the states are listed in Table A.4 in Appendix A.3. The data was computed through a steady state script of the simulation, rendered in Appendix A.16.1.

4.2 Assumptions

In Section 2.1 assumptions were made to simplify the governing equations for the dynamic states. Additional assumptions were made when modelling the Heat-to-Power cycle represented in the list below.

- The Heat-to-Power cycle is a power generating process

- No radiation

- Assumed instant mixing of the streams in the attemperator and mixer

- Steam and flue gas is assumed ideal gasses

- Constant heat capacities

- The boiling temperature of the water is assumed to be 310.9188 °C at P = 99.28 bar

- The boiling temperature of the water is assumed to be 45 °C at P = 0.096 bar

- Saturated steam in the drum evaporator

- The inlet flows into the economizer, drum evaporator and bypass flow into the attemperator is assumed to be in a liquid phase

- The steam out of the turbine is assumed to be saturated

- Constant heat transfer coefficients, UA

- Arithmetic mean was used to approximate the temperature difference over the heat exchangers

- The temperature at the heat exchanger inlet is constant and equal to 1000 °C

- A linear valve is assumed in the computation of the mass flow out of the superheater and at the turbine inlet.

- The Antoine equation was used to compute the saturation pressure out of the drum evaporator and out of the turbine.

- No pressure and temperature loss between the attemperator and the high-pressure turbine.

- The fluid density, ρ is assumed constant to be $\rho = 970 \; kgm^3$.

- The flue gas is assumed to be a product of the combustion of natural gas and consists of 13% CO_2, 7% H_2O, 5 % O_2 and 75% N_2.

4.3 Model representation

The modelled Heat-to-Power cycle is represented in Figure 4.1. Blue lines portray the liquid phase and red lines gaseous phase.
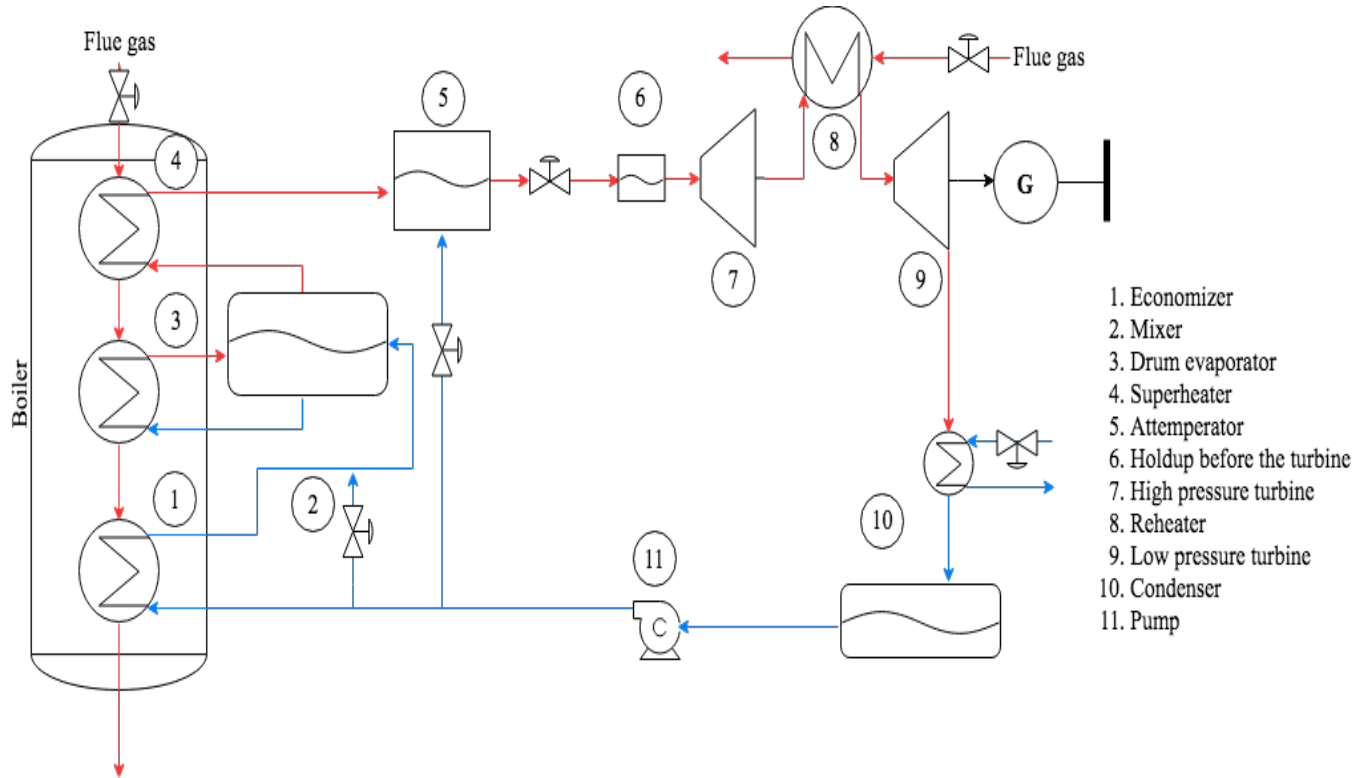
Figure 4.1: Process flowsheet of the modelled Heat-to-Power cycle

4.4   States

In order to present the states of the modelled Heat-to-Power cycle, the nomenclature and subscripts used for the variables in the simulation are first presented in Table 4.1 and 4.2, respectively.

Table 4.1: List of the nomenclature for relevant variables in the simulation

Nomenclature	Symbol	Units
Mass	M	kg
Mass flow	m	kgs^{-1}
Pressure	P	Pa
Temperature	T	K
Enthalpy	H	J
Specific enthalpy	h	Jkg^{-1}
Heat flow	Q	Js^{-1}
Valve position	z	
Rotational speed	N	rads^{-1}

Table 4.2: Description of subscripts used in the nomenclature

Subscripts	Description
eco	Economizer
mix	Mixer
b	Bypass
FG	Flue gas
d	Drum evaporator
sh	Superheater
a	Attemperator
t	Turbine
hp	High pressure
lp	Low pressure
r	Reheater
c	Condenser
p	Pump
in	Inlet
out	Outlet

The states of the Heat-to-Power cycle can be divided into dynamic and static states. The dynamic states represent a state that changes with respect to time and is computed through the integration of the state on its differential form. The static states are solved from implicit or explicit algebraic equations as they are assumed to be in steady state. The states used in the simulation are listed in Table 4.3 and divided into their corresponding subsystem and state classification. It is important to mention that power, W, is listed as a static state, even if it is not theoretically a state, but rather a function of several states such as pressure and temperature. It is still listed here, as it is an important output throughout the simulation model.

Table 4.3: The dynamic and static states of the modelled Heat-to-Power cycle

Subsystem	Dynamic states	Static states
Economizer	T_{eco}	M_{eco} $T_{FG,eco}$
Mixer		T_{mix}
Drum evaporator	M_d,H_d	$T_d,T_{FG,d},P_d$
Superheater		$T_{sh}, T_{FG,sh}$
Attemperator	M_a,T_a	P_a
Turbine	M_t	$P_{t,in}, T_{hp}, W_{hp}, T_{lp}, W_{lp}, W$
Reheater		$T_r, T_{FG,r}$
Condenser	M_c,T_c	P_c
Pump		P_p,W_p

4.5   Thermodynamic properties of water

The main thermodynamic properties used in the Heat-to-Power cycle model were heat capacities and heat of vaporization. The heat capacities of the water and steam were assumed constant and are listed in Table A.3 in Section A.2[Blackman et al., 2013].

The pressure-enthalpy diagram in Figure 2.3 in Section 2.1.3 was based on the IAPWS-97 industrial formulation for the thermodynamic properties of water and steam. The IAPWS-97 formulation is recommended for the steam power industry and provides thermodynamic steam and water properties in the ranges of 0 - 1000 bar and 0 - 2000°C[The International Association for the Properties of Water and Steam, 2007].

The IAPWS-97 formulations have been implemented in [Holmgren, 2007] as a MATLAB script: *XSteam.m*. *XSteam.m* can be used to obtain the heat of vaporization for water at different pressures through the 'h_px' function that computes the specific enthalpy of water at different pressures and vapour fractions. By computing the difference in enthalpy at 0% and 100% vapour fraction (liquid and gaseous state), the heat of vaporization is obtained at the desired pressure. The heat of vaporization can also be obtained directly from the pressure-enthalpy diagram by following the pressure lines and then noting the specific enthalpies at 0 and 100% vapour fraction.
The heat of vaporization used for the Heat-to-Power cycle are listed in Table 4.4.

Table 4.4: Thermodynamic properties of water

Pressure [MPa]	Heat of Vaporization [kJ/kg]
0.096	2394
99.28	1321.9

The IAPWS-97 formulation provides multiple thermodynamic properties and relations such as densities, heat capacities and saturation pressures. The Heat-to-Power cycle that was modelled was simple and did not go into supercritical vapour or liquid state. *XSteam.m* was not used for any other thermodynamic calculations as the main objective for building the simulation are for control purposes.

4.6 Model equations

4.6.1 Dynamic model equations

In the dynamical components, the mass and the energy of the system are modeled through ordinary differential equations represented by Equation 2.9 and 2.10 from Section 2.2, respectively. This is because these components contain a holdup that slows down the dynamics of the system leading to changes occurring over a longer period of time.

The components containing a holdup in the Heat-to-Power simulation are the economizer, drum, attemperator and condenser. The drum, attemperator and condenser components are modelled using Equation 2.9, 2.10, and 2.12 to obtain states such as holdup, enthalpy or temperature, with additional model equations for the static variables as mentioned in section 4.6.2. The holdup in the economizer is assumed to be constant, where the temperature is modelled dynamically through Equation 2.10 under the simplification from Equation 2.12 from Section 2.2.

4.6.1.1 Residence time

The holdups of the heat-to-power cycle can affect the cycle dynamics by for example dampening disturbances from the fuel load and feedwater [Kovacs, 2004, p.55]. Another important effect of the holdups is with regards to the effective delay of the plant components. The residence time of the holdups can be considered as delays leading to slower control. Realistic holdups for each of the holdup should, therefore, be compared with the expected residence time such that the main dynamics of the heat-to-power cycle model are included. The residence time can be computed through Equation 4.1.

$$\tau_T = \frac{M}{\dot{m}} \tag{4.1}$$

where M is the mass holdup [kg] and $\dot{m}$ is the mass flow [kgs^{-1}]. The holdup in the turbine, M_t, is modelled with the purpose of computing the inlet pressure of the turbine through the ideal gas law and should be set to be as low as possible to obtain the characteristic fast dynamics of the turbine subsystem. The holdup in the attemperator, M_a, has the purpose of mixing the cooling bypass water with the much larger hot superheated steam, thus, under the assumption of instant mixing, the holdup is not required to be particularly large. The main holdup dynamics are in the condenser, M_c, and drum, M_d. It is recommended to have residence times between 1 - 5 minutes for the condenser [Heat Exchange Institute, 2015] [McKetta, 1997, p.73]. The boiler drum is required to have a residence time between 2-12 minutes of holdup, depending on the amount of steam that is generated [Ganapathy, 2002, p.74].

The holdups, mass flows and computed residence times for each holdup in the simulation are listed in Table 4.5.

Table 4.5: Holdups, mass flows, and residence times for the dynamic components.

Holdup	M [kg]	$\dot{m}$ [kgs^{-1}]	τ_T [min]
M_d	1000	5.975	167.36
M_a	26.45	6.286	4.14
M_t	0.25	6.286	0.040
M_c	500	6.286	79.54

4.6.2 Algebraic model equations

The mass and energy balance for the static subsystems are modeled under the assumption that there is no or very quick change in the system with regards to time, $\frac{dM}{dt} = 0$ and $\frac{dH}{dt} = 0$. This leads to a simplification of the dynamic conservation balances from Section 2.2, shown in Equation 4.2 and 4.3 for the algebraic mass and energy balance, respectively.

Subsystems modelled by the algebraic model equations are the split of the feedwater mass flow from the pump into the boiler and attemperator, the flow and temperature of the water from the mixing of the economizer bypass and the temperature of the steam in the superheater.

$$\dot{m}_{in} - \dot{m}_{out} = 0 \tag{4.2}$$

$$\dot{m}_{in}h_{in} - \dot{m}_{out}h_{out} + Q = 0 \tag{4.3}$$

where Q is the heat transferred, m_{in} and m_{out} are the inlet and outlet mass flows and h are the specific enthalpies of the in and outlet streams computed through Equation 2.11 from Section 2.2.

4.6.2.1 Drum evaporator

A variation of the algebraic energy balance used in the drum subsystem utilizes the enthalpy, H_d, and holdup, M_d obtained from the dynamic energy and mass balance shown in Equation 2.10 and 2.9 when obtaining the temperature, T_d, out of the drum. This was done through the implicit algebraic energy balance, shown in Equation 4.4.

$$0 = H_d - M_d * h_d \tag{4.4}$$

where h_d is the specific enthalpy in the drum computed through Equation 2.11 from Section 2.2.

4.6.3 Pressure models

The pressures in the Heat-to-Power model were computed differently with respect to the phase and classification of the state or component. For pressures in dynamical pressure nodes such as in the attemperator, P_a and in the holdup before turbine, $P_{t,in}$ a pressure node approach has been used. For saturated steam such as in the drum, P_d and after the turbine, P_c, the Antoine Equation in Equation 2.1 in Section 2.1.3 has been used. In the pump, the water is in the liquid phase and the pressure is computed by the pump model represented in Section 4.6.7.

4.6.3.1 Pressure nodes

The computation of the dynamic pressure states is inspired by the pressure-flow network model described in [Rua Pazoz, 2017]. The mass, M, and temperature, T, obtained from the integration of the dynamic mass and energy balance in Equation 2.9 and 2.10 respectively, are used as inputs in the ideal gas law equation from which the pressure, P, is computed. The ideal gas law is represented in Equation 4.5.

$$P = \frac{MRT}{VM_m} \tag{4.5}$$

where R is the universal gas constant, V is the volume and M_m is the molar mass. The values for R, V and M_m used in the simulation are listed in Appendix A.2.

A visualization of the pressure node model is shown in Figure 4.2.
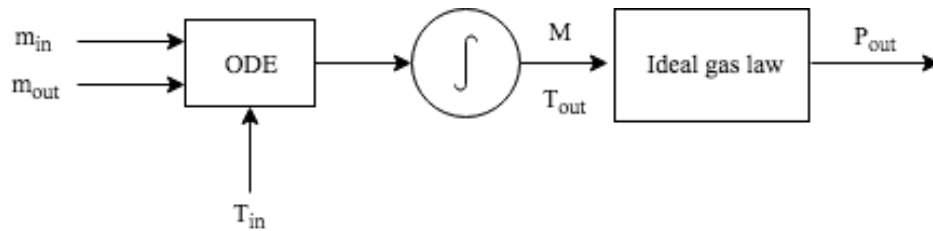
Figure 4.2: Process flowsheet of the modelled pressure nodes [Batalov, 2011, p.5].

4.6.4 Flow elements

The flow elements are described in Section 2.3 as nodes that are modelled by algebraic equations that relate the in and outlet pressure to the mass flow out of the system. The pressure nodes and their succeeding flow elements for the modelled Heat-to-Power cycle are listed in Table 4.6 below.

Table 4.6: Pressure nodes and succeeding flow elements of the Heat-to-Power simulation.

Pressure Node	Succeeding Flow Element
Drum , P_d	$\dot{m}_{sh}$
Attemperator, P_a	$\dot{m}_a$
Turbine inlet, $P_{t,in}$	$\dot{m}_t$
Condenser, P_c	$\dot{m}_p$

where the first two flows, $\dot{m}_{sh}$ and $\dot{m}_a$ are computed through the linear valve equation described in Section 4.6.4.1. The flow through the turbine, $\dot{m}_t$, is modelled by the Stodola Approximation described in Section 2.1.5.2, while the flow through the pump is computed through the pump model in Section 4.6.7.

4.6.4.1 Valve equation

The flow elements of the simulation consisted of static subsystems where the flows can be computed through the valve equation. For high-pressure steam, the linear valve equation can be used, represented in Equation 4.6

$$\dot{m}_i = C_{vi} z_i \sqrt{P_{i-1} - P_i} \tag{4.6}$$

where C_{vi} is the valve coefficient computed from nominal, $_{nom}$, and steady state, *, data through Equation 4.7.

$$C_{vi} = \frac{\dot{m}_{i,nom}}{z_{i,nom}(P_{i-1}^* - P_i^*)} \tag{4.7}$$

4.6.5 Turbine

The turbine modelled is set to have a low outlet pressure (0.096 bar) to obtain a high power output. Since the pressure sent into the turbine is high (93 bar), expansion through several stages is recommended. This is done by adding additional turbines with smaller expansion ratios, which decreases the pressure load on the individual turbine. The expansion of steam through several stages also allows for the addition of a reheater in between the turbines, minimizing the risk of condensation through the turbine and increasing the amount of heat recovered4[Sinnott and Towler, 2009, p. 121].

The turbine subsystem consists of two stages of steam expansion: a high-pressure turbine and a low-pressure turbine, where the turbines are connected to a generator to convert the mechanical energy to electrical energy. The steam is assumed to expand isentropically, leading to the isentropic pressure-temperature relation represented in Equation 4.8 [Skogestad, 2009, p. 141,201-202]. Assuming constant heat capacity of the steam, the work, W, can be computed through Equation 4.9

$$T_{out} = T_{in}\left(\frac{P_{in}}{P_{out}}\right)^{\frac{R}{C_p}} \tag{4.8}$$

$$W = mC_p(T_{out} - T_{in}) \tag{4.9}$$

where C_p is the heat capacity, R is the universal gas constant, T_{in} and T_{out} are the inlet and outlet temperature, P_{in} and P_{out} are the inlet and outlet pressure and m is the mass flow modelled by the Stodola Equation from Equation 2.4 in Section 2.1.5.2.

4.6.6 Heat exchangers

There are a total of four heat exchangers in the modelled Heat-to-Power cycle, they are positioned in the economizer, drum, superheater and between the high-and low-pressure turbines. The heat exchangers in the economizer, drum and superheater are connected through a once-through boiler such that the flue gas enters through the superheater and exits through the economizer. The heat exchanger between the high- and low-pressure turbine is commonly called the reheater. The reheater usually consists of the same flue gas as the latter heat exchangers but is modelled independently for simplicity in this case.

The transfer of heat from the flue gas to the water occurs rapidly and no dynamics are therefore included in the heat exchanger modelling on the flue gas side. The heat from the flue gas, Q, is transferred through convection and can be computed from its heat transfer coefficient multiplied with the crossectional area, UA, and temperature difference, ΔT through the empirical formula for convection as shown in Equation 4.10.

$$Q = UA\Delta T \tag{4.10}$$

The temperature difference, ΔT, in heat exchangers is normally approximated through the logarithmic mean, ΔT_{lm}. If the enthalpy is modelled on its temperature form, the logarithmic mean can be difficult to integrate. Thus, a simplified arithmetical mean will be used when modelling the convection through the heat exchanger:

$$\Delta T = \left(\frac{T_{hot,in} + T_{hot,out}}{2}\right) - \left(\frac{T_{cold,in} + T_{cold,out}}{2}\right) \tag{4.11}$$

where $T_{hot,in}$ and $T_{hot,out}$ are the inlet and outlet temperatures of the flue gas and $T_{cold,in}$ and $T_{cold,out}$ are the inlet and outlet temperatures of the steam or water.

The inlet temperature of the flue gas is assumed to be known. The outlet temperature of the flue gas can be obtained from an algebraic energy balance of the heat exchanger from the flue gas side, as represented in Equation 4.12.

$$mC_p(T_{in} - T_{out}) - Q = 0 \tag{4.12}$$

where m is the flue gas flow, C_p is the flue gas heat capacity, Q is the heat transfered and T_{in} and T_{out} are the inlet and outlet temperatures of the flue gas, respectively.

To obtain the heat transfer coefficient for the heat exchangers, a steady state script is built and can be found in Appendix A.16.1. An added purpose of this steady state script is to obtain realistic nominal values for the flue gas flow and outlet temperature. Too low outlet temperature of the flue gas risks the chance of the gas condensing from the heat transfer process, leading to corrosion of the pipes [Tanuma, 2017, p.17] [Skogestad, 2009, p. 194]. The steady state script consists of Equation 4.10, 4.12 and an energy balance for the steam side of the heat exchangers presented by Equation 4.3. The equations are solved simultaneously to obtain UA, Q and $T_{hot,out}$ given steady state and nominal data for the latter variables.

4.6.6.1 Flue gas

The flue gas is assumed to be a product of the combustion of natural gas and consists of 13% CO_2, 7% H_2O, 5 % O_2 and 75% N_2. The combustion of natural gas is represented by the mass balance in Equation 4.13.

$$CH_4 + 2O_2 \rightarrow CO_2 + H_2O \tag{4.13}$$

In reality, excess oxygen is added to the combustion and some of the oxygen does not always react during the combustion. The flue gas composition was inspired by the fractions listed in [Ivković et al., 2011, p.115]. The components heat capacities were found in SI Chemical Data [Blackman et al., 2013]. The flue gas fractions and heat capacities used in the simulation are listed in Table 4.7. The overall flue gas heat capacity is computed as 1063.1 $Jkg^{-1}K^{-1}$ and the boiling point assumed to be 100°C (373.15K) as the mixture contains a small fraction of H_2O which has the highest point of evaporation at standard conditions.

Table 4.7: Composition and heat capacities for the flue gas components

Component	Volume fraction	Heat capacity [$Jkg^{-1}K^{-1}$]
CO_2	0.13	840.91
H_2O	0.07	1888.89
N_2	0.75	1034.98
O_2	0.05	906.25

4.6.7 Pump

The modelling of the pump was inspired by the pump process model from [Oryds et al., 1994, p.183-184] and is assumed to of centrifugal type. The model described uses the pump speed, N, fluid density, ρ and inlet pressure, P_{in} as inputs and computes the mass flow rate, m, pump power consumption, W_p, fluid density, ρ and outlet pressure, P_{out}.

The model is represented in Equation 4.14 and consists of several parameters described in Table 4.8.

$$
\begin{aligned}
F &= \sqrt{\frac{k_1 N^2 - \Delta P_s / \bar{\rho}}{k_2 + k_3}} \\
\Delta P_q &= k_3 \bar{\rho} F^2 \\
\Delta P &= \Delta P_s + \Delta P_q \\
P_0 &= P_i + \Delta P \\
m &= F \rho \\
W_p &= \frac{\Delta P F}{\eta} \frac{100}{1}
\end{aligned}
\tag{4.14}
$$

where F is the volumetric flow rate, ΔP_q is the pressure drop across the load and ΔP is the pressure rise across the pump.

Table 4.8: Pump model parameters

Parameter	Description
k_1	Machine construction constant
k_2	Machine construction constant
k_3	Constant dependent on the load
η	Pump efficiency
$\bar{\rho}$	Fluid density reference value
ΔP_s	Static pressure rise across the pump

By assuming constant fluid density, the inputs are the inlet pressure, P_{in} and the pump speed, N. The inlet pressure is computed in the condenser subsystem through the Antoine Equation described in Section 2.1.3.1, thus leaving the rotational speed as an open input, that can be manipulated. A steady state script is built and solved for the parameters with steady state data for the outputs and nominal values for the inputs. In order to satisfy the degrees of freedom, k_2 is assumed to be zero. The parameters used in the simulation are listed in Appendix A.16.2.

4.7   Simulink and solvers

The Heat-to-Power cycle is modelled using the Pressure-Flow network model as described in Section 2.3. This creates a very stiff model, meaning a small-time grid is needed to solve the simulation in quick parts of the simulation while integrating over a longer time period for the much slower parts, such as the dynamic components[Perry et al., 1997, s.3,p.55-56]. To avoid the need for a constant small grid solver, a variable step solver is the most effective integration solver for this simulation.
Simulink offers several variable-step integration solvers that vary the step size dynamically during the simulation. The step size is reduced with regards to its local error in order to achieve the tolerance specified. The variable-step integration solver used in this simulation is the *ode15s* solver which is recommended for stiff systems and can achieve the highest accuracy of the stiff variable-step integration solvers offered by Simulink [The MathWorks Inc, 2019b]. *ode15s* is a multistep solver that utilizes solutions from several preceding time points when computing the model's state. *ode15s* uses variable-order numerical differentiation formulas (NDFs) [The MathWorks Inc, 2019b].

The zero-crossing options for the *ode15s* solver was enabled and the algorithm set to adaptive for faster simulation. The relative tolerance for the integration solver was set to 10^{-8} for most of the simulation. Different tolerances were also used, such as 10^{-7} or 10^{-9}, in cases where the simulation would not run at the set relative tolerance. This is an example of how stiff this system is as small differences in decimal places, run time or relative tolerance can change if the simulation runs at all.

The implicit algebraic equations are solved through an algebraic constraint solver, which was set to automatic for all the algebraic constraint blocks.

Additionally, Simulink offers a solver mode called "Accelerator", in which speeds the simulation [The MathWorks Inc, 2019c]. This mode is not necessary but can be useful in cases of long simulation time or repetitive simulations, where the accelerator reduces the total simulation time substantially.

5

The plantwide control procedure for the Heat-to-Power cycle

In this chapter, important control assumptions and approximations are presented as well as the application of the plantwide control procedure on the modelled Heat-to-Power cycle.

5.1 Control assumptions

No delays were added to the simulation. As the realistic heat-to-power cycle does contain delays this should be considered when reading this thesis. The aim of the control analysis, in this case, is to see how decoupling of a heat-to-power cycle can be made by decentralized control and how the different control structures perform compared to each other. Thus, the addition of delays scales up the time all of the controllers use to reach their setpoint and should not have an effect on the conclusions made from the simulations. The delays from the dynamic components are reflected as effective delays from their respective holdups, thus including the main dynamics of the cycle.

5.2 Top-down

5.2.1 Step S1: Definition of operational objectives

The large time scale aim of the modelled heat-to-power cycle is to maximize the profit of the process, assuming cheap energy prices. In terms of an objective function, this is the same as minimizing the loss, as can be seen in Equation 5.1.

$$J = -P = \text{cost feed} + \text{cost energy} - \text{value products} \tag{5.1}$$

$$J = p_F F + p_U U - p_w W \tag{5.2}$$

where F is the supplied fuel, U are energy utilities such as cooling water and power to the pump, W is the produced power and p is the price for the respected source or product. This is under the assumption that the modelled cycle is a pure power generating cycle (no steam is extracted) and the flue gas is delivered to the heat-to-power cycle as a heating source.

The modelled Heat-to-Power cycle is also required to contribute to grid frequency regulation on a fast time scale, thus a small time scale control objective is to achieve tight and fast power control.

The objective functions is subject to the constraints of the plant, which in the case of a heat-to-power cycle includes:

1. The produced power should be equal to its setpoint in order to match the market grid frequency.

2. The temperature after the attemperator cannot exceed material property constraints and is currently limited by a temperature of 620 °C [Breeze, 2012]. $T_a \leq 529$ °C is set as a conservative limitation for the simulation.

3. Pressure into the turbine should be controlled because of material property constraints, as well as the saturation pressure in the boiler can cause instability and should at least be below 20 MPa. $P_d < 20$ MPa.

4. The flue gas contains water, which will cause corrosion if the gas condensates, thus the temperature should be limited at 100 °C. $T_{FG,eco} \geq 151.64$ °C is set as a limitation for the simulation.

5. To reduce the risk of condensation through the turbine several constraints should be set for the pressure and temperature[Skogestad, 2009, p. 194].

    $Pt, hp \leq 4.0406$ bar and $Tt, hp \geq 144$ °C out of the high-pressure turbine.

    $Pt, lp \leq 0.096$ bar and $Tt, hp \geq 45$ °C out the low-pressure turbine (into the condenser) to increase power output and to prevent corrosion, respectively.

6. A constraint of $T_r > 478.54$ °C into the low-pressure turbine is set to prevent corrosion and to increase power output.

7. Drum holdup, M_d, should be controlled for safety reasons.

8. Water, steam and flue gas flows are limited by a lower bound of 0 kgs^{-1}.

5.2.2 Step S2: Manipulated variables and degrees of freedom

From Figure 4.1 seven manipulated variables can be established and are rendered in Table 5.1. The nominal values for the inputs are listed in Table A.5 in Appendix A.3.

Table 5.1: Inputs to the modelled Heat-to-Power cycle

Input	Description
N	Rotational speed in the pump
$\dot{m}_{eco,b}$	Bypass stream around the economizer into the mixer
$\dot{m}_{a,b}$	Bypass stream into the attemperator
$\dot{m}_{FG}$	Flue gas flow in the heat exchanger at the boiler
$\dot{m}_{FG,r}$	Flue gas flow in the heat exchanger at the reheater
$\dot{Q}_c$	Heat flow in the condenser
z_t	Valve position at the valve at the turbine inlet

The first step in determining the steady state degrees of freedom is to subtract the controlled or manipulated variables that do not have any steady state effect. From the constraints, it is clear that the drum holdup, M_d, is required to be controlled for safe operation, but does not have an effect on the other states in the simulation when the process has reached steady state. This gives one CV with no steady state effect (N_{0y} = 1). The steady-state degrees of freedom N_{ss} is then computed from Equation 3.3 as

$$N_{ss} = N_m - (N_{0m} + N_{0y}) \tag{5.3}$$
$$N_{ss} = 7 - 0 - 1 \tag{5.4}$$
$$N_{ss} = 6 \tag{5.5}$$

Inputs that can cause a disturbance in the system are called disturbance variables (DV). In the modelled Heat-to-Power cycle only one disturbance is considered, which is the power setpoint, W_s. This is because the plants' main objective is to contribute to grid frequency regulation, which sets the setpoint of the power output.

5.2.3 Step S3: Primary controlled variables

In Table 4.3 over 27 states are listed. Now that M_d is required to be controlled for safety purposes, there are 26 states, with 6 degrees of freedom left. The constraints listed in Section 5.2.1 that might become active during the simulation should be chosen first, such as the power, W, and the superheater temperature, T_a. The reheater temperature, T_r should also be controlled for the same reasons as for T_a, which is to minimize the chances of the steam condensing through the turbines as well as not reaching above maximum temperature limitations.

The pressure out of the high and low-pressure turbine is assumed constant in the simulation. In cases of increased enthalpy in the system, this will be translated into increased temperatures out of the turbines. Thus the temperature out of the condenser, T_c should be considered a primary controlled variable. Likewise, the temperature out of the heat exchanger is expected to quickly

reach its constraint and is considered a primary controlled variable.

The five identified primary controlled variables for the heat-to-power cycle are:

1. W - power production [MW]

2. T_a - steam temperature at the high pressure turbine inlet [K]

3. T_r - Temperature of the steam at the low pressure turbine inlet [K]

4. T_c - exhaust temperature out of the turbine [K]

5. $T_{FG,eco}$ - Outlet temperature of the flue gas after the heat exchanger in the boiler [K]

With five primary controlled variables, one degree of freedom is left, which can be used either for self-optimizing control, to control other variables, such as the saturation pressure, P_d, or with another MV to improve the control of the primary controlled variables.

5.2.4 Step S4: Production rate

As mentioned in Section 2.1, there exist two common options for control objectives in Heat-to-Power cycles: energy efficiency and grid frequency regulation. For high energy efficiency, the throughput manipulator (TPM) should be set at the fuel as this can be considered the bottleneck of the system. The modelled Heat-to-Power cycle, in this case, has to obtain fast and tight power control as the power is connected to the frequency grid. The TPM is, therefore, the power setpoint as it defines the production rate of the system and all the other variables should be controlled around the bottleneck caused by the grid.

5.3 Bottom-up

In this section, the bottom-up part of the plantwide procedure is completed by first building the regulatory layer in step 5 based on the analysis done in the top-down part, then improving the control structure with regards to its supervisory control layer in step 6.

5.3.1 Step S5: Regulatory control layer

SISO PID controllers were implemented in the regulatory layer of the process to ensure stable operation. The identified MV-CV pairings and their type of PID-controller are listed in Table 5.2 below. The selection of the type of PID-controller is made from a comparison of the process transfer functions derived in Appendix A.5 and the open loop input step responses based on the theory mentioned in Section 3.2.1 and might change during the sequential tuning. The pairings are based on the pair close rule, engineering logic and literature [Wu et al., 2015, p.5].

Table 5.2: List of possible controller pairings

MV	CV	PID-controller
N	M_d	P
$\dot{m}_{eco,b}$	T_{FGeco}	I
$\dot{m}_{a,b}$	T_a	PI
$\dot{m}_{FGr}$	T_r	I
$\dot{Q}_c$	T_c	PI
z_t	P_d or W	PI
$\dot{m}_{FG}$	P_d or W	PI

The latter two controllers are designated for the pressure and power control which has three possible pairing options: the boiler-driven, turbine-driven and floating pressure control structures described in Section 3.3. The implemented control structures are illustrated in Figure 5.1.

(a) Boiler-driven   **(b)** Turbine-driven   **(c)** Floating pressure
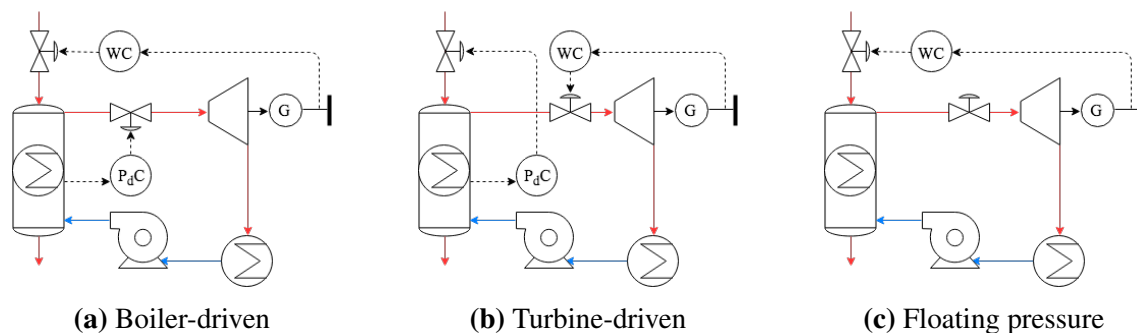
Figure 5.1: The Heat-to-Power cycle control structures

5.3.1.1 Advanced control structures

Two advanced PID-controllers were implemented in addition, utilizing the two degrees of freedom, flue gas flow and valve position, with the main objective to control the power: parallel power control and valve position control.

The parallel power and valve position control structures are illustrated in Figure 5.2.

(a) Parallel power control   (b) Valve position control
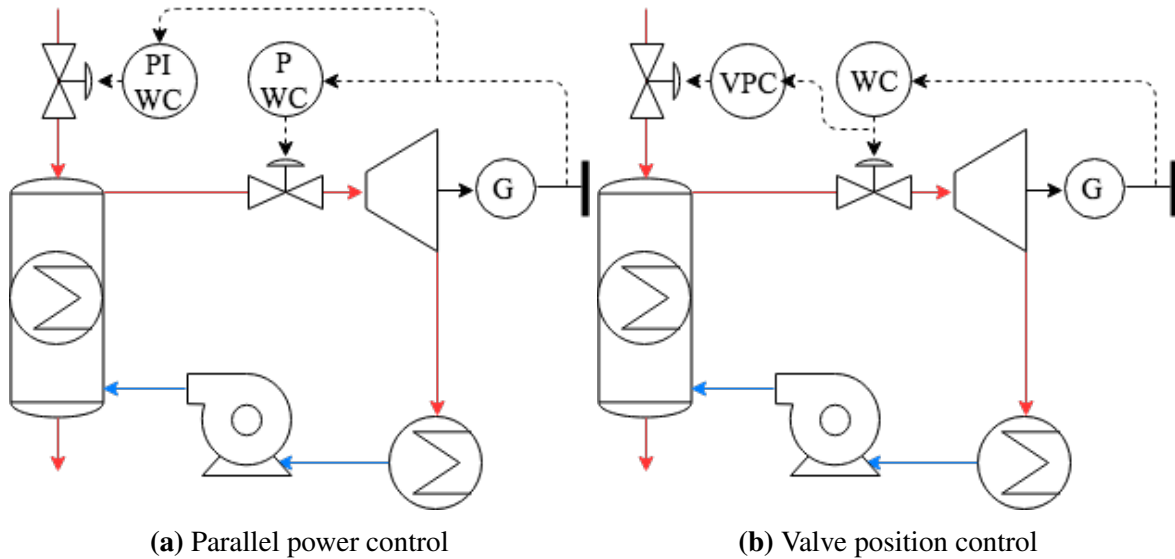
Figure 5.2: The advanced control structures implemented for the Heat-to-Power cycle.

In the case of a Heat-to-Power cycle, a parallel controller can obtain the fast power control by manipulating the valve position for small periods of time, similar to the turbine-driven control structure, whilst the large range power control is achieved by the flue gas. This links the power and flue gas together, allowing for utilization of the boiler storage, similar to what is experienced in the boiler-driven control structure. The fast power control is done through manipulating the valve position, implemented as a P-controller. The slow power control was done through the flue gas flow, implemented as a PI-controller.

The valve position controller (VPC) was added for the turbine-driven control structure to handle saturation of the valve position and thus increase the range of control (maximize throughput). In the turbine-driven control structure, the power output is paired with the valve position before the turbine, z_t. Thus by letting the saturation pressure float, the flue gas flow, $\dot{m}_{FG}$ can be paired with the valve position to bring it back to its setpoint, $z_{ts} = 0.9$. Both the power and valve position controller were implemented as PI-controllers. A block diagram of the valve position controller is shown in Figure 5.2b.
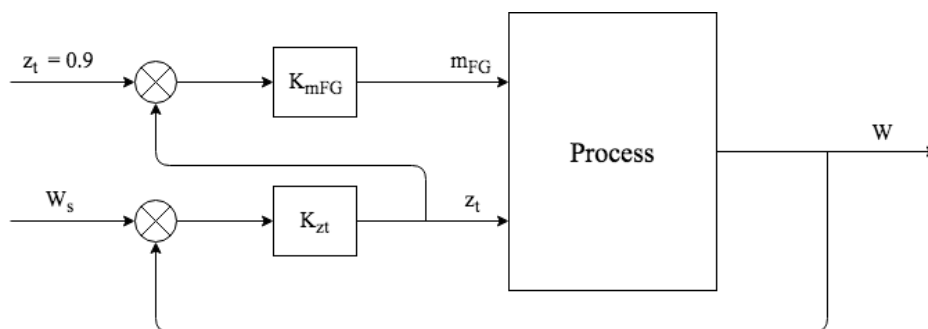
Figure 5.3: A block diagram of the implemented valve position controller.

5.3.1.2 Saturation and anti-windup

In order to set realistic values for the simulation, saturation blocks were implemented for the manipulated variables. The saturation ranges set for the manipulated variables in this simulation are listed in Table 5.3.

Table 5.3: Saturation ranges for the manipulated variables

Manipulated variable (MV)	Minimum value	Maximum value	Unit
$\dot{m}_d$	0	-*	kgs^{-1}
$\dot{m}_{eco,b}$	0	$\dot{m}_d$	kgs^{-1}
$\dot{m}_{a,b}$	0	-*	kgs^{-1}
z_t	0	1	-
$\dot{m}FGr$	0	-*	kgs^{-1}
$\dot{m}_{FG}$	0	-*	kgs^{-1}
$\dot{Q}_c$	-*	-*	Js^{-1}

  * This limitation value is large relative to the other limitation values, and was set as infinity in the simulation.

If controller pairing contains integral action, a saturation in its manipulated variable will cause the integral term in the controller to build up. In order to limit the integral windup, anti-windup has to be implemented for the controllers that contain integral action. In Simulink, this can be implemented directly into the PID-controller block by setting controller output saturation ranges. The respective output saturation ranges are listed in Table 5.4.

Table 5.4: Saturation ranges for the controller outputs

Controller	Minimum value	Maximum value	Unit
M_d	-5.9750	-*	kgs^{-1}
$T_{FG,eco}$	-0.5	5.9750	kgs^{-1}
T_a	-0.31	-*	kgs^{-1}
$P_{d,BD}$	-0.9	0.1	-
W_{TD}	-0.9	0.1	-
T_r	-5	-*	kgs^{-1}
$P_{d,TD}$	-20	-*	kgs^{-1}
W_{BD}	-20	-*	kgs^{-1}
W_{FP}	-20	-*	kgs^{-1}
T_c	-*	-*	kgs^{-1}

  * This limitation value is large relative to the other limitation values, and was set as infinity in the simulation.

Anti-windup was not implemented for the T_c-controller as the input, in this case, can be considered to be unlimited. For the rest of the temperature, pressure and power controllers, clamping anti-windup was implemented.
The back-calculation anti-windup was tested for the power controller in the turbine-driven and valve position control structure to compare the performance of the two anti-windup methods during saturation of the valve position.

The back-calculation coefficient is set as the integral action of the PI-controller which from Equation 3.5 in Section 3.2.1 results in a back-calculation coefficient, K_b, as seen in Equation 5.6 [The MathWorks Inc, 2019a] [Åström, 2002, p.230].

$$K_b = \frac{K_c T_t}{\tau_I} \tag{5.6}$$

where K_c is the controller gain and τ_I is the integral time constant as defined in Section 3.2.1. T_t is the tracking time constant and is set to be smaller than the integral time constant τ_I for the respective power controller [Åström, 2002, p.230].

5.3.2 Step S6: Supervisory control layer

A decentralized control design was chosen for the Heat-to-Power cycle as it is desired to study how simple PID-controllers can be used to handle a coupled system, such as the simulated Heat-to-Power cycle.

Both sequential and independent design approaches were tested on all of the control structures and a 1% setpoint decrease in power was made to compare the control structures on the basis of settling time for the power control.
In the sequential control procedure, each control loop is closed before tuning the next controller. Thus, it is of great importance to obtain a correct tuning order for the controllers. In [Skogestad and Morari, 1989, p. 120] it is recommended to tune the fastest control loops first. A measure of the speed of the loops is the effective delay, θ. Since the modelled Heat-to-Power cycle does not include delays, the effective delays cannot be used as a measure.
τ_1 is found for a controller pairing from an open loop input step response as the time it takes for the output to reach 63% of its steady state value. Thus, τ_1 can be used to decide the sequence order, leading to the τ_1-sequential controller tuning procedure. The closed loop time constant τ_c should ideally be the same or slower than the open loop time constant, τ_1. A secondary sequence, called the τ_c-sequential controller tuning procedure, was tested based on the closed loop time constant, τ_c.

5.4 Approximation of τ_1 in cases of no process gain

For open loop responses where the output goes back to its initial value, the other controllers in the cycle or the cycle in itself are rejecting the disturbance caused by the input step. This leads to a steady state process gain of approximately zero, making it difficult to tune a PI controller from the steady state response. In these cases, it can either be assumed that the variable is self-regulating or that the controlled variable is insensitive to the manipulated variable and can only be used for small control ranges. In the latter case, the SIMC tuning rules are applied to the initial response of the controlled variable, not the steady state response. An example of such a response is shown in Figure 5.4 below.
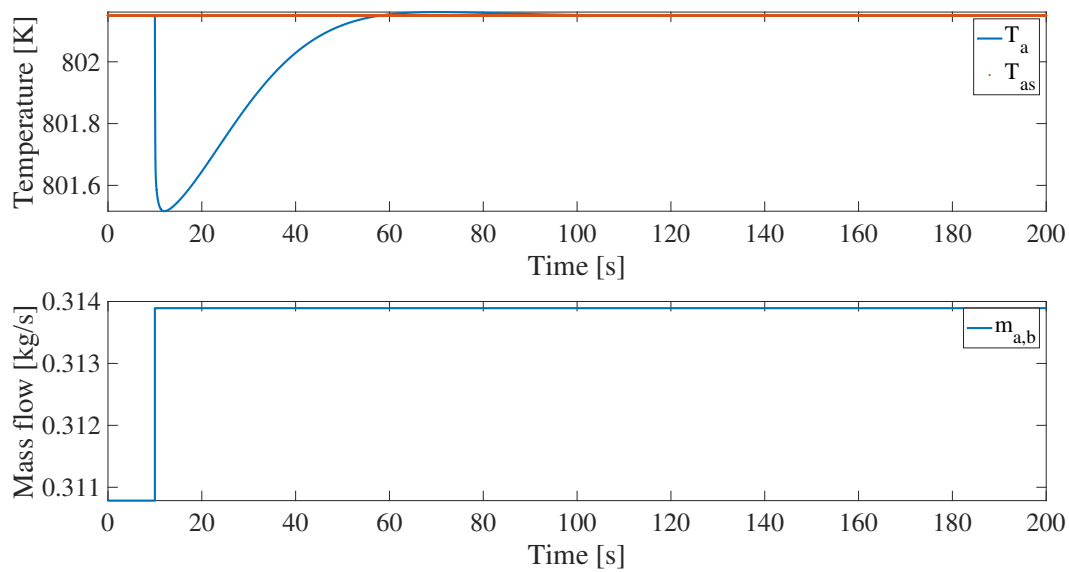
Figure 5.4: A plot of an input step response with no steady state process gain.

54

Chapter 6

Results

The aim of the thesis is to study decentralized control on a Heat-to-Power cycle. In order to implement the decentralized controllers in the best possible manner, both independent and sequential controller tuning was implemented for the boiler-driven, turbine-driven and the floating pressure control structure to see which controller tuning method that should be recommended. Two advanced control structures were implemented: parallel power control and valve position control. The control structures utilized two manipulated variables, the flue gas flow ($\dot{m}_{FG}$) and the valve position (z_t), to control the power output in parallel or cascade. The valve position controller was implemented for the turbine-driven control structure in order to increase the range of power control. The regulatory control structures were compared with regards to their ability to control the power after a step decrease of 1% in the power setpoint. Settling time, degree of overshoot and undershoot, as well as the quality of the response curve are studied.

6.1 Obtaining the τ_1 and τ_c sequence

When determining the controller sequence, the effective time delay should be used as a measure of the speed for each loop. Since the modelled Heat-to-Power cycle does not include delays, the effective delays cannot be used as a measure. Therefore τ_1 and τ_c are chosen as a basis for the order in the tuning sequences.

In the independent tuning process, both open loop and closed loop step responses are performed for each controller in the Heat-to-Power cycle. The τ_1- and τ_c-sequence are designed with regards to the τ_1s and τ_cs obtained from the independent tunings in each control structure. The first controller to be tuned in a sequence is the fastest loop, thus, the loop with the lowest value of τ_1 or τ_c for the τ_1 and τ_c-sequence, respectively. The control loop is closed before the second fastest controller is tuned. The last control loop to be tuned is therefore the loop with the highest value of τ_1 or τ_c, for the τ_1 and τ_c-sequence, respectively.

The drum holdup and temperature controllers are paired with the same respective inputs in all of the five control structures. The parameters and controller tunings are assumed to be the same in the control structures for the independent controller tuning. The latter two degrees of freedom are paired differently with regards to the five control structures, leading to different values for τ_1 and τ_c from the independent controller tunings.

6.2 Controller pairings for the different control structures

The implementation of the drum holdup, M_dC, and temperature TC controllers are the same for all five control structures. The CV-MV pairing and the respective process gain (k) units are listed in Table 6.1. The pairings are illustrated by a process flow diagram in Figure 6.1.
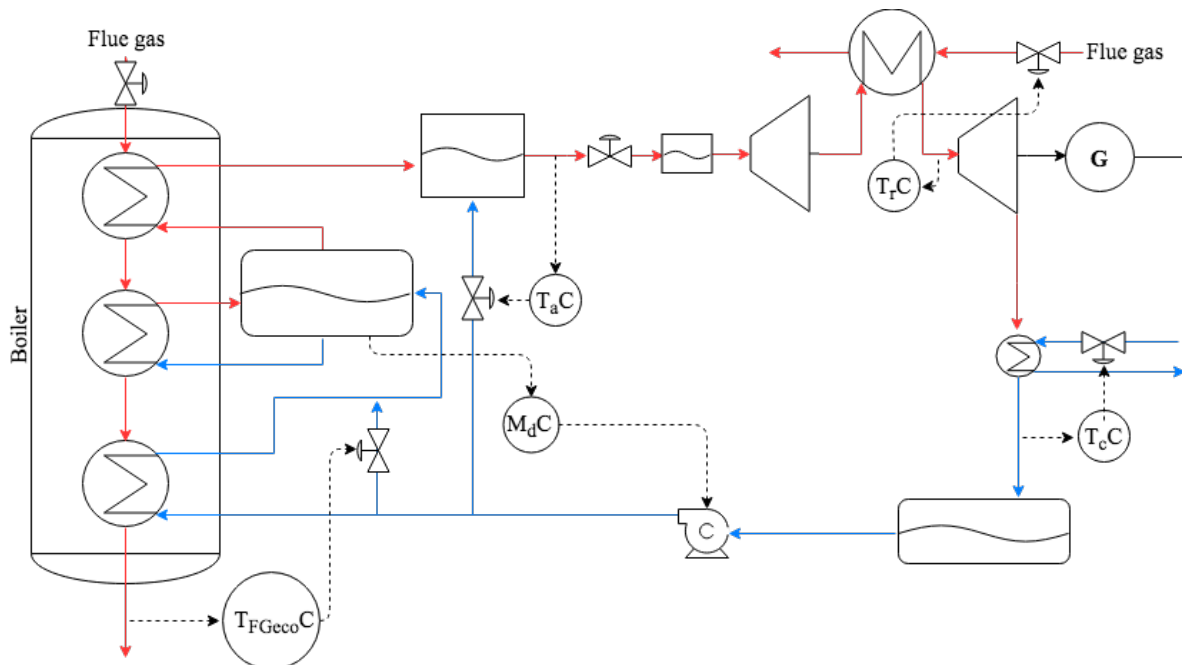
Figure 6.1: A process flow diagram of the Heat-to-Power cycle with the drum holdup and temperature controllers.

Table 6.1: Controller pairings and process gain (k) units for the drum holdup and temperature controllers in the Heat-to-Power cycle

CV	MV	k unit
M_d	N	10^{-2}kg rad^{-1}s
$T_{FG,eco}$	$\dot{m}_{eco,b}$	10^{-2}Kkg^{-1}s
T_a	$\dot{m}_{a,b}$	10^{-2}K kg^{-1}s
T_r	$\dot{m}_{FG,r}$	10^{-2} Kkg^{-1}s
T_c	$\dot{Q}_c$	10^{-2}KJ^{-1}s

The pairings with the flue gas flow, $\dot{m}_{FG}$, and valve position, z_t, in the boiler-driven, turbine-driven, floating pressure, parallel power and valve position control structure, as well as the general process gain (k) units, are listed in Table 6.2.

Table 6.2: Controller pairings and process gain (k) units for the boiler-driven, turbine-driven, floating pressure, parallel power and valve position control structures

Control structure	CV	MV	k unit
Boiler-driven	P_d	z_t	10^{-6}Pa
	W	$\dot{m}_{FG}$	10^{-6}Wkg^{-1}s
Turbine-driven	P_d	$\dot{m}_{FG}$	10^{-6}Pakg^{-1}s
	W	z_t	10^{-6}W
Floating pressure	W	$\dot{m}_{FG}$	10^{-6}Wkg^{-1}s
Parallel power	W	z_t	10^{-6}W
	W	$\dot{m}_{FG}$	10^{-6}Wkg^{-1}s
Valve position controller	W	z_t	10^{-6}W
	z_t	$\dot{m}_{FG}$	kg^{-1}s

6.3 Decentralized independent controller tuning

The open loop input step responses and the closed loop setpoint responses for the boiler and turbine-driven control structures are plotted in Appendix A.6 and A.7, respectively. The resulting independent controller tunings are listed in Table 6.3 for the boiler-driven (BD) and turbine-driven (TD) control structure. Since the floating pressure control structure is similar to the boiler-driven control structure it is assumed to have the same independent controller tunings.

Table 6.3: Decentralized independent controller tunings.

Controller	k	τ_1 [s]	θ [s]	τ_c [s]	PID
M_d	0.0210	∞	0	1.0000	P
$T_{FG,eco}$	0.1228	8.5860e-4	0	0.0350	I
T_a	-2.2222	0.0895	0	1.3425	PI
T_r	0.3210	0	0	0.0250	I
T_c	4.2489e-7	0.8848	0	1.3272	PI
$P_{d,BD}$	-0.4900	0.0022	0	3.0000	PI
$P_{d,TD}$	0.3886	0.7167	0	1.5990	PI
W_{BD}	-0.3646	0.6624	1.1369e-13	1.6000	PI
W_{TD}	-0.0962	0.0038	0.1396	30.000	PI

6.3.1 Inverse response in power output

The open loop step response in the valve position caused the power output to settle towards zero process gain as seen in Figure 6.2, indicating a low steady-state effect on the power from the valve position. In order to tune a power controller, the power controller was tuned at the initial response. The resulting independent closed loop setpoint response in power is shown in Figure 6.3 for the power output and valve position.
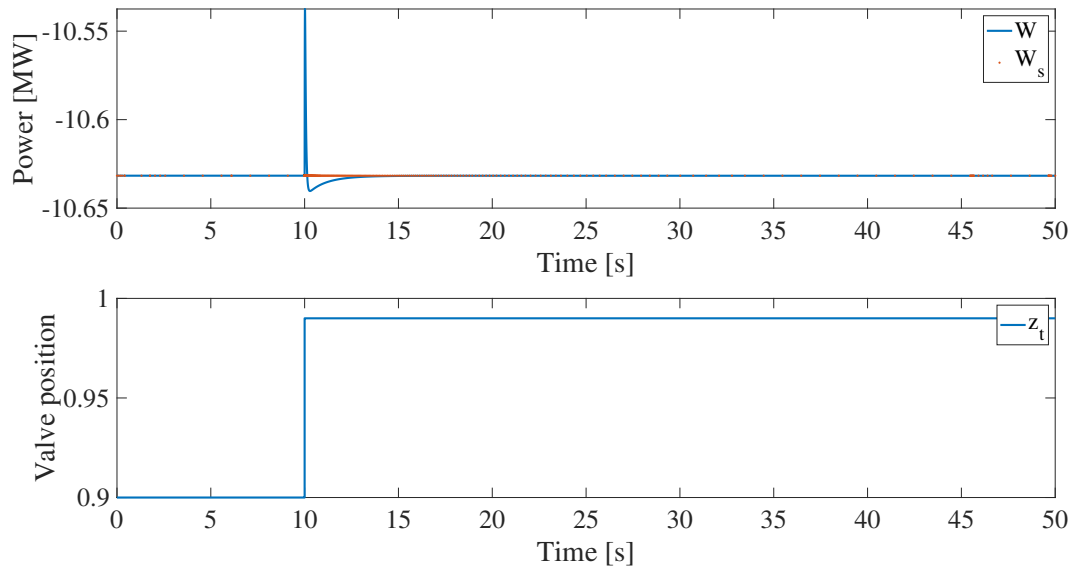
Figure 6.2: Plot of W and z_t after a 10 % open loop step response in z_t.
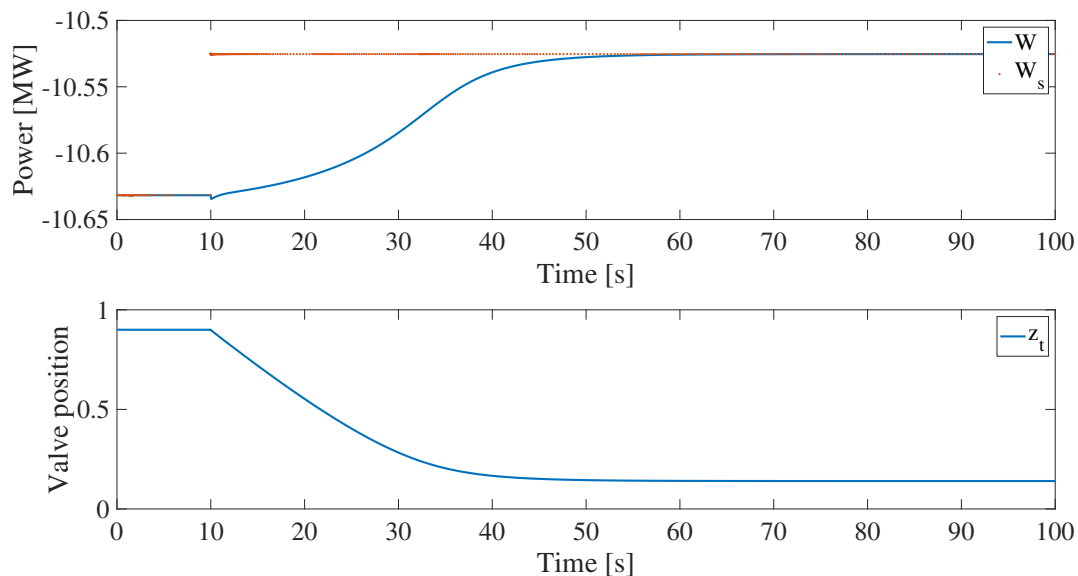
Figure 6.3: Plot of the power, W, and the valve position, z_t after a 1% step decrease in W_s with M_dC and WC active, $\tau_c = 30$s.

A plot of the drum pressure, P_d, attemperator pressure, P_a, turbine inlet pressure, $P_{t,in}$, from the same setpoint change is shown in Figure 6.4.
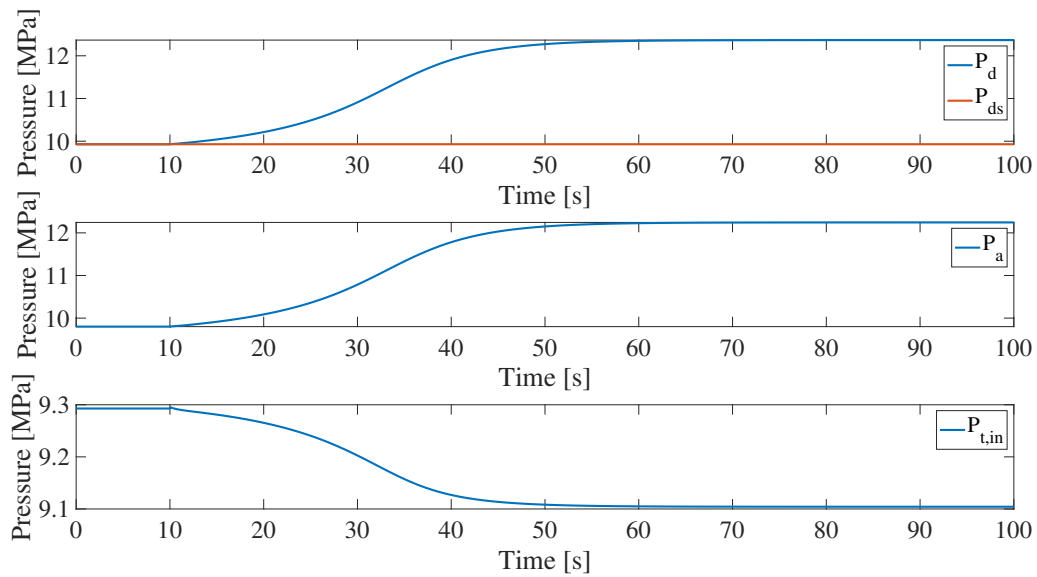
Figure 6.4: Plot of the valve position and the drum, attemperator and turbine inlet pressure after a 1% step decrease in W_s with only M_dC and WC active, τ_c = 30s.

To illustrate the control limitations in the power, a plot with τ_c = 20 was made of a 1 % step decrease in the power setpoint shown in Figure 6.5
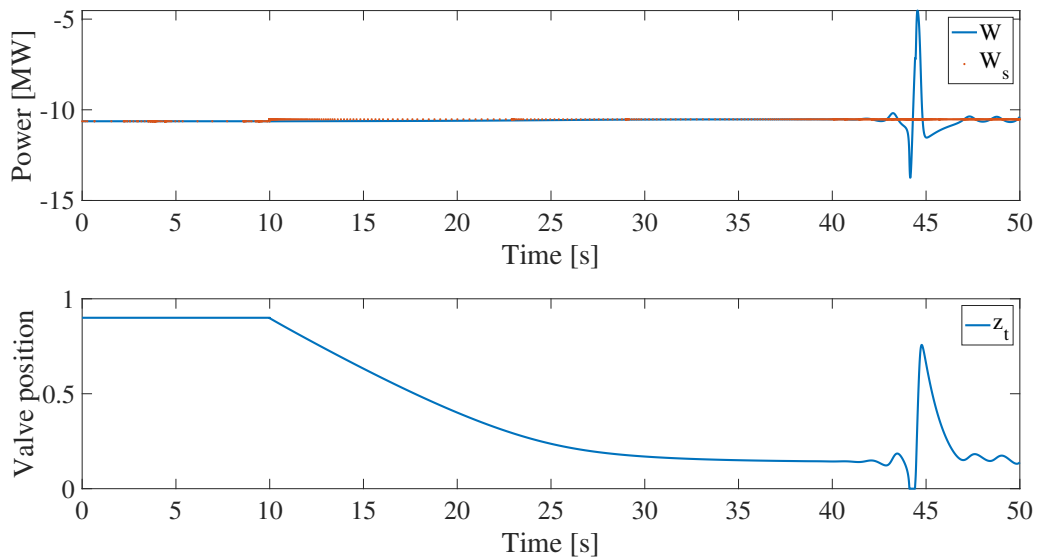
Figure 6.5: Plot of the power, W, and the valve position, z_t after a 1% step decrease in W_s with M_dC and WC active, τ_c = 20s.

6.3.2 1% step decrease in the power setpoint

All control loops were closed and a 1% step decrease in the power setpoint, W_s was made for the independently tuned boiler-driven (BD), turbine-driven (TD), and floating pressure (FP) control structures, shown in Figure 6.6.
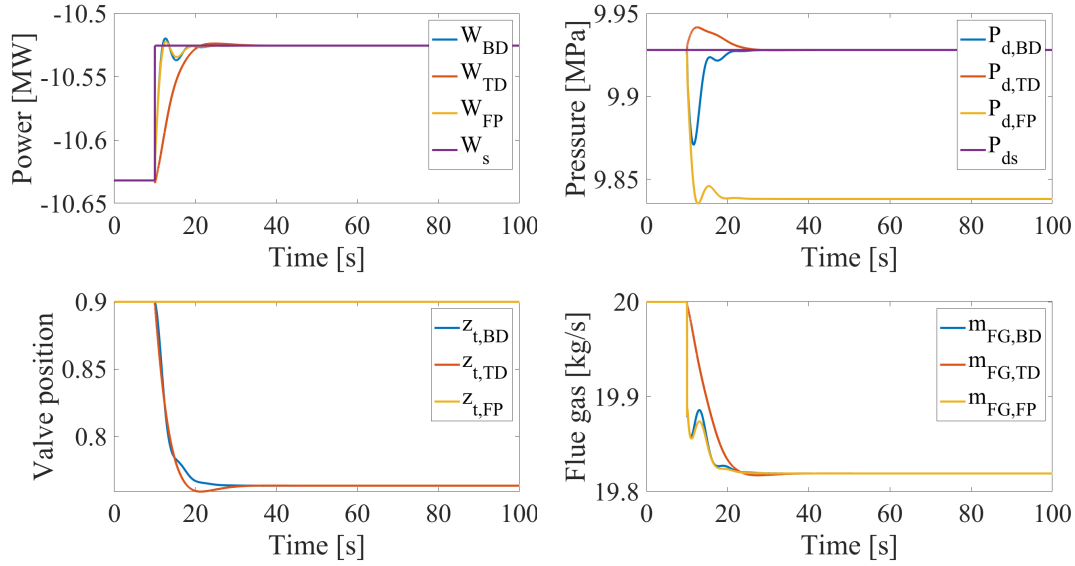
Figure 6.6: Plot of W, P_d, $\dot{m}_{FG}$ and z_t for the three control structures after a 1% closed loop setpoint decrease in W_s.

6.4 Decentralized τ_1 - sequential controller tuning

From the previous section, the open loop constants, τ_1 for each controller was determined, leading to the tuning order described in Table 6.4a, 6.4b and 6.4c for the boiler-driven, turbine-driven and floating pressure control structure, respectively. The drum holdup controller has an integrating response, meaning that τ_1 is large. In order to maintain stability in the system, this controller is required to be closed before tuning the other controllers. As it is the first controller to be tuned in the sequence, the tunings for the M_d-controller is the same as the independent control tunings listed in Table 6.3.

Table 6.4: Independent τ_1-based tuning sequences for the control structures.

(a) Boiler-driven

Controller	τ_1 [s]
T_r	0
$T_{FG,eco}$	8.5862e-4
P_d	0.0022
T_a	0.0895
W	0.6624
T_c	0.8848

(b) Turbine-driven

Controller	τ_1 [s]
T_r	0
$T_{FG,eco}$	8.5862e-4
W	0.0038
T_a	0.0895
P_d	0.7167
T_c	0.8048

(c) Floating pressure

Controller	τ_1 [s]
T_r	0
$T_{FG,eco}$	8.5862e-4
T_a	0.0895
W	0.6624
T_c	0.8848

The controllers for the the boiler-driven, turbine-driven and floating pressure control structures were tuned again in the τ_1 - sequence. This leads to different values for the process gain (k), τ_1 and τ_c for the respective controllers. The open loop input step responses and the closed loop setpoint changes are plotted in Appendix A.8, A.9, and A.10.

6.4.1 Boiler-driven control structure

The resulting τ_1 - sequential controller tunings for the boiler-driven control structure are listed in Table 6.5 below.

Table 6.5: τ_1 - sequential controller tunings for the boiler-driven control structure.

Controller	k	τ_1 [s]	θ [s]	τ_c [s]	PID
T_r	0.3161	0	0	0.0250	I
$T_{FG,eco}$	0.0491	1.5740e-04	0	0.0350	I
P_d	-0.3151	0.0015	0	2.1111	PI
T_a	-3.4097	2.0568	0	24.9999	PI
W	-1.6280	2.1587	0	40.9900	PI
T_c	3.8061e-7	0.6729	0	180.1110	PI

6.4.2 Turbine-driven control structure

In the turbine-driven control structure, the power controller is tuned early in the sequence, leading to a very fast controller. The subsequent controller to be tuned is the attemperator temperature, T_a,-controller, which obtained a steady state process gain of approximately zero, with a response curve similar to a pure gain response as seen in Figure 6.7.
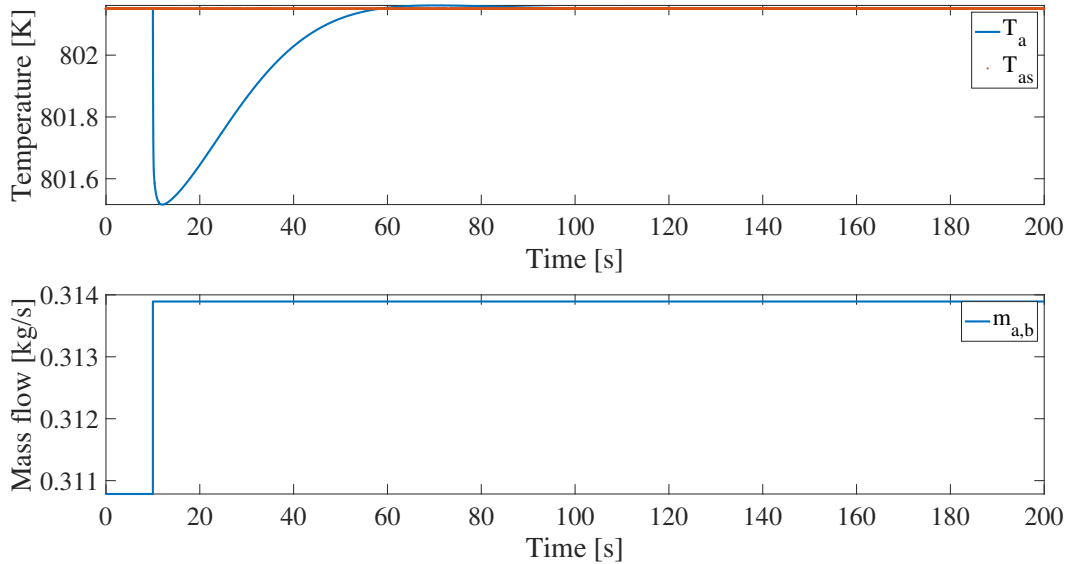
Figure 6.7: A plot of T_a and $\dot{m}_{a,b}$ after a 1% open loop step response in $\dot{m}_{a,b}$.

Two different tuning approaches can be made with regards to the T_a-controller in this case. The first is to assume that the attemperator temperature is self-regulating, such that the other control loops already closed in the cycle or the cycle itself are rejecting the disturbance caused by the input step in the attemperator bypass steam. The second approach is similar to the approach in Section 6.3.1 of tuning the controller by its initial response instead of the steady state response. This assumes that the attemperator bypass steam has a small steady state effect in the attemperator temperature, which is logical when considering the dynamic energy balance Equation 2.10 in Section 4.6.1, where a change in the enthalpy is more affected by change in the inlet superheater temperature, T_{sh}, or the much larger mass flows such as the inlet flow from the superheater, $\dot{m}_{sh}$.

6.4.2.1 Self regulating T_a

The T_a-controller was left as a self regulating variable while completing the tuning of the latter controllers in the sequence: P_dC and T_cC.

First an open loop step response of $\dot{m}_{FG}$ was made in order to tune the P_d-controller, shown in Figure 6.8. The P_d-controller was then verified through a closed loop setpoint response, shown in Figure 6.9
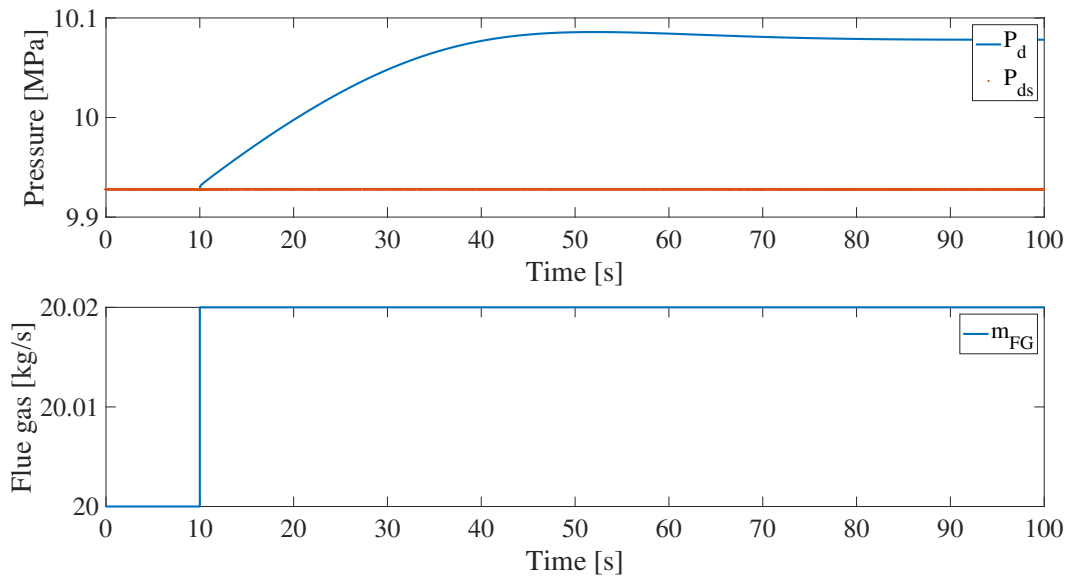
Figure 6.8: A plot of P_d and $\dot{m}_{FG}$ after a 0.1% open loop step response in $\dot{m}_{FG}$.
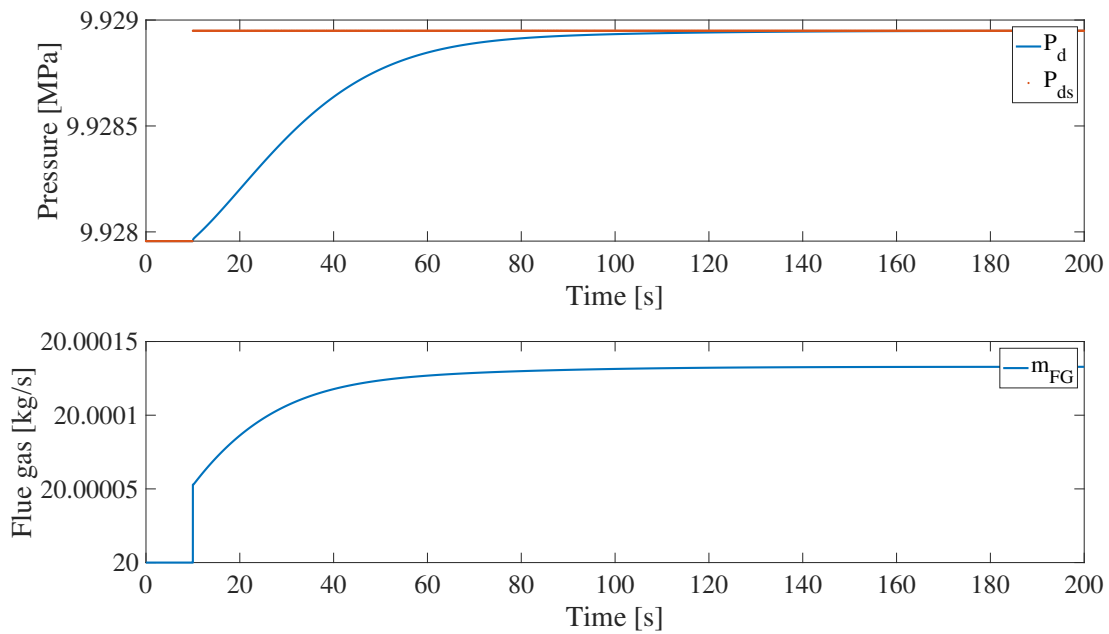
Figure 6.9: A plot of P_d and $\dot{m}_{FG}$ after a 0.01% closed loop setpoint step increase in P_{ds}.

The last controller to be tuned in the τ_1-sequence of the turbine-driven control structure is the condenser temperature, T_c. The open loop step response in $\dot{Q}_c$ showed undampened osciallting behaviour of T_c, seen in Figure 6.10. It was still possible to tune a satisfactory controller as seen by the closed loop setpoint response of T_{cs} in Figure 6.11
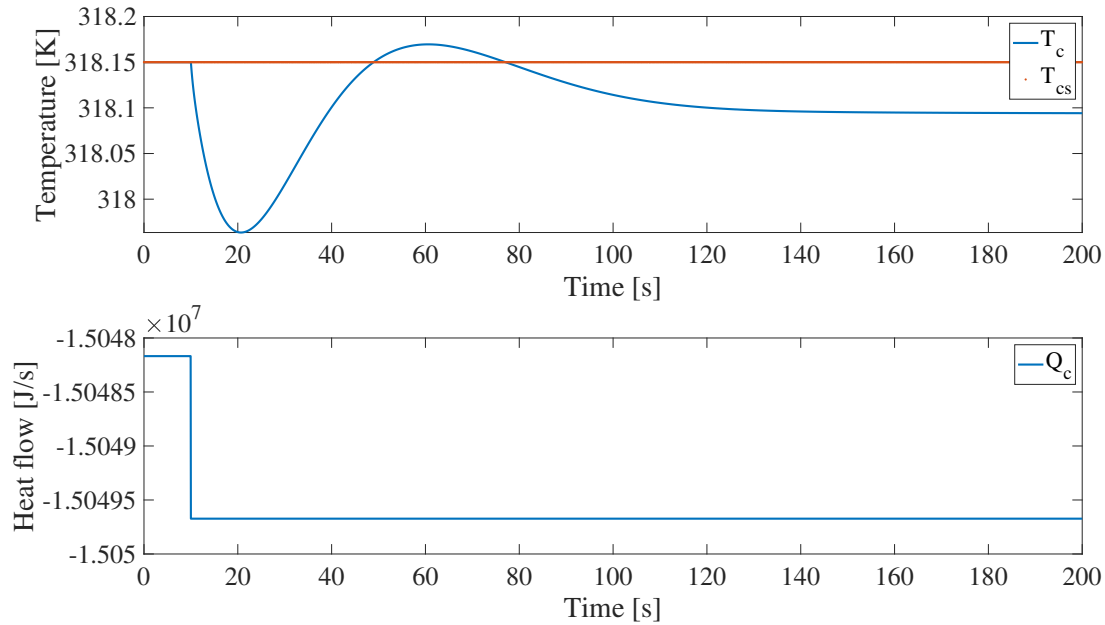
Figure 6.10: A plot of T_c and $\dot{Q}_c$ after a 0.01% open loop step response in $\dot{Q}_c$.
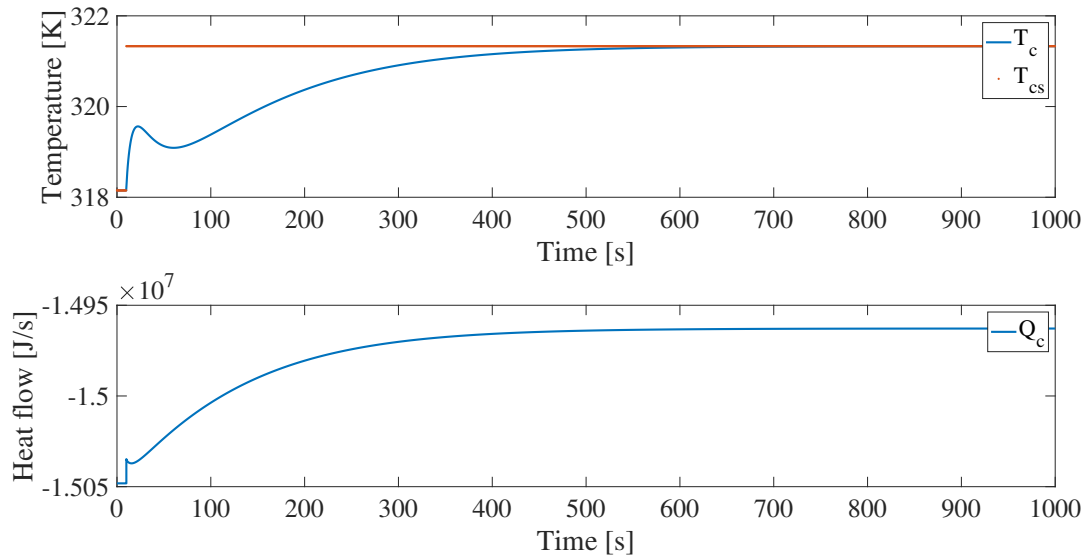
Figure 6.11: A plot of P_d and $\dot{m}_{FG}$ after a 1% closed loop setpoint step increase in T_{cs}.

In order to check if T_a has remained a self regulating variable, a 1% step decrease in the power setpoint, W_s, was made after the completion of the sequential tuning, shown in Figure 6.12. It is clear that T_a is not a self-regulating variable after the completion of the sequential tuning as it does not reach its setpoint after the disturbance in W_s.
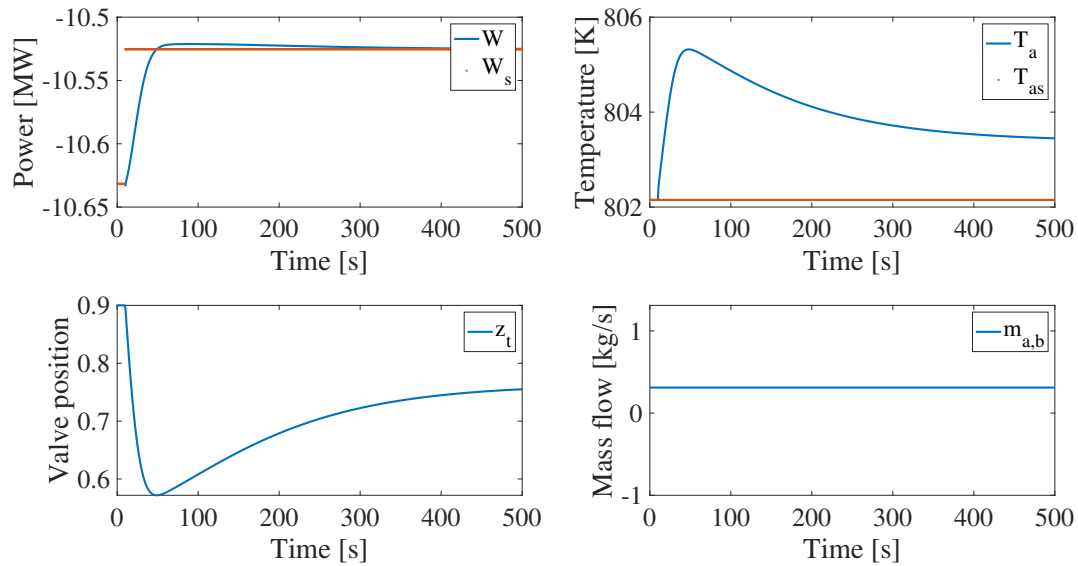
Figure 6.12: Plot of the power, W, valve position, z_t, attemperator temperature, T_a and bypass flow, $\dot{m}_{a,b}$ after a 1% step decrease in W_s

The τ_1-sequential controller tunings from the self-regulating approach are listed in Table 6.6

Table 6.6: τ_1 - sequential controller tunings for the turbine-driven control structure assuming T_a is self regulating.

Controller	k	τ_1 [s]	θ [s]	τ_c [s]	PID
T_r	0.3161	0	0	0.0250	I
$T_{FG,eco}$	0.0491	1.5740e-4	0	0.0350	I
W	-0.2528	0.0129	0.1164	19.9990	PI
T_a		Self regulating			
P_d	7.5019	14.4974	0	2.5000	PI
T_c	1.2393e-6	21.8778	0	42.000	PI

6.4.2.2 Tuning of T_a at initial response

The T_a-controller was tuned from the initial response in Figure 6.7. The resulting controller was tested through a 0.01% step increase in T_{as}, shown in Figure 6.13. The strange response in $\dot{m}_{a,b}$ is caused by the saturation of the economizer bypass flow, which has not been experienced in other, much larger, setpoint changes in T_{as}. An explanation for this can be that since T_a, in this case, has a low sensitivity to $\dot{m}_{a,b}$, a small setpoint change in T_a requires a large initial response in $\dot{m}_{a,b}$, saturating other streams. T_a is not required to meet a change in its setpoint, only to be kept at its setpoint. Thus, a 1% decrease in power setpoint is made to verify the T_a controller at the end of the sequential tuning, shown in Figure 6.14.
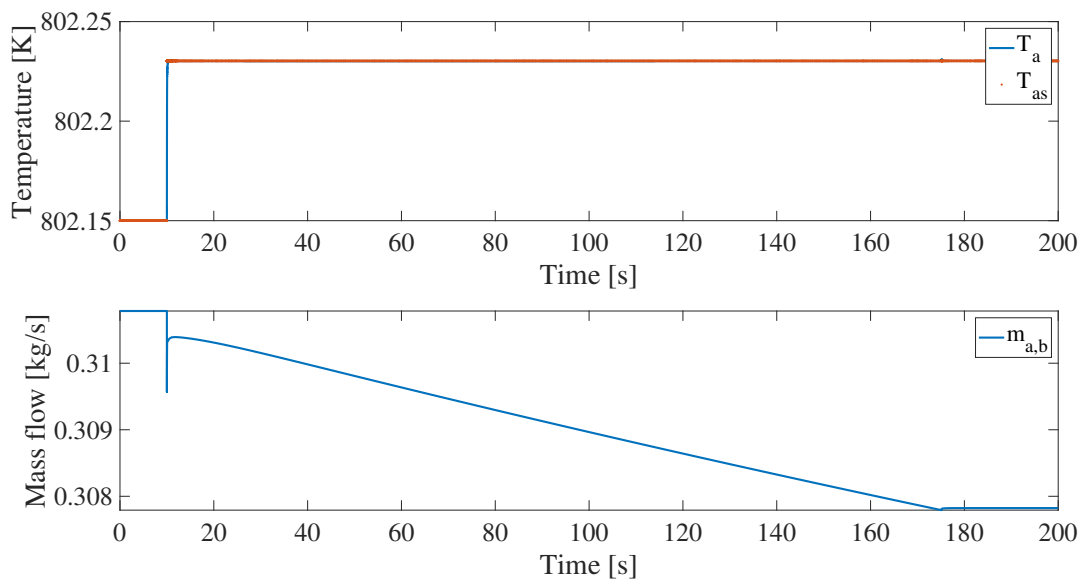
Figure 6.13: A plot of T_a and $\dot{m}_{a,b}$ after a 0.01% closed loop change in T_{as}.
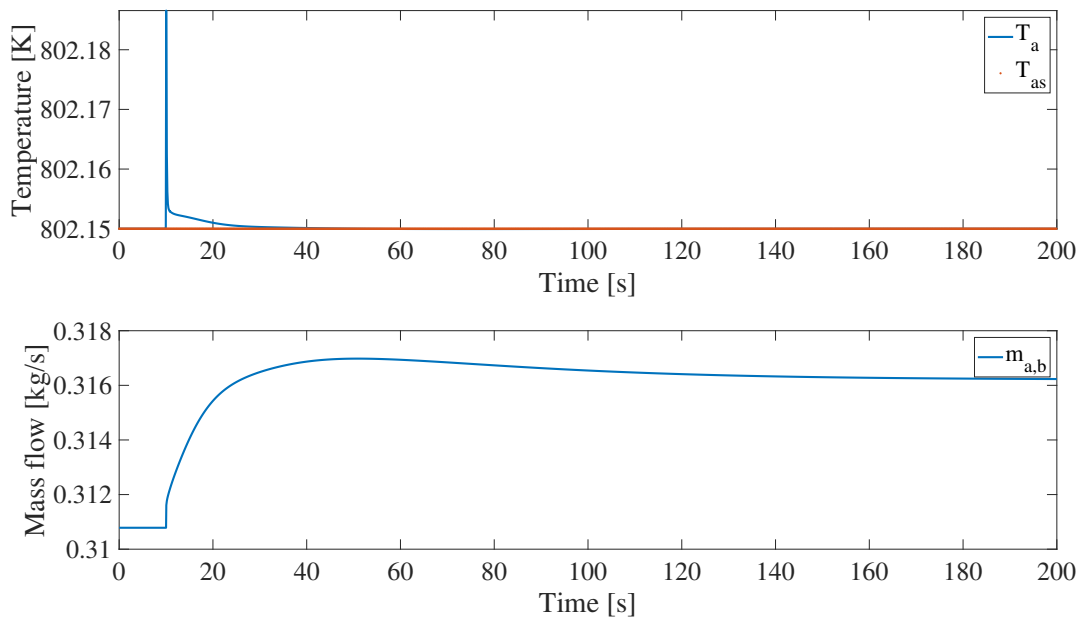
Figure 6.14: A plot of T_a and $\dot{m}_{a,b}$ after a 1% setpoint decrease in the power.

The sequential tuning also encountered another abnormal response in the next controller tuning of the τ_1-sequence, the saturation pressure, P_d-controller. The expected response for this controller is a first order steady state response, as can be seen from its independent open loop step response in Figure 6.15.
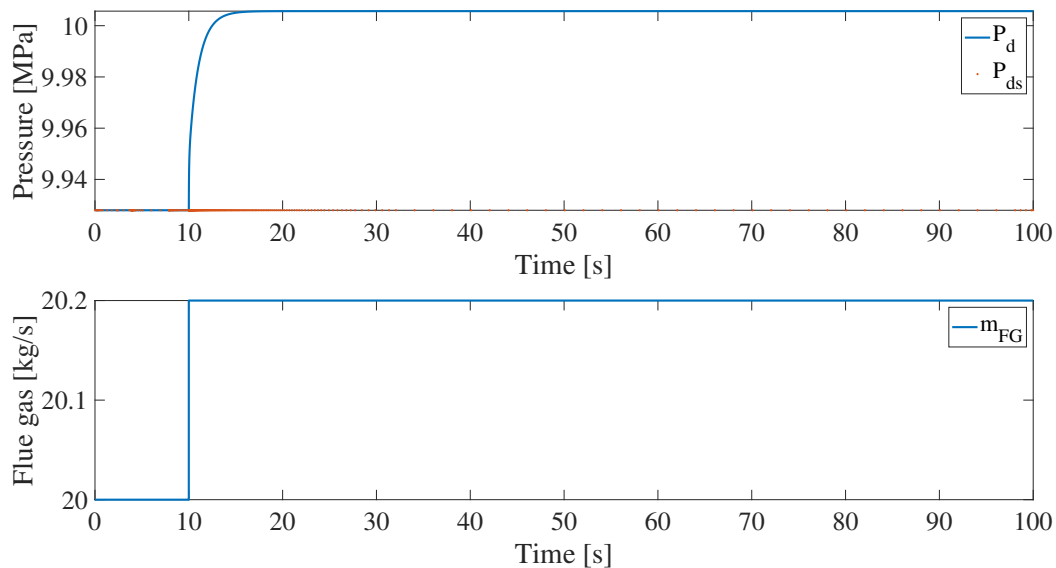
Figure 6.15: A plot of T_a and $\dot{m}_{FG}$ after a 1% step in $\dot{m}_{FG}$ from the decentralized independent controller tuning.

The open loop input step response of the flue gas flow, $\dot{m}_{FG}$, from the sequential tuning resulted instead in an integrating response as seen in Figure 6.16. This is most likely caused by the

previously tuned T_a-controller, as the open loop step in $\dot{m}_{FG}$ when assuming T_a to be self-regulating in Figure 6.8 in Section 6.4.2.1 gave a first order steady state response in P_d.
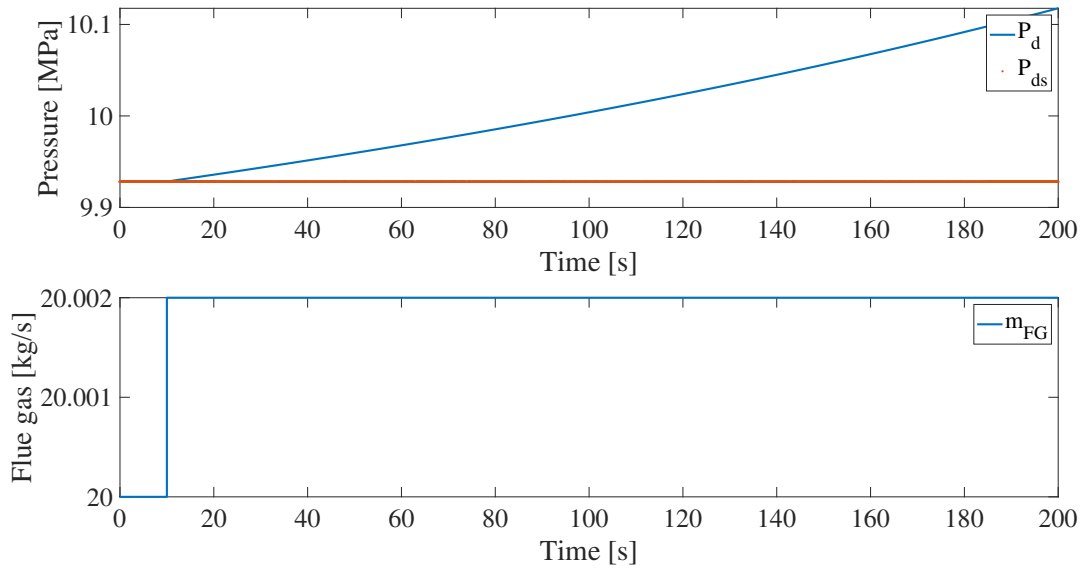
Figure 6.16: A plot of P_d and $\dot{m}_{FG}$ after a 0.1% open loop step response in $\dot{m}_{FG}$.

An integrating response leads to a high or infinite open loop constant. The SIMC tuning rules for integrating responses from Table 3.1 in Section 3.2.1 should therefore be applied. With τ_1 = ∞ and $\theta = 0$, the only remaining parameters when designing the PI controller is the process gain (k) and the closed loop constant, τ_c, where τ_c is the only parameter that can be varied. It is difficult to tune this controller as increasing τ_c to reduce the overshoot from the saturation pressure setpoint, P_{ds}, also reduces the integral action in the controller. The low integral action in the controller creates a controller containing mainly proportional action, making it difficult for the controller to regulate the pressure to its setpoint. A small overshoot of 0.0015% is therefore accepted as seen in Figure 6.17.
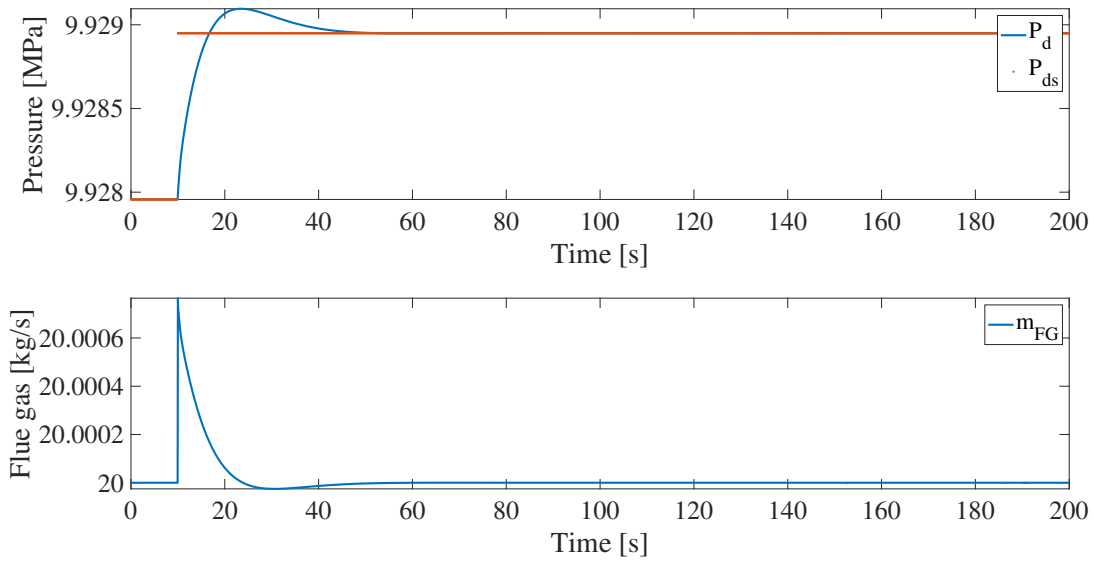
Figure 6.17: A plot of P_d and $\dot{m}_{FG}$ after a 0.001% closed loop change in P_{ds}.

The final τ_1 - sequnetial controller tunings for the turbine-driven control structure are listed in Table 6.7.

**Table 6.7:** τ_1 - sequential controller tunings for the turbine-driven control structure.

Controller	k	τ_1 [s]	θ [s]	τ_c [s]	PID
T_r	0.3161	0	0	0.0250	I
$T_{FG,eco}$	0.0491	1.5740e-4	0	0.0350	I
W	-0.2528	0.0129	0.1164	19.9990	PI
T_a	-2.0389	0.0733	0	0.0250	PI
P_d	0.4992	∞	0	2.59990	PI
T_c	3.8060e-7	0.6780	0	41.5999	PI

6.4.3 Floating pressure control structure

The floating pressure control structure is identical to the boiler-driven control structure except for having no pressure control. The removal of the pressure controller in the sequence had a lot of effect on the speed of the open loop responses and thus the tuned controllers became much faster than experienced in the boiler-driven control structure. The resulting τ_1-sequential controller tunings are listed in Table 6.8.

Table 6.8: τ_1 - sequential controller tunings for the floating pressure control structure.

Controller	k	τ_1 [s]	θ [s]	τ_c [s]
T_r	0.3161	0	0	0.0250
$T_{FG,eco}$	0.0491	1.5740e-4	0	0.0350
T_a	-2.0987	0.0842	0	5.1111
W	1.6141	12.3216	0	4.1110
T_c	3.8095e-7	0.7060	0	4.5999

6.4.4 1 % step decrease in the power setpoint

A 1% decrease in power setpoint was made for the τ_1-sequential tuned boiler-driven (BD), turbine-driven (TD) and floating pressure (FP) control structures, shown in Figure 6.18.
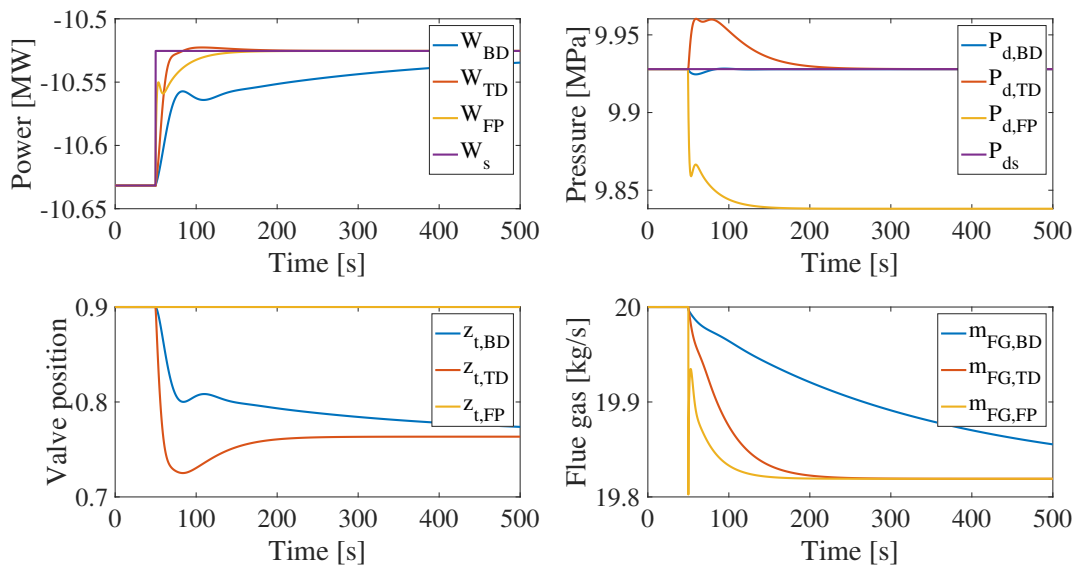
Figure 6.18: Plot of W, P_d, $\dot{m}_{FG}$ and z_t for the three control structures after a 1% closed loop setpoint decrease in W_s.

6.5 Decentralized τ_c - sequential controller tuning

The sequence for the boiler-driven, turbine-driven and floating pressure control structure based on the τ_cs from the independent controller tunings are listed in Table 6.9 below.

Table 6.9: Independent τ_c - tuning sequences for the control structures.

(a) Boiler-driven

Controller	τ_c [s]
T_r	0.0250
$T_{FG,eco}$	0.0350
T_c	1.3272
T_a	1.3425
W	1.6000
P_d	3.0000

(b) Turbine-driven

Controller	τ_c [s]
T_r	0.0250
$T_{FG,eco}$	0.0350
T_c	1.3272
T_a	1.3425
P_d	1.5990
W	30.0000

(c) Floating pressure

Controller	τ_c [s]
T_r	0.0250
$T_{FG,eco}$	0.0350
T_c	1.3272
T_a	1.3425
W	1.6000

The controllers are tuned again, sequentially, but now with regards to a sequence determined from the closed loop time constants, τ_c, obtained from the independent tuning. This leads to different values for the process gain (k), τ_1 and τ_c for the respective controllers compared to the independent and τ_1-sequential controller tunings. The τ_c sequential tunings for the boiler-driven, turbine-driven and floating pressure control structure are the same for the drum holdup and temperature controllers since the sequences are identical up to this point. The results are listed in Table 6.10 for the drum holdup and temperature controllers, and the individual pressure and power controllers in Table 6.11.

Table 6.10: The τ_c - sequential controller tunings for the drum holdup and temperature controllers.

Controller	k	τ_1 [s]	θ [s]	τ_c [s]	PID
T_r	0.3161	0	0	0.0250	I
$T_{FG,eco}$	0.0491	1.540e-4	0	0.0350	I
T_c	2.2458e-6	7.9524	0	2.5999	PI
T_a	-2.2544	0.1010	0	2.5999	PI

Table 6.11: The τ_c - sequential controller tunings for the pressure and power controllers.

Control structure	Controller	k	τ_1 [s]	θ [s]	τ_c [s]	PID
Boiler-driven	W	-0.5882	0.4995	0	12.5999	PI
	P_d	-0.5122	0.0023	0	10.9990	PI
Turbine-driven	P_d	0.4969	0.45991	0	12.9999	PI
	W	-0.6086	7.6577	0.1061	59.9999	PI
Floating pressure	W	-0.5882	0.4995	0	12.5999	PI

The open loop step responses used to tune the controllers are found in Appendix A.11 and A.12 for the boiler-driven and turbine-driven control structure, respectively. The same controller tunings as the boiler-driven control structure were used for the floating pressure control structure since their sequences are completely identical except for the floating pressure control structure not containing the P_d-controller at the end of the sequence.

6.5.1   1% step decrease in the power setpoint

A 1 % step decrease in the power setpoint, W_s, was made for the boiler-driven (BD), turbine-driven (TD), and floating pressure (FP) control structure with the τ_c-sequential controller tunings, shown in Figure 6.19.
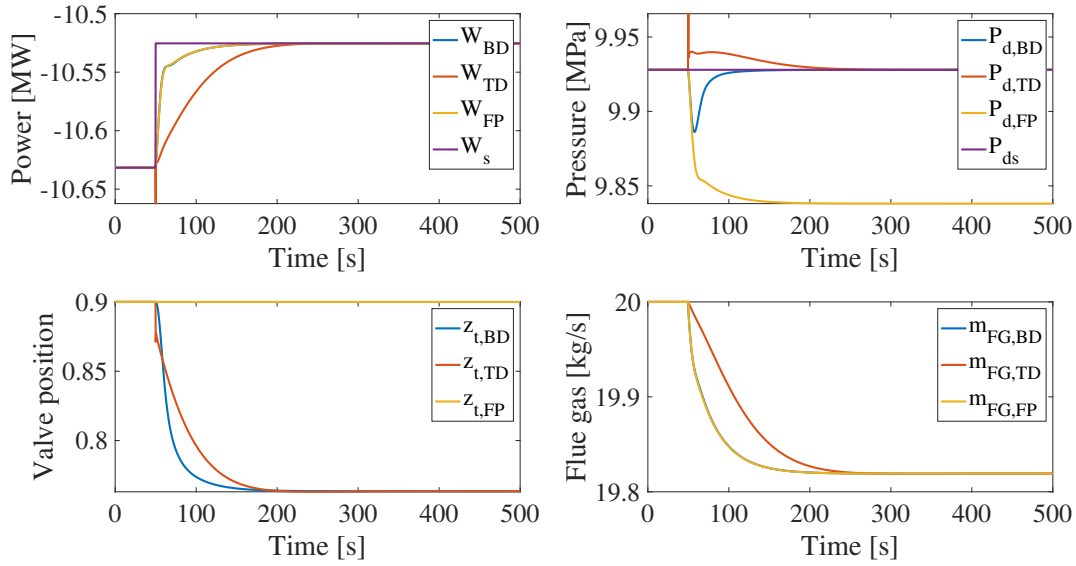
Figure 6.19: Plot of W, P_d, $\dot{m}_{FG}$ and z_t for the three τ_c - sequential tuned control structures after a 1% closed loop setpoint decrease in W_s.

6.6   Valve position controller

The turbine valve is easily saturated, especially with regards to the turbine-driven control structure. This is not desirable as the power output (being our throughput manipulator) should not be paired with a MV that may saturate[Reyes-Lúa et al., 2018]. A valve position controller was implemented for the turbine-driven control structure, to account for the saturation. The τ_1 - sequence was used for tuning, where the valve position controller was tuned right after the power controller. After closing the valve position control loop the latter temperature controllers, T_aC and T_cC, were tuned and closed, sequentially. The open loop input step responses and setpoint changes made to tune and verify the controllers can be found in Appendix A.14. The controller tunings are listed in Table 6.12

Table 6.12: Controller tunings for the valve position controller.

Controller	k	τ_1 [s]	θ [s]	τ_c [s]	PID
T_r	0.3161	0	0	0.0250	I
$T_{FG,eco}$	0.0491	1.540e-4	0	0.0350	I
W	-0.2528	0.0129	0.1164	19.9999	PI
VPC	-10.3222	22.5865	0	29.9900	PI
T_a	-2.2025	0.0925	0	209.9990	PI
T_c	3.8097e-7	0.6747	0	359.9990	PI

6.6.1   1% step increase and decrease in the power setpoint

A 1% decrease and increase in the power setpoint was made for the turbine-driven (TD) and the valve position control structure (VPC) as seen in Figure 6.20 and 6.21, respectively. Clamping is the implemented method of anti-windup.
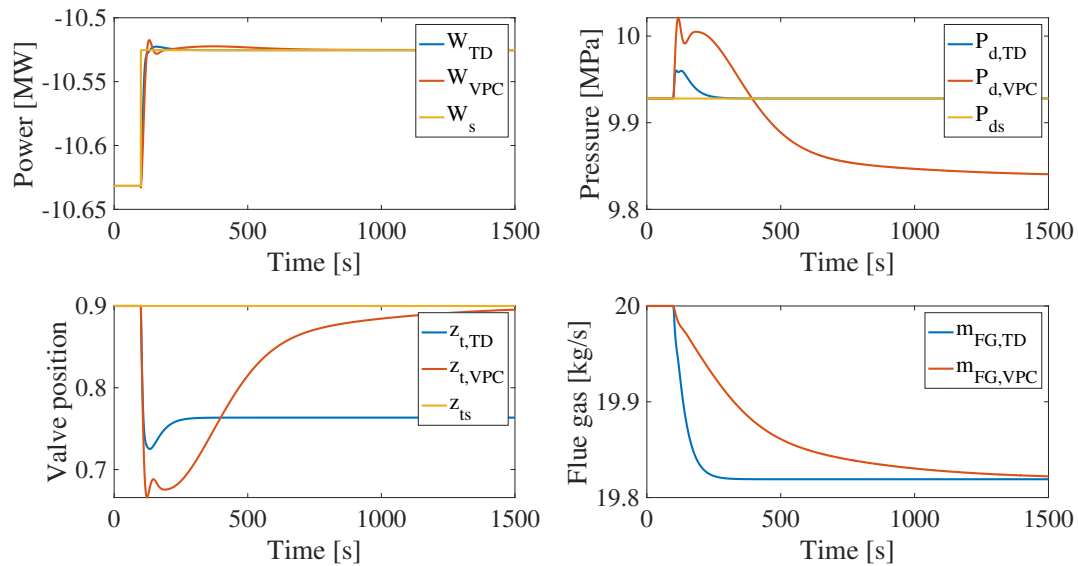
Figure 6.20: A plot of a 1% step decrease in W_s for the turbine-driven and the valve position control structure.
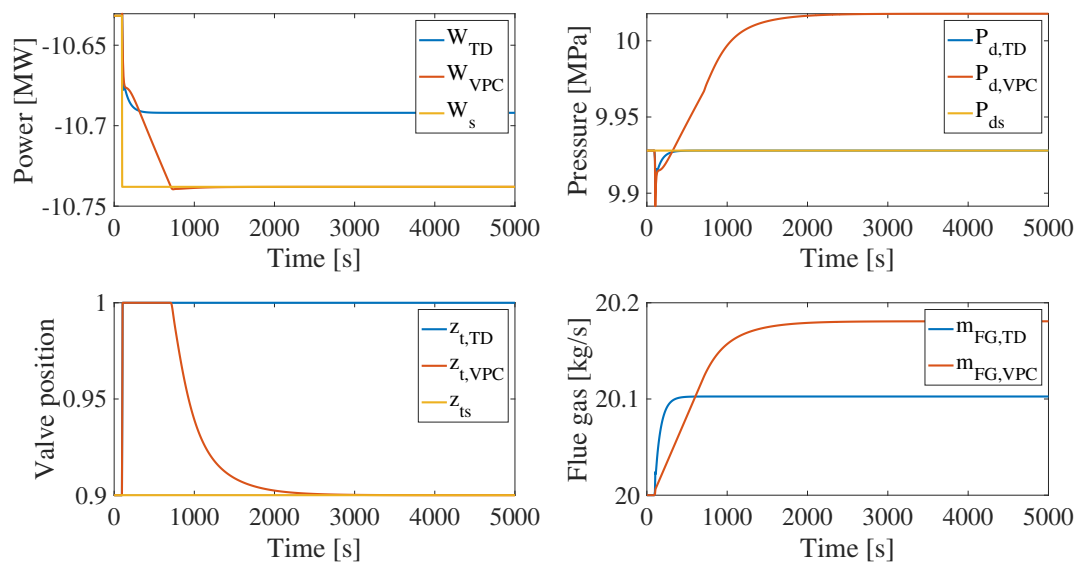
Figure 6.21: A plot of a 1% step increase in W_s for the turbine-driven and the valve position control structure, with clamping anti-windup.

6.6.2 Back-calculation anti-windup

To illustrate the two methods of anti-windup Simulink has to offer a 1% step increase of the power setpoint is made again, but now implementing back-calculation as a method of anti-windup, shown in Figure 6.22. The tracking constant, T_t, was set to be 0.01, as it is smaller than $\tau_I = 0.0129$.
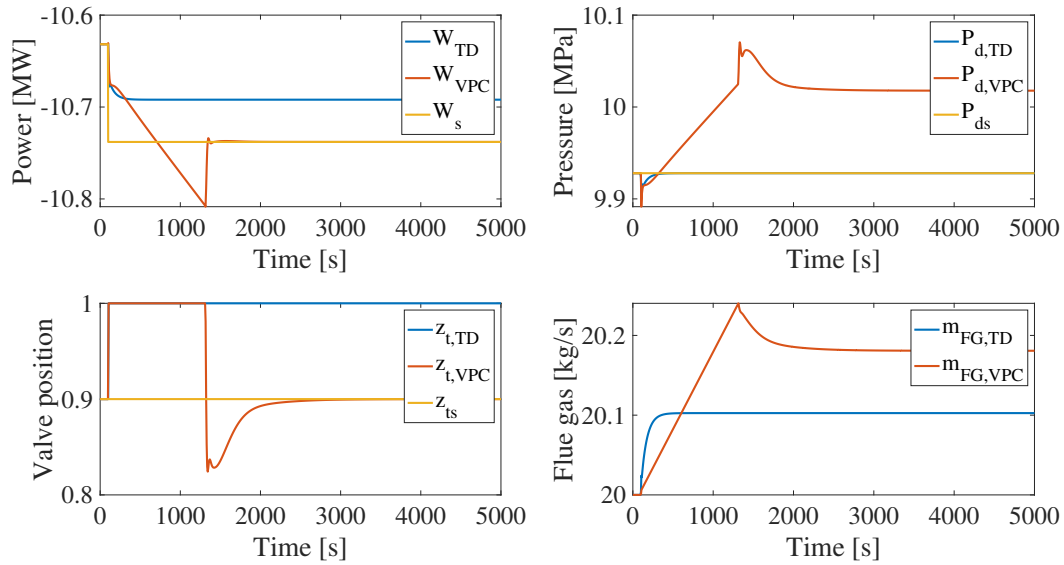
Figure 6.22: A plot of W, z_t and $\dot{m}_{FG}$ after a 1% step increase in W_s with back-calculation anti-windup.

It is clear in Figure 6.22 that there is still some integral windup with the back-calculation anti-windup. This also shows that the back-calculation works dynamically, such that an insufficient back-calculation coefficient leads to worse results for the anti-windup compared to the static clamping anti-windup.

6.7 Parallel power control

The parallel power controller was tuned using the τ_1-sequence similar to the sequence of the valve position controller. In the parallel controller tuning, the overshoot in the power output was removed. During the tuning procedure, it was possible to get a quite fast response in the power controller as seen in Figure 6.23.
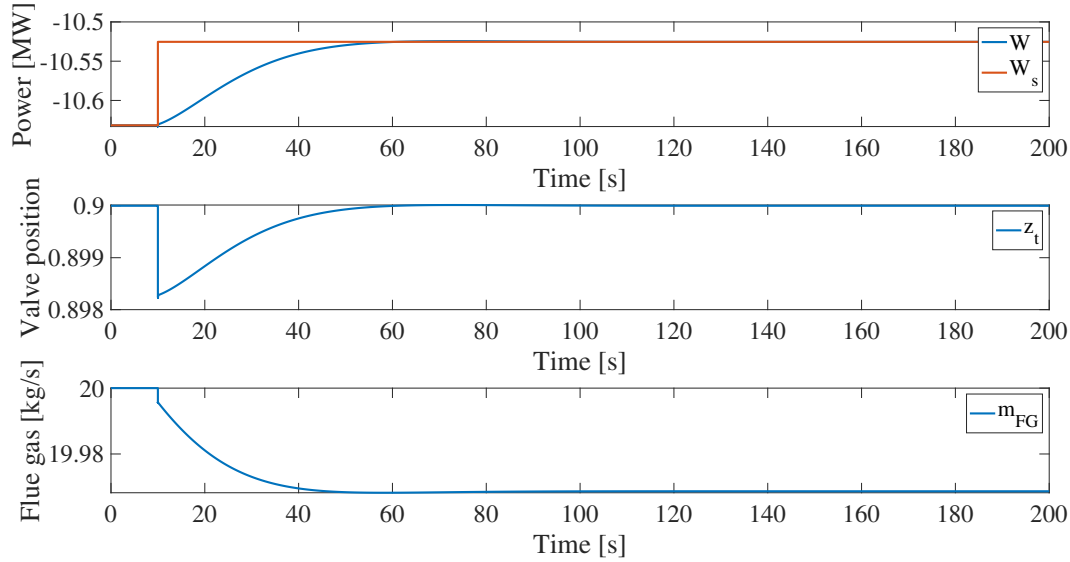
Figure 6.23: A plot of the response after a 1% step decrease in W_s for the parallel power control structure.

The last two controller tunings in the sequence, T_aC and T_cC, causes the power controller to become slow at the completion of the sequential tuning procedure. To better identify which controller that is causing this effect in the power controllers, the setpoint responses for T_a and T_c are presented in Figure 6.24 and 6.25, respectively.

The open loop input step responses and the closed loop setpoint responses used to tune the controllers are found in Appendix A.13. The resulting controller tunings are listed in Table 6.13 in the sequential order they were tuned.

Table 6.13: Controller tunings for the parallel power control structure.

Controller	k	τ_1 [s]	θ [s]	τ_c [s]	PID
T_r	0.3161	0	0	0.0250	I
$T_{FG,eco}$	0.0491	1.540e-4	0	0.0350	I
W-z_t	-0.2528	0.0129	0.1164	3.0000	P
W-$\dot{m}_{FG}$	-1.5995	12.2835	0	35.0000	PI
T_a	-2.2027	0.0947	0	2.2999	PI
T_c	3.8083e-7	0.6579	0	9.9999	PI
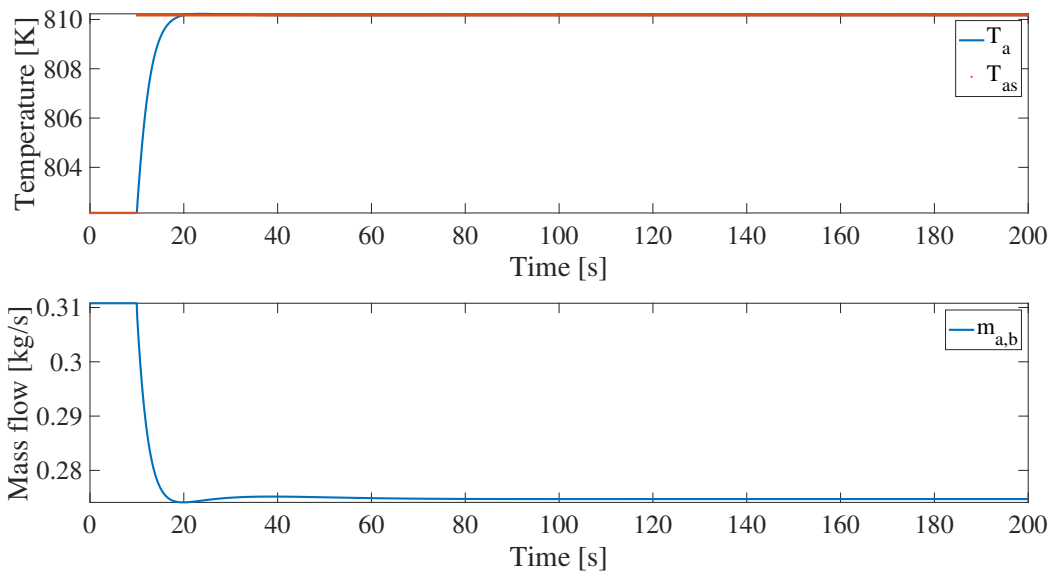
Figure 6.24: A plot of the response after a 1% step increase in T_{as} for the parallel power control structure.
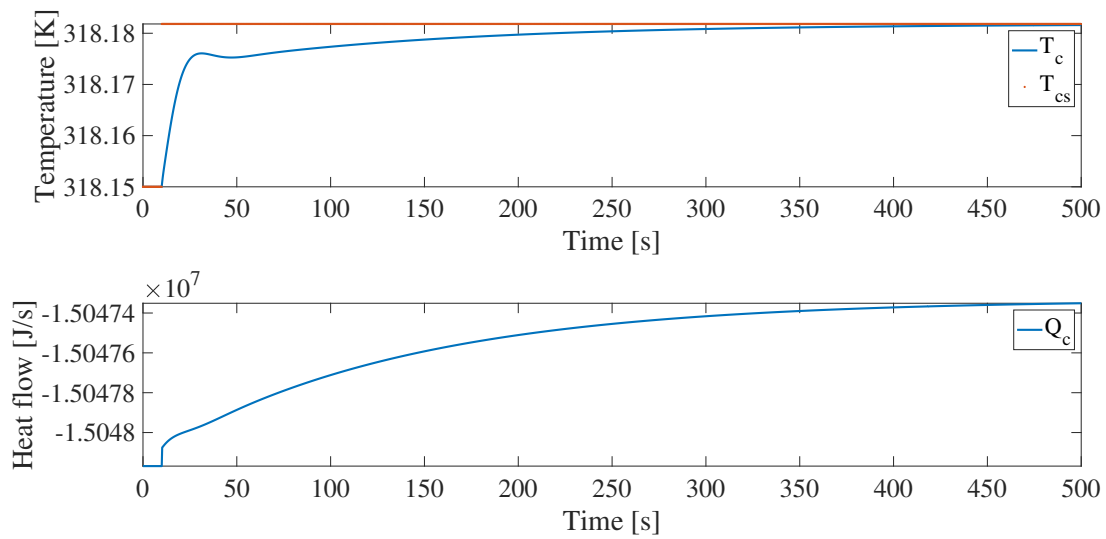
Figure 6.25: A plot of the response after a 0.001% step increase in T_{cs} for the parallel power control structure.

6.7.1   1% step decrease in the power setpoint

A 1% step decrease in the power setpoint, W_s, was made for the valve position (VPC) and parallel power (P) control structure, shown in Figure 6.26.
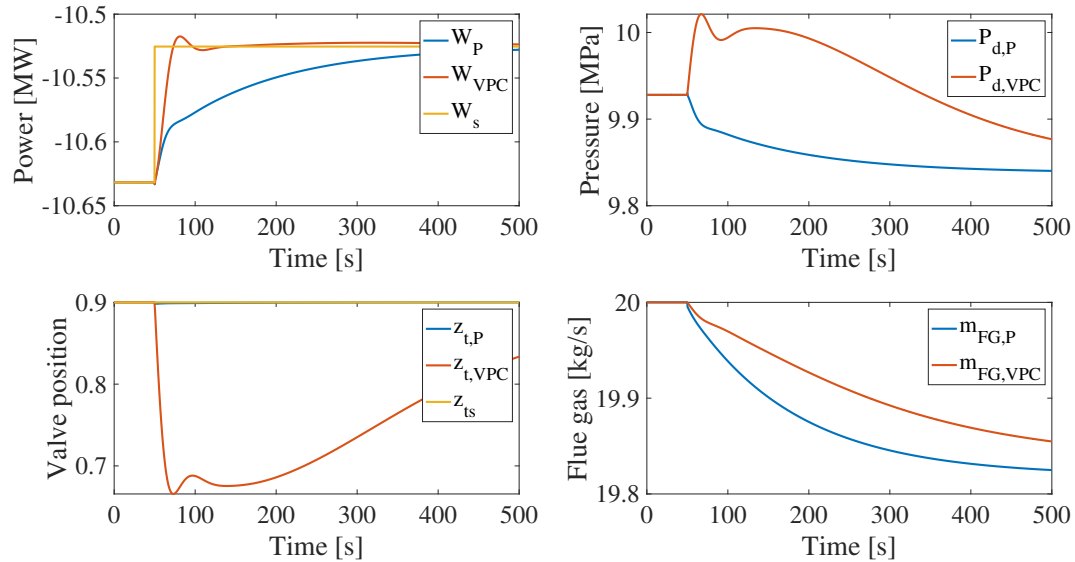
Figure 6.26: A plot of the response after a 1% step decrease in W_s for the valve position and parallel power control structure.

6.8   Settling times

The time the power output for each control structure and tuning method uses to reach steady state is listed in Table 6.14.

Table 6.14: Steady state times for the power output in each control structure and tuning design.

|	Steady state time [s]		
Control structure	Independent	τ_1-sequential	τ_c-sequential
Boiler-driven	25	>500	250
Turbine-driven	35	220	280
Floating pressure	25	180	250
Valve position controller	-	220[1]	-
Parallel power controller	-	>500	-

[1] Not including the overshoot

The τ_c-sequential controller tuning sequence is chosen for the boiler-driven control structure as it delivers a considerably faster response in the power controller compared to the response from τ_1 -sequential tuning. The turbine-driven and floating pressure control structures are both much faster with the τ_1 -sequential tuning sequence. The valve position control structure was only tested through a τ_1-sequential controller tuning sequence. It was attempted to tune the valve position controller towards the end of the sequence, similar to a τ_c-sequential controller tuning approach, but this lead to an even higher overshoot of the power controller as the valve position controller now had to become much slower in controlling the valve position back to its setpoint. The parallel controller was also only tested through a τ_1-sequential controller tuning sequence, even if the slow power controller technically should be placed towards the end since the open loop time constant is much larger than the latter loops in the sequence. This is not possible in this case as both of the power controllers needs to be tuned in parallel. From the τ_c-sequential controller tuning of the turbine-driven control structure it is clear that the power control becomes much slower, such that it is desired to tune the power controllers early in the sequence, similar to the τ_1-sequential tuning sequence.

6.8.1 Fastest control tuning sequences for each control structure

A new plot with each control structure with their fastest control tuning sequence is shown in Figure 6.27. A zoomed in plot of the power responses is shown in Figure 6.28.
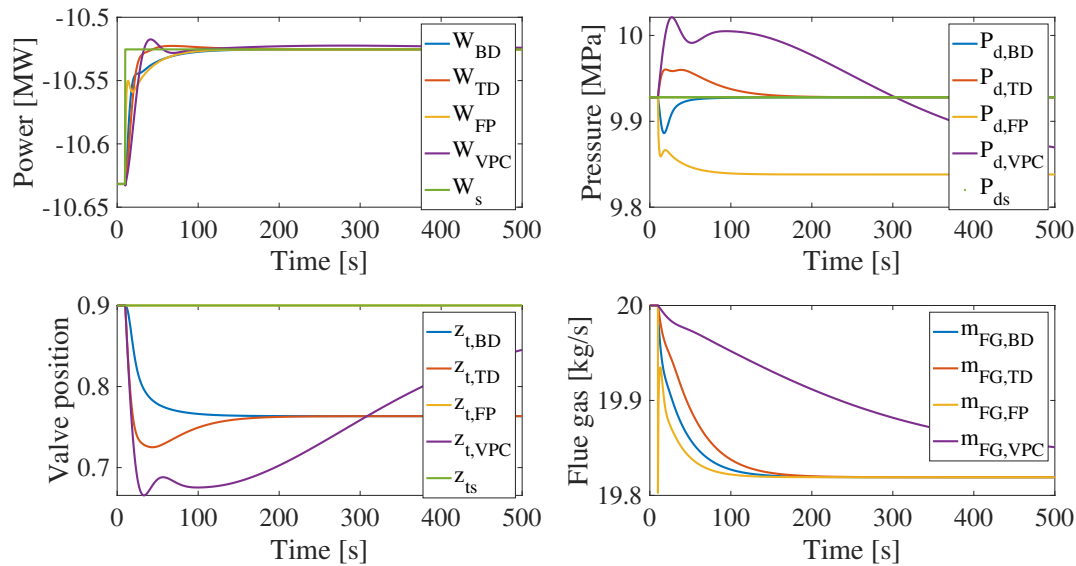
Figure 6.27: A plot of the response after a 1% setpoint decrease in W_s for the boiler-driven, turbine-driven, floating pressure and valve position control structures.
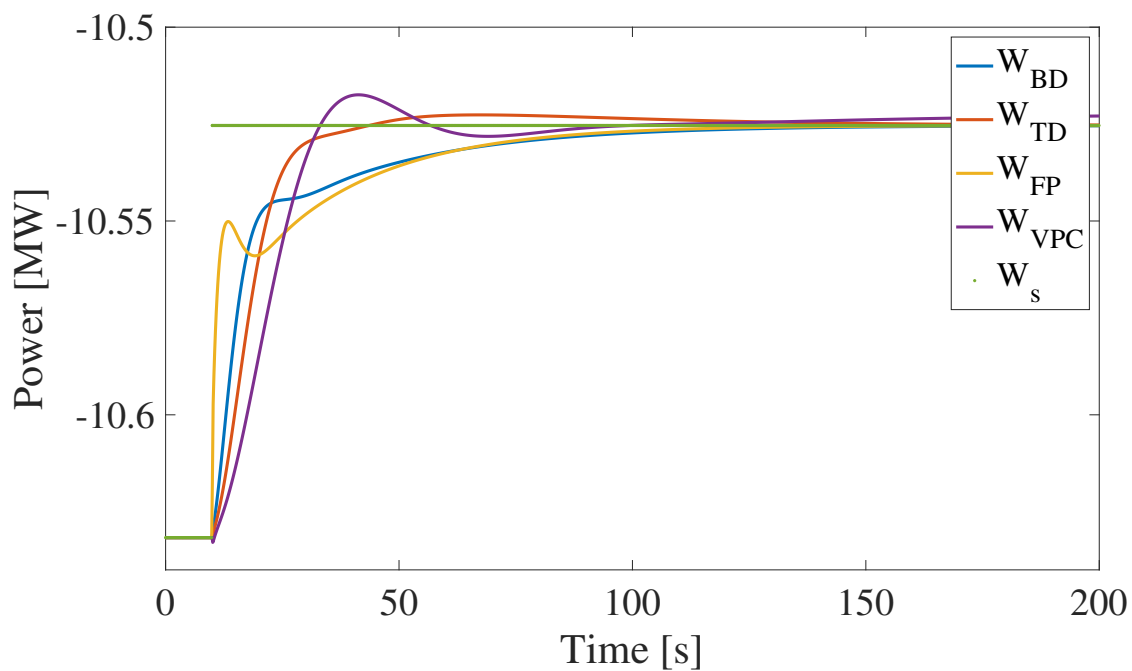
Figure 6.28: A plot of the response in the power after a 1% setpoint decrease in W_s for the boiler-driven, turbine-driven, floating pressure and valve position control structures-

6.8.2 The effect of the residence time in the condenser

In the previous specialization project, a future recommendation was to decrease the holdups in the simulation [Andersskog, 2018]. The drum holdup remained 1000kg, while the attemperator and turbine holdup was reduced substantially to improve the speed of the dynamics in the turbine section. The condenser holdup was also reduced, from 1000kg to 40kg. After checking with the literature of the residence times of the boiler and condenser, 40kg is too low. The current simulation contains a condenser holdup of 500kg, reflecting the residence times found in the literature. A plot of the fastest control tuning procedures for the boiler-driven, turbine-driven, floating pressure and valve position controller after a 1% setpoint decrease in power with 40kg condenser holdup is made in Figure 6.29 to compare the control performance with the 500kg condenser holdup results in Figure 6.27. The fastest tuning sequences for the control structures was found to be the same as in the 500kg simulation where τ_c-sequential is chosen for the boiler-driven control structure and τ_1-sequential for the latter control structures.
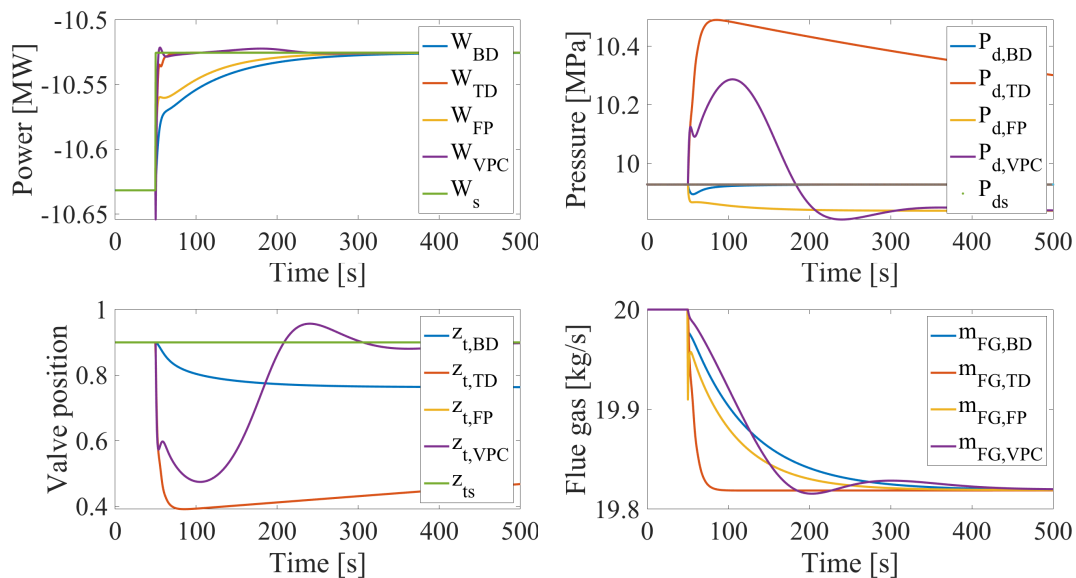
Figure 6.29: A plot of the fastest control sequences for the boiler-driven, turbine-driven, floating pressure and valve position control structures for a condenser holdup of 40kg.

Chapter 7

Discussion

7.1 Decentralized independent controller tuning

It is clear from the 1% power setpoint step decrease of the independently tuned boiler-driven, turbine-driven and floating pressure control structures in Figure 6.6 that the independent decentralized tuning does not account for interactions in the Heat-to-Power cycle. Specifically, the coupled loops result in undampened oscillating behaviour for the boiler-driven and floating pressure control structure. The coupling might be taken care of in the turbine-driven control structure by having larger τ_c, which also leads to the turbine-driven control structure obtaining slightly higher settling time for the power output compared to the boiler-driven and floating pressure control structure.

In the open loop step response in the valve position for the turbine-driven control structure in Figure 6.2, the power output to settled towards its original value and had to be tuned at its initial response. A reason for this might be the fact that the power is mainly a function of temperature (or enthalpy), which is constant from the valve inlet to the valve outlet. The power is also a function of mass flow, but the change caused by the step in the valve position will have an overall small effect on the power output. This leads to a small steady-state effect on the power from the valve position, indicating that the valve position can only be used to control the power within small ranges as large changes in power can only be made by changing the fuel load into the system.

In the turbine-driven control structure it is not possible to completely remove the inverse response in the power controller, as seen by Figure 6.3 and 6.4. The only way to reduce this inverse response is to design a slow controller, which is not desired and not realistic as the inverse response is a characteristic of the system and cannot be completely removed. The inverse response is a result of the RHP-zeros in the system. The RHP-zeros can come from the interaction between the valve opening and the pressure, defining the computed power output. Closing the valve causes a sudden increase in inlet pressure to the turbine, but also a decrease in mass flow, higher pressure from the attemperator, thus leading to the steady state decrease in pressure at the turbine inlet as seen from Figure 6.3 and 6.4. As mentioned in Section 3.2.2, the inverse response is considered a delay when tuning the power controller. Still, the closed loop time constant had to be selected relatively large to avoid unstable response in the power output. To illustrate this, the same setpoint response in the power was made with a $\tau_c = 20$ in Figure 6.5,

indicating that the power controller is sensitive to high controller gain. Still, the turbine-driven control structure reached its setpoint without any form of oscillation. The response in power output did contain a slight overshoot, which is most likely caused by coupling loops still being present.

The boiler and floating pressure control structures did not experience any inverse responses as the power, in this case, was not paired with the valve position. Still, this could show up after closing the latter controllers as the inverse response is a characteristic of the turbine. One of the reasons that it is not present in the boiler-driven and floating pressure control structures can be the long distance of pairing, decoupling the pressure and power controller. The manipulated variables paired with the power output in these two cases are the flue gas flow which gives a first order steady state response in power in the open loop tunings, leading to smooth power control. In the floating pressure control structure, the valve position is fixed and thus the effects of the valve opening are not present. In the boiler-driven control structure, the valve position is paired with the drum pressure, which allows for several dampening holdups between the measured output and the controller action.

7.2   Decentralized τ_1 - sequential controller tuning

The three control structures: boiler-driven, turbine-driven and floating pressure, behaved somewhat differently with regards to the method of tuning. Smooth and fast response in power output after a 1% setpoint decrease in power from the independent tuning in Figure 6.6 only gives satisfactory response for the turbine-driven control structure. This changes after the implementation of the τ_1 sequential controller tuning shown in Figure 6.18 where the turbine-driven control structure settles smoother but 40 seconds slower than the floating pressure control structure. An explanation for this could initially seem to be based on the fact that floating pressure has one less control loop in its system. By allowing the pressure to float, fewer variations occur through the coupling with the pressure controller. But by studying the curve of the power output in the boiler-driven control structure it shows similar behaviour in the response curve, just on a much slower scale. The reason for the lower settling time in the floating pressure control structure compared to the boiler-driven control structure is, therefore, mostly connected to the difference in tuning sequences.

There is still a clear presence of coupling with the power controller for the floating pressure control structure as the power response curve does not reach its setpoint without undampened oscillating behaviour. The turbine-driven control structure has a power output response similar to the response curve in Figure 6.6 from the independent tuning, with a small overshoot, but is now reaching steady state much later. The long settling time is most likely caused by coupling with the relatively slow T_c-control loop and the sequential tuning of the control structure. It is still expected that the increase in settling time for the power controller would lead to a decrease in overshoot. The overshoot might occur as a result of the pressure controller, that is limited by its integrating open loop response. The PI action in the drum pressure, P_d, controller is not able to regulate the pressure towards its setpoint without giving an overshoot. This is because when using the SIMC tuning rules for a PI-controller from an integrating response large values for τ_c in will reduce the integral action in the controller. Reduction in the integral action in the drum

pressure PI-controller can lead to the drum pressure not reaching its setpoint at all.

The change in open loop response of the attemperator temperature and drum pressure controller in the τ_1-sequential tuning of the turbine-driven control structure reflects the disadvantages of the sequential tuning procedure. As each controller closes the next loop will change from its predictable independent process transfer function if it is coupled by any of the previous loops. This leads to open loop responses such as for example for the P_d-controller in Figure 6.15 and the T_a-controller in Figure 6.7, which makes it difficult to not only tune the controllers, but to also obtain satisfactory closed loop responses. This indicates that controllers that are required to regulate their output quick and tightly should be tuned early in the sequence to maintain a more predictable behaviour.

T_a did not stay self-regulating through the completion of the τ_1-sequential tuning of the turbine-driven control structure as seen in Figure 6.12, indicating that it still requires a controller. The implemented T_a-controller that was tuned from its initial response did work as seen in Figure 6.14, but also caused saturation of the economizer bypass stream or valve position during the tuning procedure. This problem did not continue once the sequential controller tuning was completed, thus, the τ_1-sequential controller sequence can still be used for the turbine-driven control structure, but with the knowledge that the T_a-controller might not guarantee failure tolerance.

Considering the response curves in Figure 6.18 for the τ_1 sequential tuning procedure, the response curves for boiler-driven and floating pressure control structure show clear effects of still being coupled with other control loops that are tuned later in the sequence, thus a strategic approach is required for these control structure when designing a tuning sequence for smooth and fast power control. In this case, the coupled control loop can only be with the condenser temperature loop as it is the next and last control loop to be closed after the power controller.

The boiler-driven and floating pressure control structure only differ with regards to a pressure controller. Still, the slight change in the tuning order (lack of pressure controller in the floating pressure control structure) gave much faster controllers in the floating pressure control structure compared to the boiler-driven control structure as seen from the controller tunings in Table 6.8. It is also clear in the 1% setpoint decrease in power from Figure 6.18 and the respective settling times in Table 6.14 that the addition of a pressure controller adds significantly longer settling time for the power output and has large effect on the tunings of the latter controllers in the sequence. On the other hand, the pressure control in the boiler-driven control structure is much faster compared to the floating pressure and turbine-driven control structures, again showing the effect of the position of a controller in the sequential controller tuning.

7.3 Decentralized τ_c - sequential controller tuning

The τ_c - sequential tuning procedure leads to longer settling times for all of the control structures as seen in Figure 6.19. The advantage with the τ_c - sequential controller tuning is that it was overall much more straight forward to tune and gave smoother response curves. All of the open loop step responses were of the same response type as the open loop responses in the independent tuning, but now also allowed for tuning at steady state for the power controller in

the turbine-driven control structure. This might occur as a result of the temperature controllers all being tuned early in the process, thus stabilizing the cycle by slowing down the open loop responses for the power and pressure controllers. The change in sequence creates a separation between the controllers, allowing for decoupling between control loops such as the power and pressure control loops from the attemperator and condenser temperature controllers.

In Figure 6.19, the turbine-driven control structure uses about 30 seconds longer to reach steady state compared to the boiler-driven and floating pressure control structure. This is directly linked to the sequence of tuning, as now the power controller is tuned last in the sequence. The pressure control in the turbine-driven control structure is slow, but not changing its settling time much from the τ_1 sequential tuning procedure. As well the response curve for power output in the turbine-driven control structure had a much larger inverse response than what was experienced from the independent and τ_1 sequential tuning. This indicates, that the τ_c sequence is not beneficial for the turbine-driven control structure and that if a fast power controller is desired this should be done either through an independent tuning or τ_1 sequential tuning. Excluding the inverse response, the response curve seen for the power output in the turbine-driven control structure now does not contain the overshoot that was experienced in the independent and τ_1-sequential controller tuning. The change in the turbine-driven control structure with regards to the different tuning procedures indicate that the turbine-driven control structure is not as coupled as the boiler-driven and floating pressure control structure with regards to undampened oscillating behaviour, but more with regards to control speed.

The settling time for the power output in the floating pressure control structure has also increased from the τ_c-sequential controller tuning. The only change in the sequence compared to the τ_1 sequence is the position of the T_c-controller, that is now placed early in the sequence, slowing down the latter controllers.

The only control structure to improve from the τ_c sequential tuning procedure compared to the τ_1-sequential tuning is the boiler-driven control structure. The power output of the boiler-driven control structure does not only reach steady state twice as fast but also contains less underdamped oscillating behaviour, indicating that there is less coupling between the control loops from this sequence. The distance between the power and condenser temperature in the sequence is much greater, allowing for the regulating action in the condenser temperature to occur before the power controller.

Overall, the sequential tuning procedure has a large effect in the response of the power output, especially for the floating pressure and boiler-driven structures. Even if the responses are slower, the undampened oscillating behaviour from the independent tuning is substantially reduced, indicating that the sequential tuning does indeed account for some of the couplings between the control loops.

7.4   Valve position controller

The implemented valve position controller was successful in controlling the valve position back to its setpoint, allowing for maximum throughput but trading off the performance of the power control as it experienced an overshoot. This can come from the coupling between the control loops in the two controllers, causing the valve position controller to introduce disturbances into the power output. The overshoot was reduced with slower valve position controller, but not removed. Designing a slow valve position controller made the latter and most importantly, the T_c-controller much slower as well, affecting the valve position and power controller through the coupling with the flue gas and the temperatures in the system. Removing the integral action in one of the controllers was attempted in both the power controller and valve position controller. Removing the integral action in the power controller can cause problems when tight control of the power setpoint is desired to meet the demands in the electric grid. Removing the integral action in the valve position controller, on the other hand, is more reasonable, but defying the purpose of the valve position controller in the first place.

In the valve position controller, the power control is done through the valve position, utilizing the fast dynamics in the turbine, resulting in fast power control. As well, the valve position controller does manage to set the valve position back to its setpoint, which is a great advantage in cases where the valve position saturates as seen from Figure 6.21. Especially for the turbine-driven control structure, the valve position is very limited with regards to increasing the power output as it easily saturates. This can also be a problem in the boiler-driven control structure at large increases in drum pressure. For the floating pressure control structure, the valve position is fixed, which will limit throughput as well. Additionally, the problems with the tuning of the attemperator temperature, T_a, - controller did not occur during the tuning of the valve position control structure. If the overshoot is accepted or removed through a decoupling filter, the valve position control structure will contain the advantages of the turbine-driven control structure of fast and smooth power control, in addition to the advantages of the valve position control of maximum throughput.

When comparing the turbine-driven and valve position control structure to the floating pressure control structure with regards to settling time, the floating pressure control structure seems to obtain the fastest power control. The control structure also has the advantage of linking the fuel load to the power output. If high energy efficiency is desired, then the floating pressure should be the selected control structure based on these results. The disadvantage of the floating pressure control structure, on the other hand, is that it leaves the pressures uncontrolled, which in large setpoint changes can become unsafe and create instabilities in the cycle. This is an advantage that the turbine-driven control structure has, while still maintaining quite fast power response. If it is important to maintain stability and pressure control, for example in a supercritical heat-to-power cycle, where the temperatures and pressures into the high-pressure turbines are critically large, a turbine-driven control structure should be selected control structure.

The clamping and back-calculation anti-windup methods in Simulink was tested through a 1% setpoint change in the power in Figure 6.21 and 6.22, respectively. The results reflect the theory in Section 3.2.3 as the clamping anti-windup seemed to perform better than the back-calculation anti-windup. The back-calculation anti-windup case contained a large overshoot once the valve became unsaturated, showing that the anti-windup is not removing the integral windup fast

enough. This can be improved by increasing the tracking time constant, T_t. Because of time limitations, this was not done in this simulation. Improving the back-calculation coefficient is time-consuming and does not guarantee better results than the clamping method if not done properly.

7.5   Parallel power controller

When comparing the parallel power and the valve position control structures, the parallel control structure seemed to give better responses during the tuning process as seen in Figure 6.23. The parallel controller only contains integral action in the slow power controller, removing the overshoot of the power output that was experienced in the valve position control structure, seen in Figure 6.26. In the 1% decrease in power setpoint during the tuning of the parallel controller shown in Figure 6.23 it is clear that the valve position is used for only a very small range. The rest of the power control is done through manipulating the flue gas, thus slowing down the power control as well. If the settling time of the power control had stayed the same during the tuning of the latter controllers in the sequence, this control structure would have been optimal for tight and smooth power control with a large throughput range. Considering the setpoint changes of T_{as} and T_{cs} in Figure 6.24 and 6.25, it is clear that the T_c-controller is required to be much slower than the T_a-controller in order to deliver a satisfactory response in its output. The disadvantage with this is that the power controller that manipulates the flue gas is still very much coupled with the condenser temperature control loop, thus leading to the overall slow power control in Figure 6.23.

7.6   Condenser holdup residence time

From the 40kg simulation results in Figure 6.29, the turbine-driven control structure was found to be substantially faster than the other control structures, as well as maintaining this speed with the added valve position controller. The overshoot from the valve position controller was still present, but not on the same scale as in the current 500kg simulation. This is first of all because the sequences were slightly different from the larger holdup. In the current 500kg condenser holdup simulation, the T_c controller is tuned last in the τ_1 sequence, requiring a very slow controller. Throughout the simulations, a strong coupling is noticed between the power controller and the temperature condenser controller, which can explain why the results changed this much.

7.7   Simulink

In Section 2.4 Simulink as a simulation environment is explained. The Heat-to-Power cycle has been built in Simulink, with the subsystems representing the individual components and actions of the Heat-to-Power cycle. One of the advantages found by utilizing the subsystem blocks is obtaining a clear separation between the components and an easier overview, considering the large complexity and number of variables the Heat-to-Power cycle contains. The disadvantage of using the subsystems is concerning debugging of the cycle and loss of the direction in which the simulation is solved. In general, the Simulink blocks create an easier modelling experience, but on a trade-off for the transparency of how the blocks themselves are modelled. As well,

as mentioned in Section 4.7 the simulation struggled with sensitivity. At certain tolerances or values for the control parameters, the simulation would stop running. This was in most of the cases solved by reducing or increasing the relative tolerance to 1e-7 or 1e-9. In a few cases, especially during longer runtimes, for example in the 1% setpoint increase of the power in Figure 6.21, the tunings for the valve position controller had to be changed from 49.9999 to 50.0. These changes should not give a difference in the results of the simulation, but for some reason made the simulation run. The problems with the Heat-to-Power cycle simulation are most likely caused by the stiff system and the *ode15s* solver.

Chapter 8

Conclusion

The first objective of this master thesis was to model the heat-to-power cycle in Simulink. The second objective was to apply the plantwide procedure on the cycle to design a decentralized control structure with good performance for a highly coupled system. The control objective of the plant is to have fast and tight power control as it is required to contribute to supply power to the grid. The five control structures boiler-driven, turbine-driven, floating pressure, parallel power control and valve position control were implemented and compared based on their ability to control the power after a setpoint change. Three decentralized tuning procedures were implemented for the boiler-driven, turbine-driven and floating pressure control structure to identify the optimal method of tuning with regards to reducing the coupling between the control loops and delivering fast power control.

Independent tuning was found to only be possible for the turbine-driven control structure as the boiler-driven and floating pressure control structures suffered from undampened oscillating behaviour in their power output. This is because the floating pressure and the boiler-driven control structures contained stronger coupling between its loops and will require τ_1 and τ_c-sequential tuning, respectively. The sequential tuning was found to reduce the coupling effects on the power control substantially for these two control structures, but trading-off shorter settling times for the power controllers.

In cases where fast and smooth power control is desired and pressure is allowed to float, the floating pressure control structure tuned through the τ_1-sequence was found to give the lowest settling time. This structure is still not recommended as it delivers low throughput.

The coupling between the flue gas and the condenser temperature was found to be the main cause of slow power control in the boiler-driven control structure. Positioning the condenser temperature controller early in the sequence improved the speed of the power control.

The opposite is seen in the turbine-driven control structure, where the τ_c-sequential tuning results in slow power control. This is not caused by the position of the condenser temperature controller but rather is only affected by the position of the power controller in the sequence. If sequential tuning is used for the turbine-driven control structure, τ_1-sequential is recommended. Similarly, for the floating pressure, parallel power and valve position control structures, τ_1-sequential is recommended.

If an overshoot and floating pressure are accepted, the addition of valve position control is recommended for the turbine-driven control structure as it suffers from a small control range by pairing the power controller with the valve position. The clamping anti-windup was found to reduce the integral windup sufficiently and bring the power towards its setpoint within a reasonable time.

The parallel power controller was found to give smooth power control, eliminating the overshoot that the valve position control structure contained. Still, the coupling between the flue gas and the condenser temperature resulted in long settling time for the power output.

A decrease in the condenser residence time changed the tuning sequences and the conclusions that can be made with regards to power settling time. This shows that the condenser has a large effect on the stability and coupling between the control loops in the Heat-to-Power cycle.

It was possible to design a decentralized control structure for a Heat-to-Power cycle, but with a trade-off for each control structure. Allowing for the overshoot in the valve position control structure leads to a conclusion of a τ_1-sequential tuned turbine-driven control structure, with an added valve position with clamping anti-windup as the most optimal control structure for a plant that is required to control the power for grid frequency regulation.

Chapter 9

Further recommendations

The turbine-driven control structure is supposed in theory to give the fastest power control, which for the 40kg case of the condenser holdup was the case. In the simulated case with 500kg, the floating pressure was faster. This shows clearly the sensitivity of the model on the results. A future recommendation is, therefore, to improve the quality of the modelled dynamics in the simulation to be able to study the control structures more clearly. This can be done by for example including valve dynamics and delays to the simulation, increasing the complexity of the heat exchanger model and to research the effects of the holdups in the economizer and attemperator. Especially for the turbine-driven control structure, the sequence of tuning had a large effect on the performance of the controllers. Even if three sequences (independent, τ_1 and τ_c) was studied in this case, it would be interesting to see other sequences as well and how it affects the speed and the performance of the controllers in this control structure. Ideas for other sequences are sequences based on the settling times for the respective independent setpoint responses, effective delays and intuition based trial-and-error built sequences.

It was attempted to compute a RGA of the model, to study the coupling between the controlled variables and the manipulated variables. The system contains many equations, both static and dynamic, which made this a difficult task to be done accurately with reliable results. Because of time limitations, this was not completed and therefore not presented in this thesis, and is recommended to be studied in the future. The RGA will not only indicate the optimal controller pairings but also show clearly which other manipulated variables that might interfere with the optimal control pairings. The RGA can then be utilized when designing the optimal sequence where the controllers which are desired to be fast are tuned early in the sequence and the controllers in which are coupled and can be allowed to be slow are tuned late in the sequence, thus reducing the coupling between the controllers even more. Another important aspect of the RGA is that the process transfer functions obtained in this process can be utilized to design decouplers for the controllers assuming independent controller tuning. It would, therefore, be interesting to compare a control structure with decentralized control and optimal sequential tuning design with a decentralized independent tuned control structure containing decouplers.

Another future recommendation is to design a multivariable controller that can handle the change of active constraints, such as an NMPC and compare it to the decentralized control structures with regards to controller performance.

The valve position controller brought the valve position back to its setpoint, whilst introducing disturbances in the power output leading to the overshoot. A future recommendation is to add a filter to the valve position controller that can remove the overshoot and improve the overall performance of the controller. A recent source of valve position control decoupling filter can be found in [Slätteke, 2006, p.149-151].

Bibliography

Alobaid, F., Mertens, N., Starkloff, R., Lanz, T., Heinze, C., and Epple, B. (2017). Progress in dynamic simulation of thermal power plants. *Progress in Energy and Combustion Science*, 59:79–162.

Andersskog, I. (2018). Control Oriented Modelling of a Steam Cycle. Technical report, Norwegian University of Science and Technology.

Åström, K. J. (2002). Control system design. `http://clux.x-pec.com/files/ fronter/ENE103%20-%20Reguleringsteknikk/fagstoff/suplement% 20Reg%20tek%20engelsk%20.pdf`.

Batalov, A. (2011). Pressure-Flow Network Modeling. Technical report, Department of Engineering Cybernetics, NTNU, Trondheim.

Blaazer, M. J. (2010). *Advanced process control for power plants - Improving overall performance through control of internal process variables*. PhD thesis, Delft University of Technology.

Blackman, A., Gahan, L. R., Aylward, G. H., and Findlay, T. J. V. (2013). *Aylward and Findlay's SI Chemical Data*. John Wiley & Sons Australia.

Breeze, P. (2012). Pushing the steam cycle boundaries. `https://www. powerengineeringint.com/articles/print/volume-20/issue-4/ features/pushing-the-steam-cycle-boundaries.html`.

Celis, C., Pinto, G. R., Teixeira, T., and Xavier, É. (2017). A steam turbine dynamic model for full scope power plant simulators. *Applied Thermal Engineering*, 120:593–602.

ChemicaLogic Corporation (1998). Pressure-Enthalpy Diagram for Water and Steam. `http: //www.chemicalogic.com/Documents/mollier_chart_metric.pdf`.

Cooke, D. H. (1985). On Prediction of Off-Design Multistage Turbine Pressures by Stodola's Ellipse. *Journal of Engineering for Gas Turbines and Power*, 107(3):596.

Ganapathy, V. (2002). *Industrial Boilers and Heat Recovery Steam Generators: Design, Applications, and Calculations*. Dekker Mechanical Engineering. Taylor & Francis.

Greene, C. (2014). fullfig. `https://se.mathworks.com/matlabcentral/ fileexchange/48071-fullfig`.

Gustavsson, A. and Rönnberg, J. K. (2016). *Investigating an iterative method for tuning decentralised PI-controllers in TITO systems*. PhD thesis, Chalmers University of Technology.

Halevi, Y., Palmor, Z. J., and Efrati, T. (1997). Automatic tuning of decentralized PID controllers for MIMO processes. *Journal of Process Control*.

Heat Exchange Institute (2015). Condenser hotwells. `https://www.heatexchange.org/pdf/techsheets/TechSheet136.pdf`.

Himmelblau, D. M. and Riggs, J. B. (2012). *Basic Principles and Calculations in Chemical Engineering*. Always learning. Prentice Hall.

Holmgren, M. (2007). XSteam.m. `https://se.mathworks.com/matlabcentral/fileexchange/9817-x-steam-thermodynamic-properties-of-water-and-steam`.

Hovd, M. and Skogestad, S. (1993). Improved independent design of robust decentralized controllers. *Journal of Process Control*.

Ivković, M., Ivković, D., and Ivković, H. (2011). Technical solution abilities of flue gas thermal power consumption on compressor station Struzec. Technical report.

Jha, S. K. and Kaistha, N. (2007). Valve Positioning Control for Process Through-put Maximization. *Chemical Engineering Research & Design - CHEM ENG RES DES*, 85:1465–1475.

Kovacs, J. (2004). Power Plant Control, Lecture notes. Technical report.

Mazzi, N., Rech, S., and Lazzaretto, A. (2015). Off-design dynamic model of a real Organic Rankine Cycle system fuelled by exhaust gases from industrial processes. *Energy*, 90:537–551.

McKetta, J. J. (1997). *Encyclopedia of Chemical Processing and Design: Volume 61 - Vacuum System Design to Velocity: Terminal in Setting: Estimation*. Chemical Processing and Design Encyclopedia. Taylor & Francis.

Oryds, A., Pike, A., Johnson, M., Katebi, R., and Grimble, M. (1994). *Modelling and simulation of power generation plants*. Springer-Verlag.

Øverli, J. (1981). *Strømningsmaskiner, Bind 3 Termiske maskiner*. Tapir akademisk forlag.

Perry, R., Green, D., and Maloney, J. (1997). *Perry's chemical engineers' handbook*. McGraw-Hill, 7 edition.

Reyes-Lúa, A., Zotica, C., Das, T., Krishnamoorthy, D., and Skogestad, S. (2018). Changing between Active Constraint Regions for Optimal Operation: Classical Advanced Control versus Model Predictive Control. *Computer Aided Chemical Engineering*, 43:1015–1020.

Rua Pazoz, J. (2017). *Dynamic Modeling and Process Simulation of Steam Bottoming Cycle*. PhD thesis, Norwegian University of Science and Technology.

Scaife, W. G. (1985). The Parsons Steam Turbine. *Scientific American*, 252(4):132–139.

Sinnott, R. and Towler, G. (2009). *Chemical Engineering Design: SI edition*. Chemical Engineering Series. Elsevier Science.

Skogestad, S. (2003). Simple analytic rules for model reduction and PID controller tuning. *Journal of Process Control*, 13(4):291–309.

Skogestad, S. (2004). Control structure design for complete chemical plants. *Computers & Chemical Engineering*, 28(1-2):219–234.

Skogestad, S. (2009). *Prosessteknikk Masse- og energibalanser*. Tapir akademisk forlag.

Skogestad, S. and Grimholt, C. (2012). The SIMC method for smooth PID controller tuning. *Advances in Industrial Control*, pages 147–175.

Skogestad, S. and Morari, M. (1989). Robust performance of decentralized control systems by independent designs. *Automatica*, 25(1):119–125.

Skogestad, S. and Postlethwaite, I. (2005). *Multivariable Feedback Control: Analysis and Design*. John Wiley and Sons Ltd.

Slätteke, O. (2006). *Modeling and Control of the Paper Machine Drying Section*. PhD thesis, Lund University.

Tanuma, T. (2017). *Advances in Steam Turbines for Modern Power Plants*. Elsevier.

The International Association for the Properties of Water and Steam (2007). IAPWS Industrial Formulation 1997 for the Thermodynamic Properties of Water and Steam. `http://www.iapws.org/relguide/IF97-Rev.pdf`.

The MathWorks Inc (2018). Simulink. `https://se.mathworks.com/products/simulink.html?s_tid=hp_ff_p_simulink`.

The MathWorks Inc (2019a). Anti-Windup Control Using a PID Controller. `https://se.mathworks.com/help/simulink/slref/anti-windup-control-using-a-pid-controller.html?requestedDomain=`.

The MathWorks Inc (2019b). Choose a solver. `https://se.mathworks.com/help/simulink/ug/types-of-solvers.html`.

The MathWorks Inc (2019c). How Acceleration Modes Work. `http://www.mathworks.de/de/help/simulink/ug/how-the-acceleration-modes-work.html`.

van Putten, H. and Colonna, P. (2007). Dynamic modeling of steam power cycles: Part II - Simulation of a small simple Rankine cycle system. *Applied Thermal Engineering*, 27(14):2566–2582.

Welfonder, E. (1999). Dynamic interactions between power plants and power systems. *Control Engineering Practice*, 7(1):27–40.

Wu, X., Shen, J., Li, Y., and Lee, K. Y. (2015). Steam power plant configuration, design, and control. *WIREs Energy Environment*, 4(6):537–563.

Ziegler, J. G. and Nichols, N. B. (1993). Optimum Setting for Automatic Controllers. *Transactions of ASME*, pages 759–768.

Appendix A

Appendix

A.1 Units

The symbol and units for the respected quantities used during the simulation are listed in Table A.1 below.

Table A.1: Symbols and SI units for the quantities in the steam cycle

Quantity	Symbol	SI Units
Mass	M	kg
Rotational speed	N	rads^{-1}
Enthalpy	H	J
Specific enthalpy	h	Jkg^{-1}
Temperature	T	K
Heat flow	Q	Js^{-1}
Pressure	P	Pa
Power	W	W
Mass flow	$\dot{m}$	kgs^{-1}
Volumetric flow rate	q	$m^3 s^{-1}$
Universal gas constant	R	J$mol^{-1}K^{-1}$
Molar mass	Mm	kgmol^{-1}
Volume	V	m^3
Heat capacity	C_p	J$kg^{-1}K^{-1}$
Heat of vaporization	ΔH_{vap}	Jkg^{-1}
Heat transfer coefficient multiplied with the surface area	UA	W$m^{-2}K^{-1}$
Valve coefficient	K_v	kgPa$^{-1}s^{-1}$
Stodola coefficient	K_t	m^{-3}

Table A.2: SI unit conversion table

Quantity	Unit	Conversion factor to SI units
P	Bar	10^5 Pa
T	°C	T + 273.15 K

A.2 Parameters

The parameters used during the simulation are listed in Table A.3.

Table A.3: Parameter values

Parameter	Symbol	Value	Units
Volumetric flow	q	0.2506	$\mathrm{m^3s^{-1}}$
Universal gas constant	R	8.3145	$\mathrm{Jmol^{-1}K^{-1}}$
Molar mass of water	Mm_{water}	18e-3	$\mathrm{kgmol^{-1}}$
Volume in the attemperator	V_{mix}	1	$\mathrm{m^3}$
Volume in the turbine	$V_{turbine}$	0.01	$\mathrm{m^3}$
Specific heat capacity of steam	$C_{p,Steam}$	2000	$\mathrm{Jkg^{-1}K^{-1}}$
Specific heat capacity of the flue gas	$C_{p,FG}$	1063.1	$\mathrm{Jkg^{-1}K^{-1}}$
Specific heat capacity of water	$C_{p,Water}$	4180	$\mathrm{Jkg^{-1}K^{-1}}$
High pressure turbine outlet pressure	$P_{t,hp}$	4.0406e5	Pa
Low pressure turbine outlet pressure	$P_{t,lp}$	9.6146e3	Pa
Pump outlet pressure	P_p	100e5	Pa
Inlet temperature of flue gas	$T_{FG,0}$	1273.15	K
Reference temperature at P = 9.6146e3 Pa	T_{ref}	318.15	K
Reference temperature at P = 99.28e5 Pa	$T_{ref,bp}$	584.0688	K
Heat of vaporization for water at T_{ref}	$\Delta_{vap,45}H$	2394e3	$\mathrm{Jkg^{-1}}$
Heat of vaporization for water at $T_{ref,bp}$	$\Delta_{vap,311}H$	1321.9e3	$\mathrm{Jkg^{-1}}$
UA for the HEX in the economizer	UA_{eco}	5.2104e4	$\mathrm{Wm^{-2}K^{-1}}$
UA for the HEX in the drum	UA_d	2.5095e4	$\mathrm{Wm^{-2}K^{-1}}$
UA for the HEX in the superheater	UA_{sh}	7.5964e3	$\mathrm{Wm^{-2}K^{-1}}$
UA for the HEX in the reheater	UA_r	1.6560e4	$\mathrm{Wm^{-2}K^{-1}}$
Valve coefficient for $\dot{m}_{sh}$	$K_{v,sh}$	4.6851e-5	$\mathrm{kgPa^{-1}s^{-1}}$
Valve coefficient for $\dot{m}_a$	$K_{v,a}$	1.3759e-5	$\mathrm{kgPa^{-1}s^{-1}}$
Machine construction constant	k_1	1.1837e-17	$\mathrm{m^2}$
Machine construction constant	k_2	0	$\mathrm{m^4}$
Load dependent constant	k_3	7.8993e+07	$\mathrm{m^{-4}}$
Pump efficiency	η	0.9	-
Fluid density reference value	ρ_{ref}	974	$\mathrm{kgm^{-3}}$
Static pressure rise across pump	ΔP_s	6.7595e+06	Pa

A.3 Steady state data and nominal values

The steady state data (initial values) and nominal values used in the simulation are rendered in Table A.4 and A.5 below, respectively. The variables were scaled during the simulation for numerical purposes.

Table A.4: Table with the design data for the Heat-to-Power cycle states

State	Steady state values	Scaling	Units
M_{eco}	1	-	kg
T_{eco}	5.8407	10^{-2}	K
$T_{FG,eco}$	4.2480	10^{-2}	K
T_{mix}	5.6182	10^{-2}	K
M_d	1.000	10^{-2}	kg
H_d	2.4334	10^{-9}	J
T_d	5.8407	10^{-2}	K
$T_{FG,d}$	7.1102	10^{-2}	K
T_{sh}	8.7678	10^{-2}	K
$T_{FG,sh}$	1.1086	10^{-3}	K
M_a	2.6450	10^{-1}	kg
T_a	8.0215	10^{-2}	K
$M_{turbine}$	2.5080	10	kg
M_c	5.0000	10^{-2}	kg
T_r	7.5169	10^{-2}	K
$T_{FG,r}$	4.1772	10^{-2}	K

Table A.5: Nominal values used for the inputs in the simulation

Input	Nominal value	Units
$\dot{m}_d$	5.9750	$\text{kg}s^{-1}$
$\dot{m}_{a,b}$	0.3108	$\text{kg}s^{-1}$
$\dot{m}_{eco,b}$	0.5000	$\text{kg}s^{-1}$
z	0.9000	-
$\dot{Q}_c$	-1.5048e+07	$\text{J}s^{-1}$
$\dot{m}_{FG}$	20.000	$\text{kg}s^{-1}$
$\dot{m}_{FG,r}$	5.0000	$\text{kg}s^{-1}$

A.4   Setpoints for the PID-controllers

The setpoints for the Heat-to-Power cycle controllers are listed in Table A.6.

Table A.6: Setpoints for the Heat-to-Power cycle PID controllers

State	Setpoint	Scaling	Unit
$T_{FG,eco}$	4.2480	10^{-2}	K
M_d	1.0000	10^{-2}	kg
T_a	8.0215	10^{-2}	K
P_d	9.9280	10^{-6}	Pa
W	-10.6317	10^{-6}	W
T_r	7.5169	10^{-2}	K
T_c	3.1815	10^{-2}	K
z_t	0.9000	-	-

A.5 Process transfer functions for the controllers

The independent process transfer function for each controller pairing are derived and represented in Equations A.1-A.6 below by linearization (Taylor approximation) and Laplace transformation of the design equations. The process transfer function for the saturation pressure, P_d and the flue gas, $\dot{m}_{FG}$ was not computed because of the complexity of the Antoine Equation. The same is for the process transfer function for the power output, W, and z_t and $\dot{m}_{FG}$.

$$M_d(s) = \frac{1}{s}\dot{m}_d(s) \tag{A.1}$$

$$\Delta T_{FG,eco} = \left[\frac{2}{UA_{eco}}(T_{eco} - T_c)\right]^* \Delta \dot{m}_{eco,b} \tag{A.2}$$
$$\Delta T_{FG,eco} = 0.0102\Delta meco, b$$

$$\Delta T_a(s) = \left[\frac{C_{p,Water}(T_c - T_{ref}) - C_{p,Steam}T_a}{C_{p,Steam}M_a s + \dot{m}_a C_{p,Steam}}\right]^* \Delta ma_b(s) \tag{A.3}$$
$$\Delta T_a(s) = \frac{-127.61}{4.21s + 1}\Delta ma_b(s)$$

$$\Delta T_r = \left[\frac{C_{p,FG}(T_{FG,0} - T_{FG,r})}{\dot{m}_t C_{p,Steam}}\right]^* \Delta \dot{m}_{FG,r} \tag{A.4}$$
$$\Delta T_r = 72.34\Delta \dot{m}_{FG,r}$$

$$\Delta T_c = \left[\frac{1}{M_c C_{pWater}s + \dot{m}_p C_{p,Water}}\right]^* \Delta Q_c \tag{A.5}$$
$$\Delta T_c = \frac{3.807e-5}{6.365s + 1}\Delta Q_c$$

$$\Delta P_d = \left[-\frac{\dot{m}_a}{K_{v,a}z_t^2}\right]^* \Delta z_t \tag{A.6}$$
$$\Delta P_d = -5.64e5\Delta z_t \tag{A.7}$$

A.6 Decentralized independent controller tuning of the boiler-driven and floating pressure control structures

Independent open loop step responses were made for each controller and a subsequent closed loop setpoint step response for closed loop tuning (varying τ_c) shown in the Figure A.1 - A.14 in the subsections below.

A.6.1 Drum holdup controller
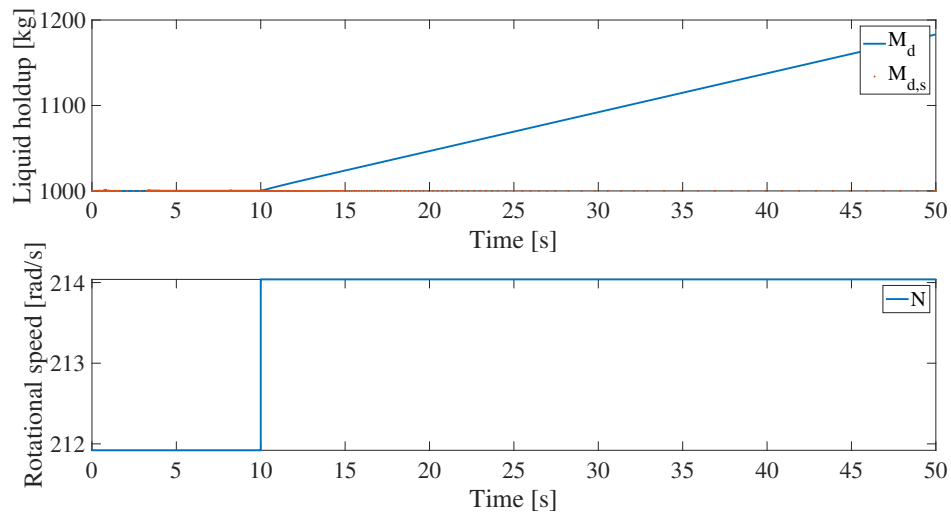
Figure A.1: Plot of M_d and N after a 1% open loop step response in N
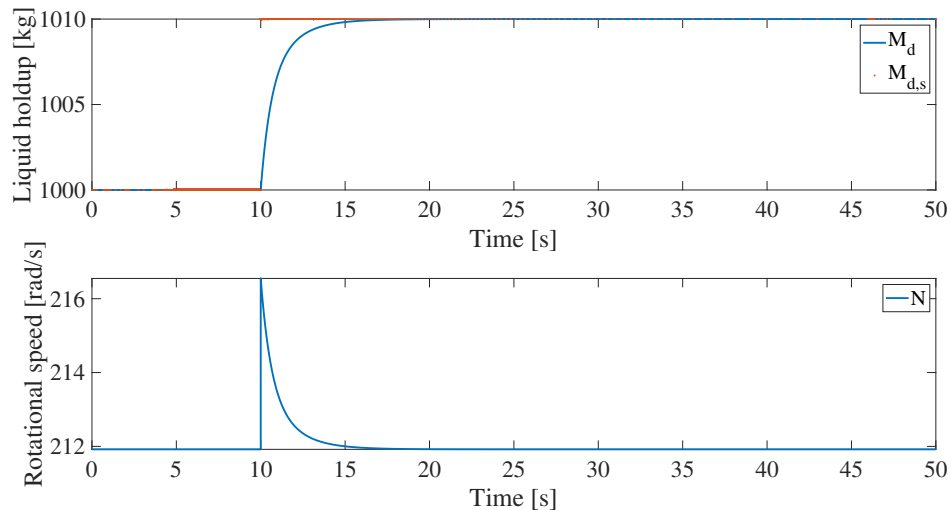
Figure A.2: Plot of M_d and N after a 1% closed loop setpoint change in M_{ds}
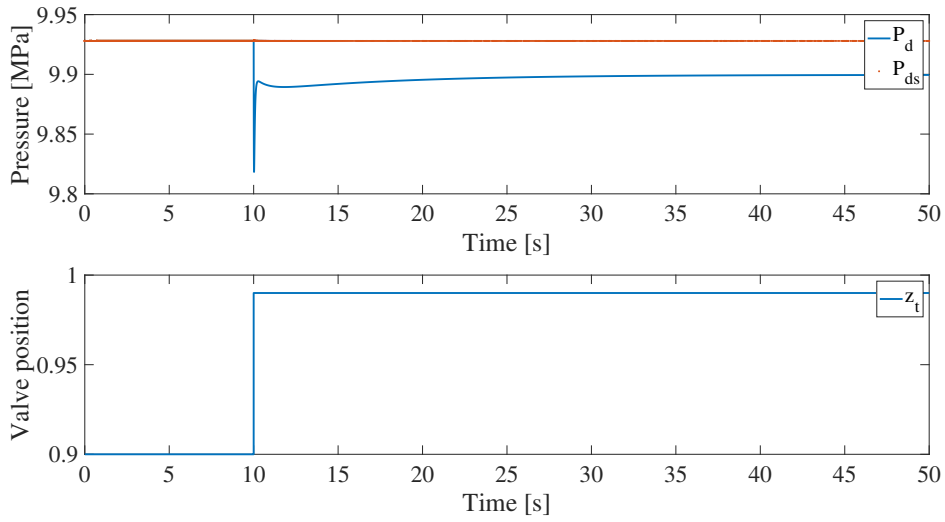
A.6.2 Flue gas temperature controller
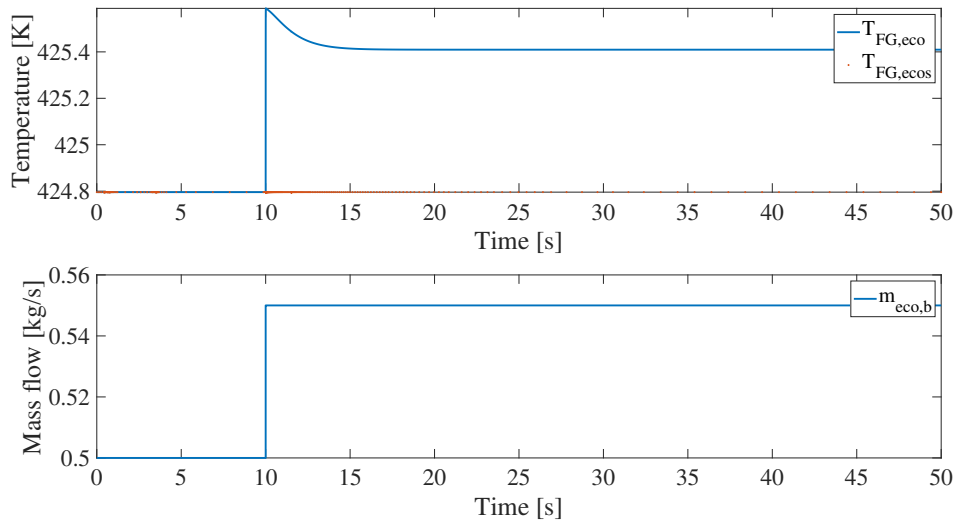
**Figure A.3:** Plot of $T_{FG,eco}$ and $\dot{m}_{eco,b}$ after a 10% open loop step response in $\dot{m}_{eco,b}$
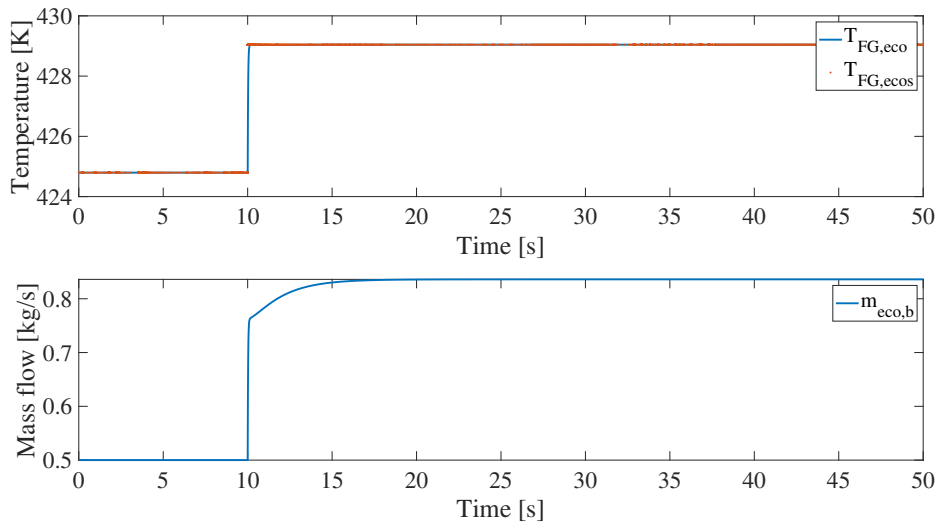
Figure A.4: Plot of $T_{FG,eco}$ and $\dot{m}_{eco,b}$ after a 1% closed loop setpoint change in $T_{FG,eco,s}$
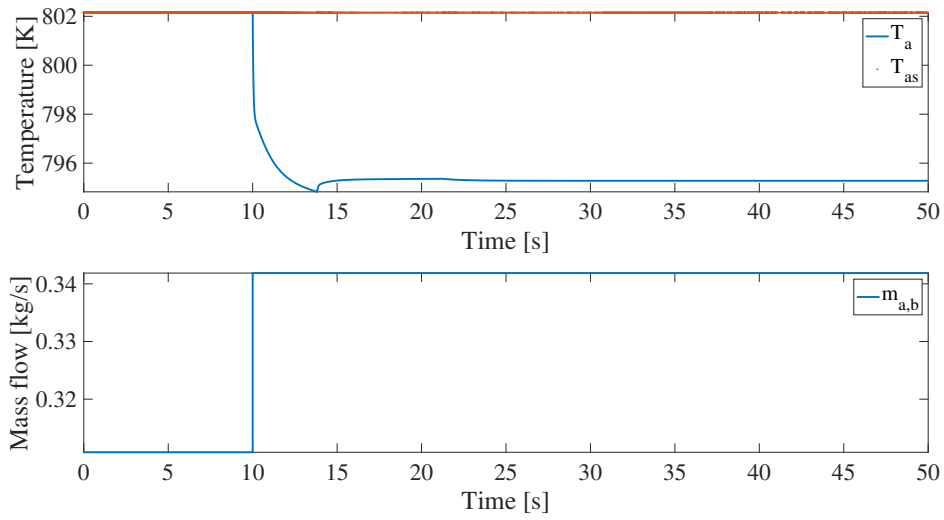
A.6.3 Attemperator temperature controller
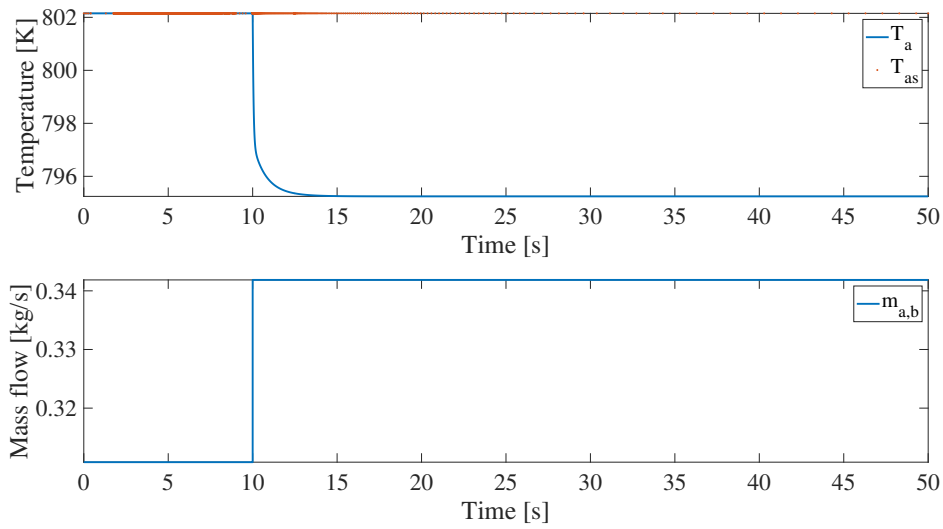
Figure A.5: Plot of T_a and $\dot{m}_{a,b}$ after a 10% open loop step response in $\dot{m}_{a,b}$
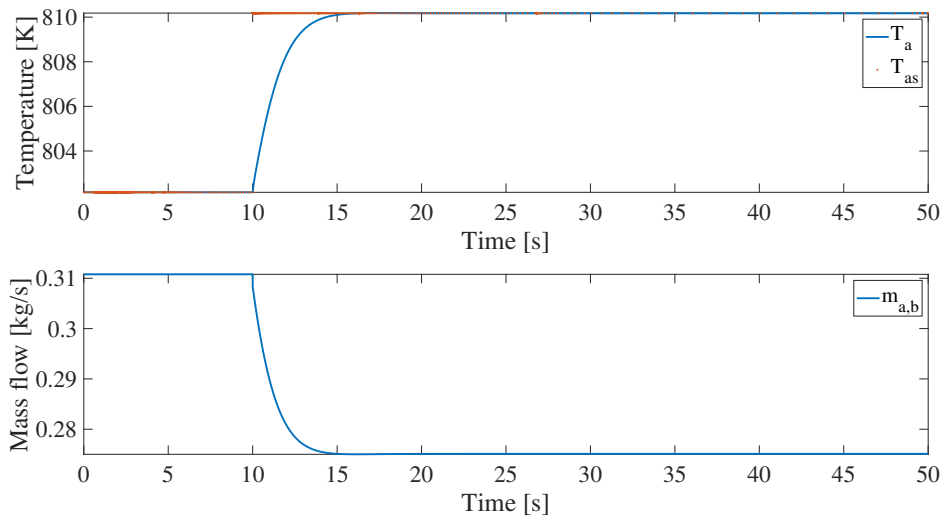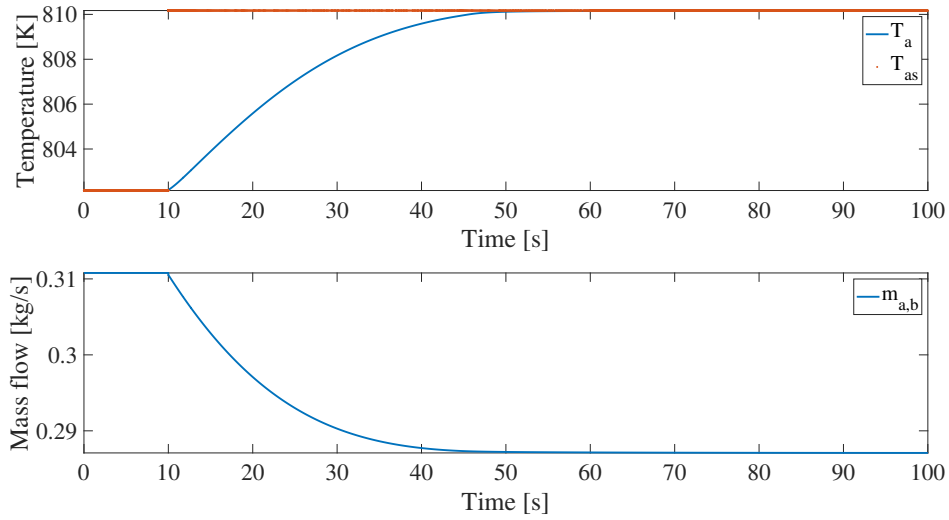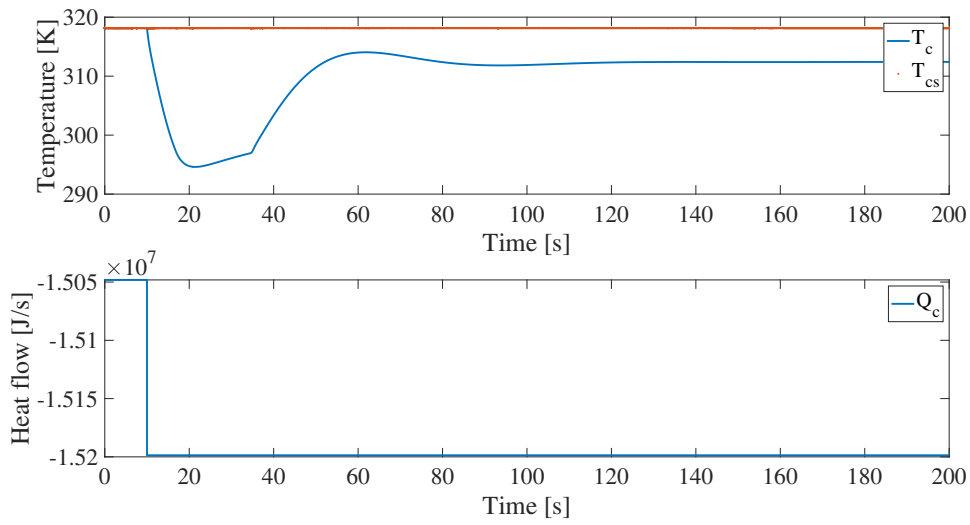

Figure A.6: Plot of T_a and $\dot{m}_{a,b}$ after a 1% closed loop setpoint change in T_{as}

A.6.4 Reheater temperature controller
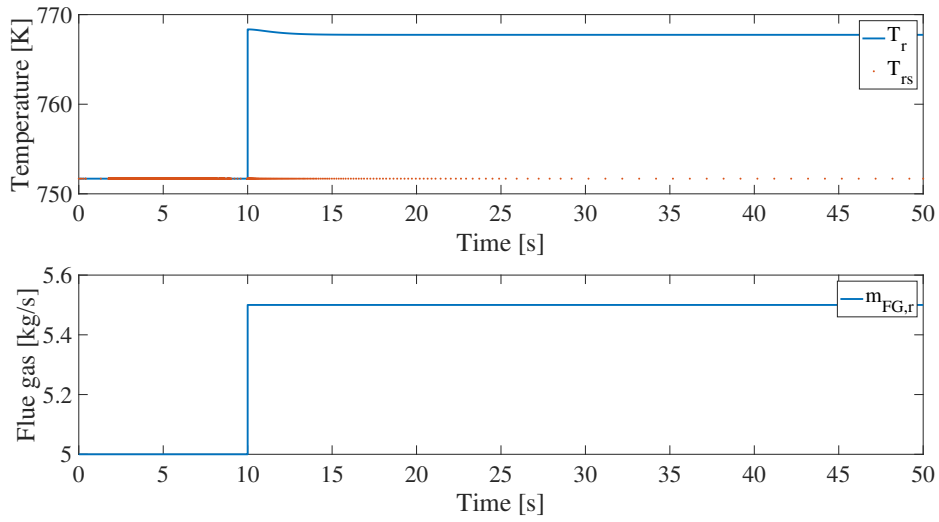
**Figure A.7:** Plot of T_r and $\dot{m}_{FG,r}$ after a 10% open loop step response in $\dot{m}_{FG,r}$
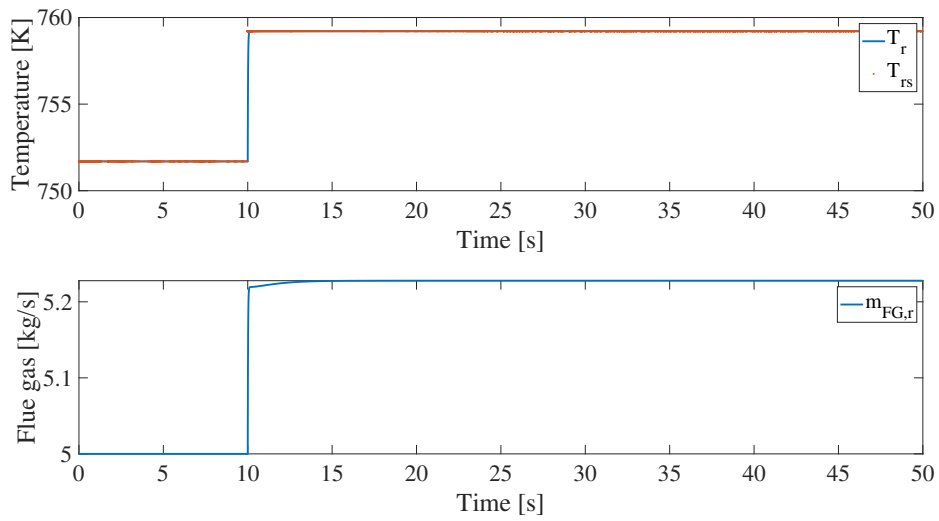
Figure A.8: Plot of T_r and $\dot{m}_{FG,r}$ after a 1% closed loop setpoint change in T_r

A.6.5 Condenser temperature controller
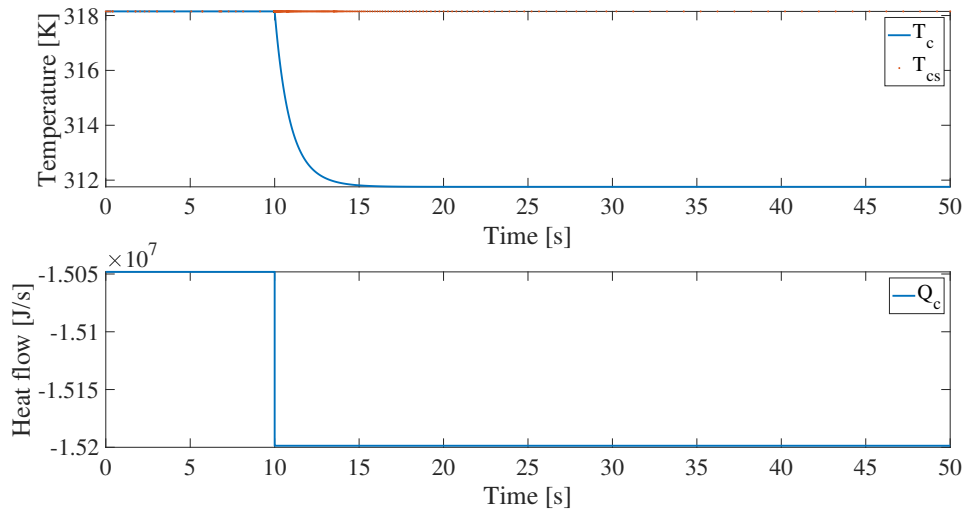
Figure A.9: Plot of T_c and $\dot{Q}_c$ after a 1% open loop step response in $\dot{Q}_c$
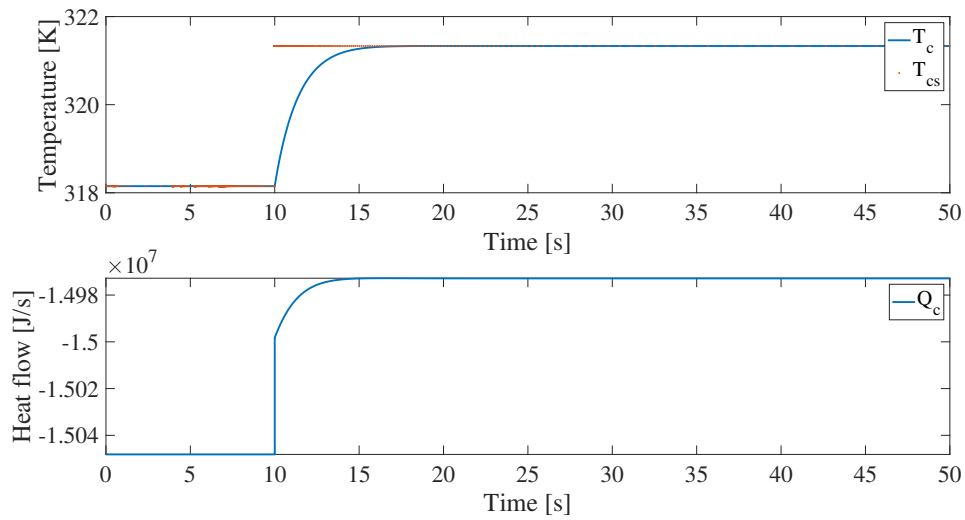
Figure A.10: Plot of T_c and $\dot{Q}_c$ after a 1% closed loop closed loop setpoint change in T_{cs}

A.6.6   Drum pressure controller
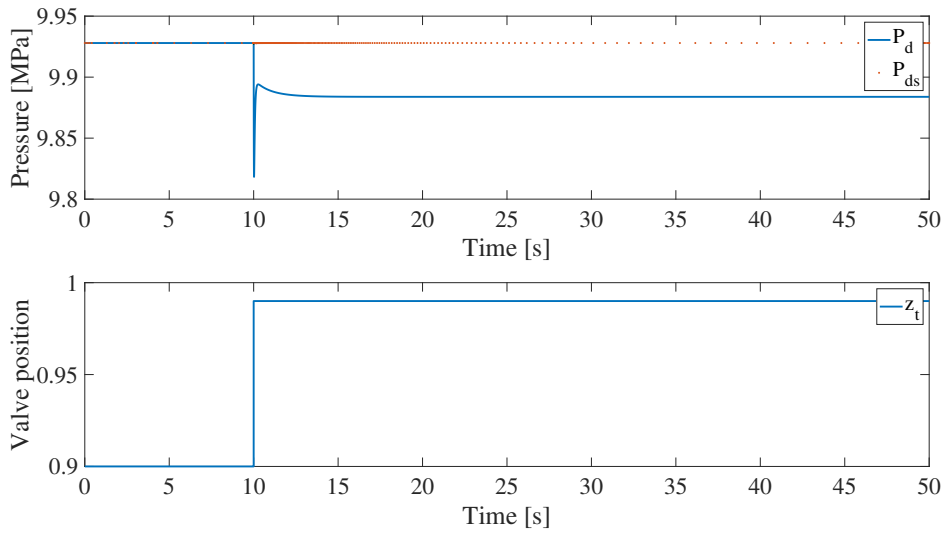
Figure A.11: Plot of P_d and z_t after a 10% open loop step response in z_t
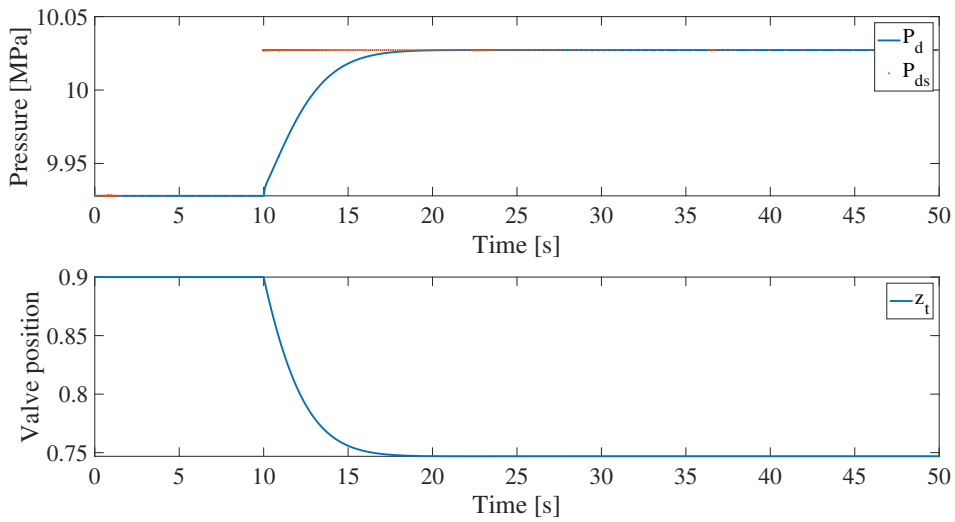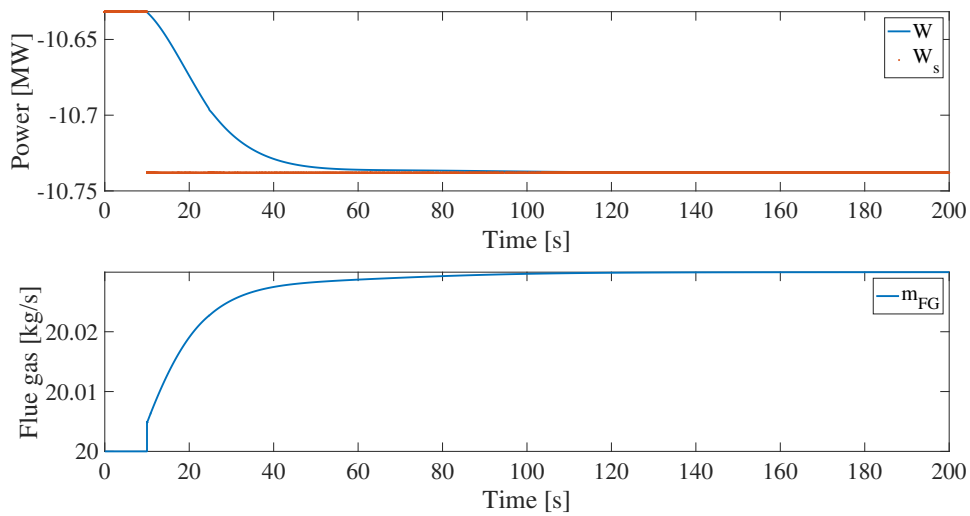

Figure A.12: Plot of P_d and z_t after a 1% closed loop setpoint change in P_{ds}

A.6.7 Power controller
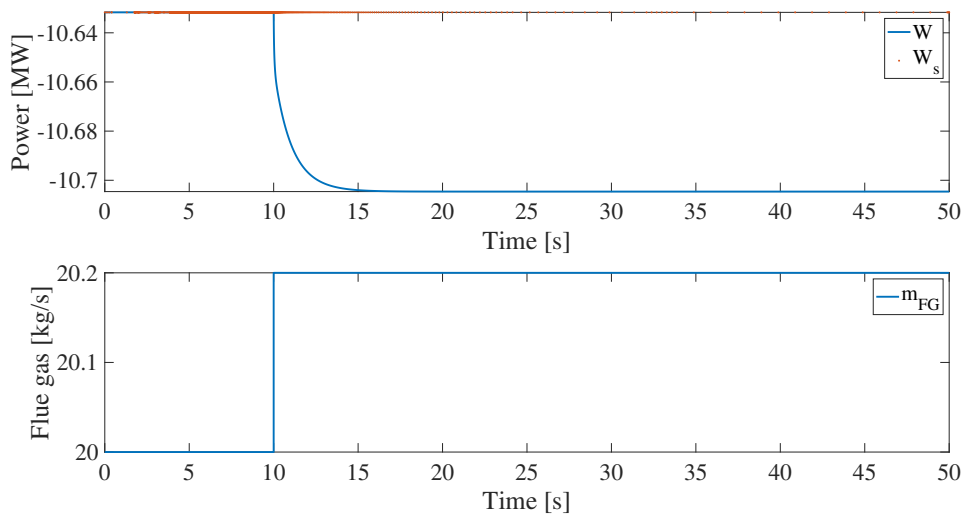
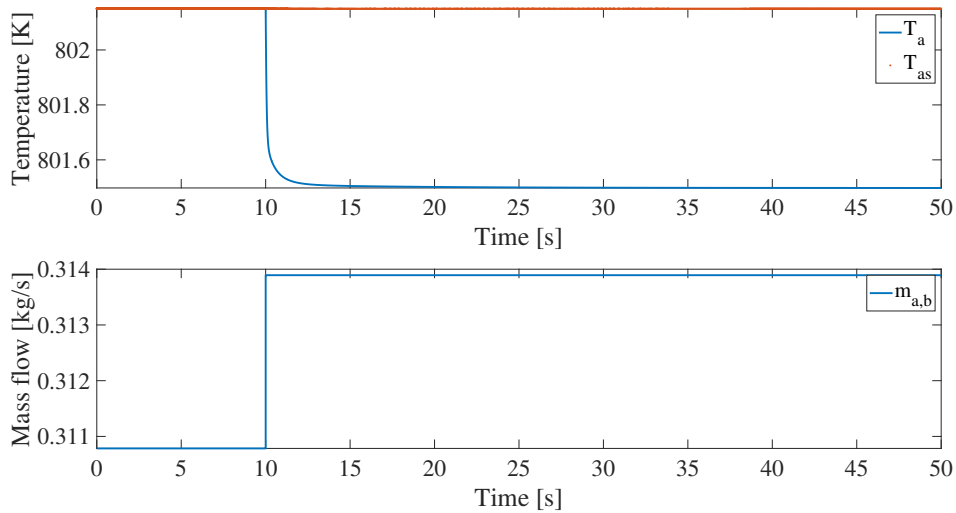**Figure A.13:** Plot of W and $\dot{m}_{FG}$ after a 1% open loop step response in $\dot{m}_{FG}$
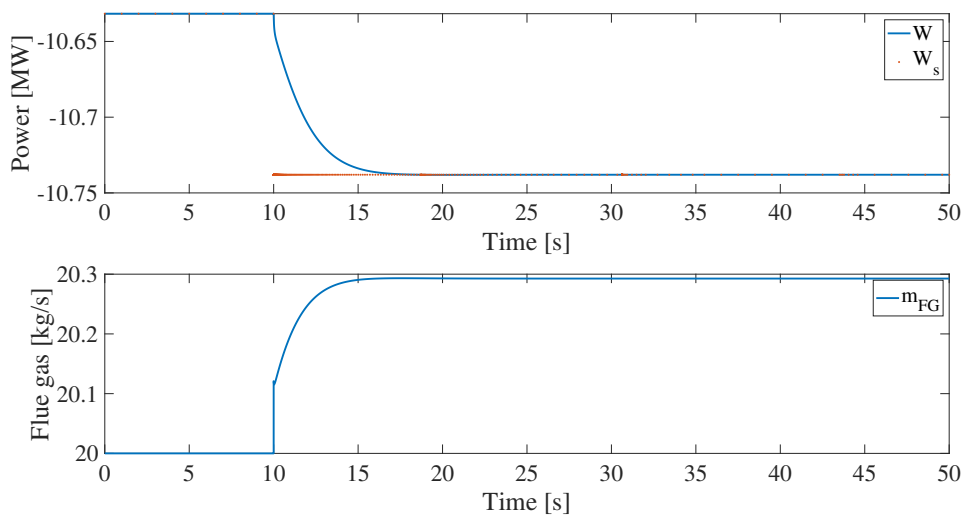
Figure A.14: Plot of W and $\dot{m}_{FG}$ after a 1% closed loop setpoint change in W_s

A.7 Decentralized independent controller tuning of the turbine-driven structure

The same open loop input step responses and closed loop setpoint responses can be accounted for the turbine-driven control structure for the drum holdup and temperature controllers as shown in Figure A.1 - A.10. Independent open loop step responses were made for the drum pressure, P_d, and power, W,- controller and a subsequent closed loop setpoint step response, shown in Figure A.15 - A.18.

A.7.1 Drum pressure controller
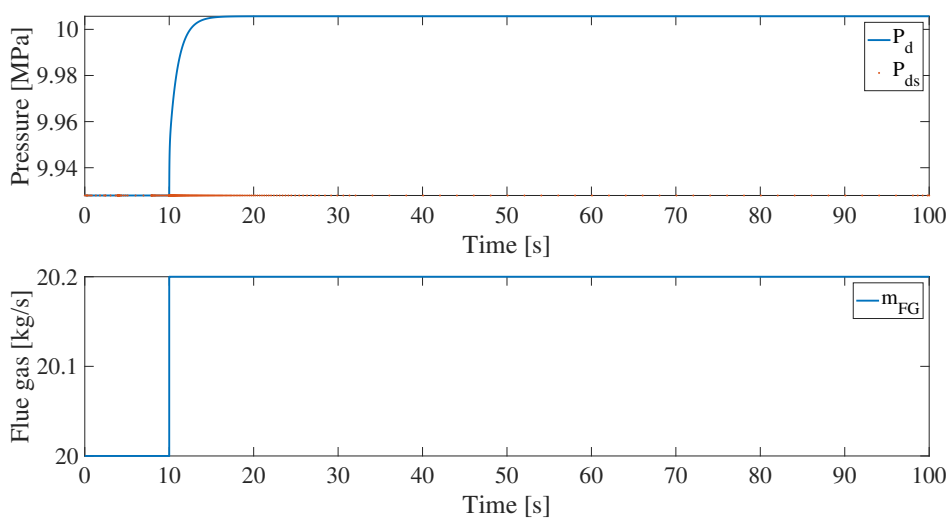
Figure A.15: Plot of P_d and $\dot{m}_{FG}$ after a 1% open loop step response in $\dot{m}_{FG}$
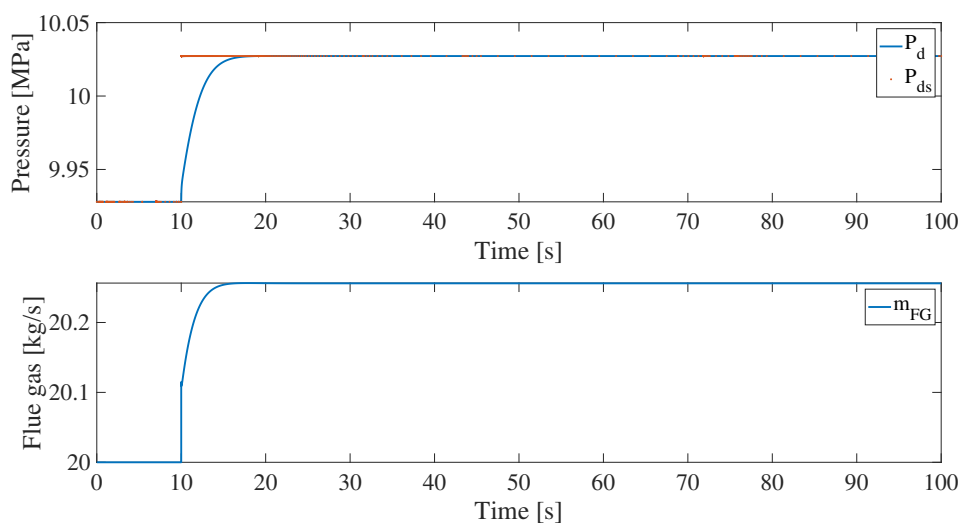
Figure A.16: Plot of P_d and $\dot{m}_{FG}$ after a 1% closed loop setpoint change in P_{ds}

A.7.2 Power controller
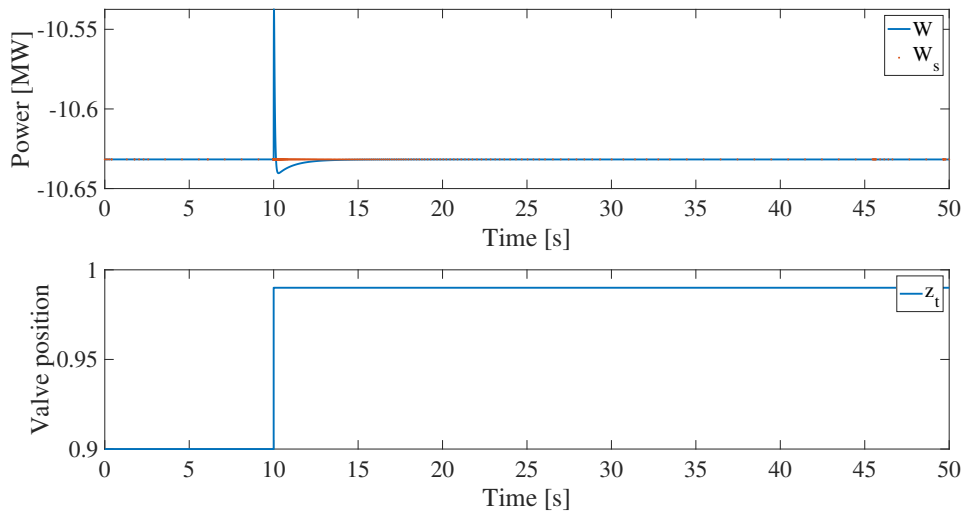
Figure A.17: Plot of W and z_t after a 10% open loop step response in z_t
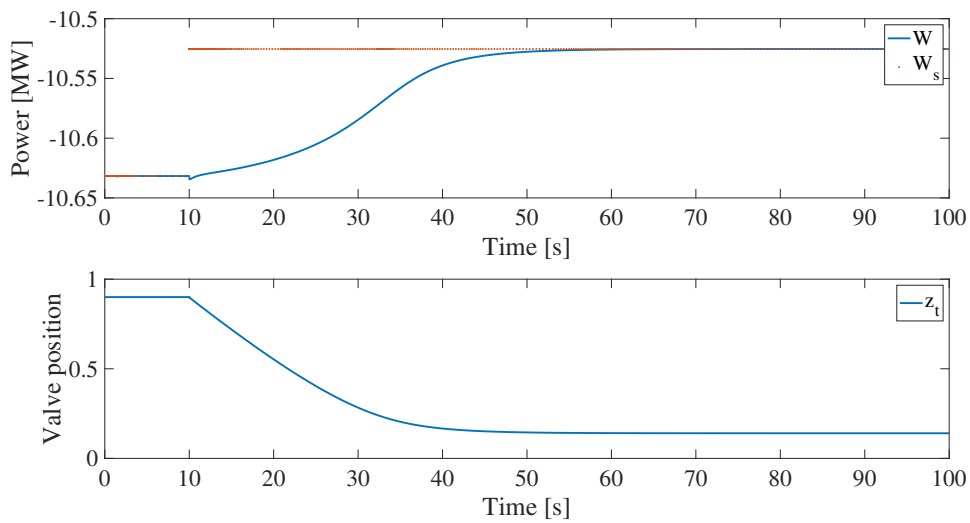
Figure A.18: Plot of W and z_t after a 1% closed loop setpoint decrease in W_s

A.8 Decentralized τ_1 - sequential controller tuning of the boiler-driven control structure

The M_d-controller was closed first as it is required to be active for safety purposes, the independent tunings can, therefore, be used in this case. The latter controllers in the τ_1-sequence for the boiler-driven control structure are tuned through open loop input step responses and verified through closed loop setpoint responses shown in the Figures A.19- A.30 below.

A.8.1 Reheater temperature controller
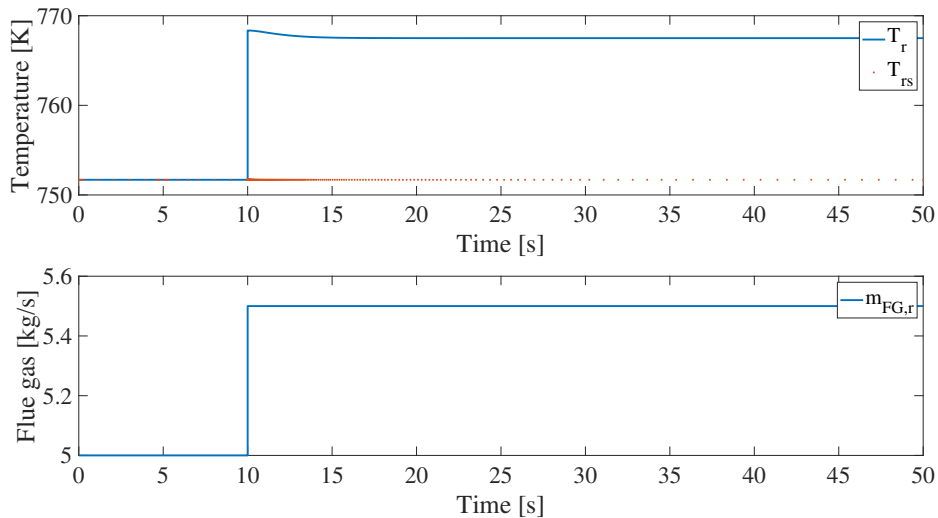
**Figure A.19:** Plot of T_r and $\dot{m}_{FG,r}$ after a 10% open loop step response in $\dot{m}_{FG,r}$
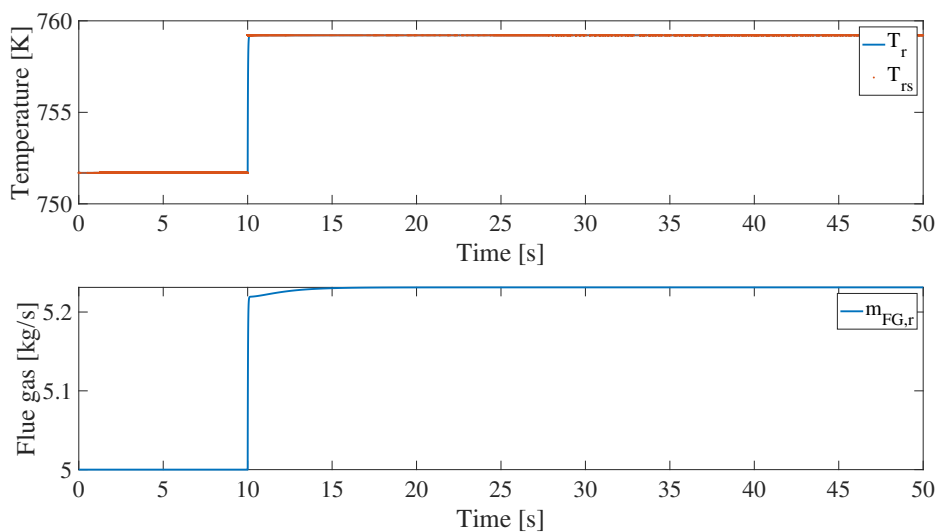
Figure A.20: Plot of T_r and $\dot{m}_{FG,r}$ after a 1% closed loop setpoint change in T_r

A.8.2 Flue gas temperature controller
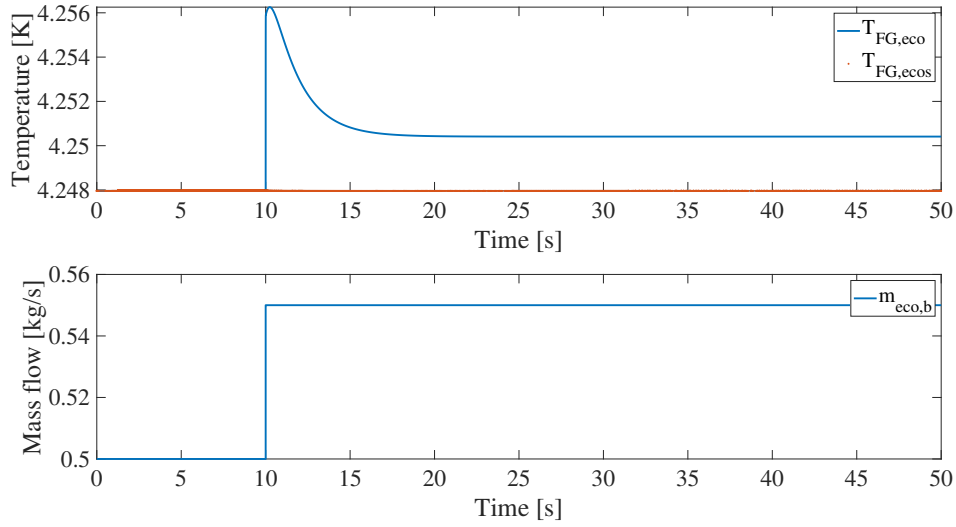
Figure A.21: Plot of $T_{FG,eco}$ and $\dot{m}_{eco,b}$ after a 10% open loop step response in $\dot{m}_{eco,b}$
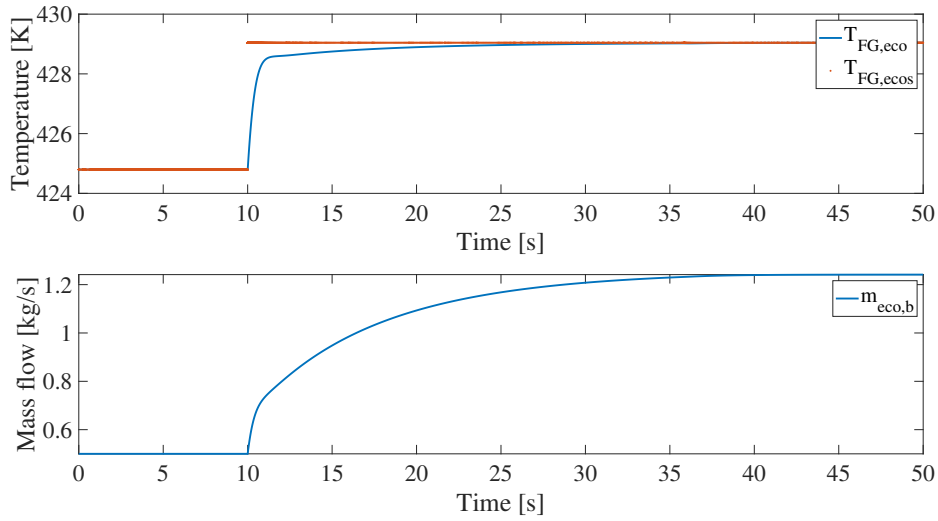
Figure A.22: Plot of $T_{FG,eco}$ and $\dot{m}_{eco,b}$ after a 1% closed loop setpoint change in $T_{FG,eco,s}$

A.8.3 Drum pressure controller

Figure A.23: Plot of P_d and z_t after a 10% open loop step response in z_t
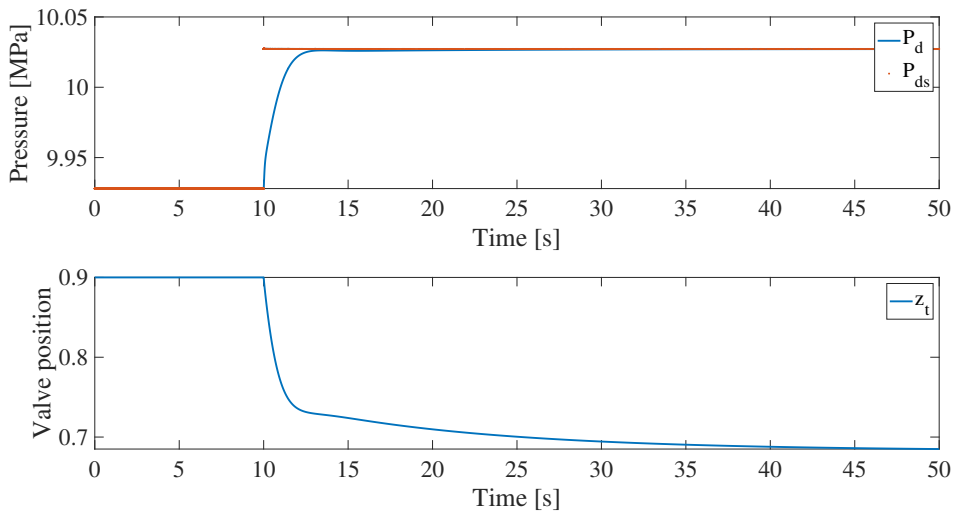
Figure A.24: Plot of P_d and z_t after a 1% closed loop setpoint change in P_{ds}

A.8.4 Attemperator temperature controller

Figure A.25: Plot of T_a and $\dot{m}_{a,b}$ after a 10% open loop step response in $\dot{m}_{a,b}$

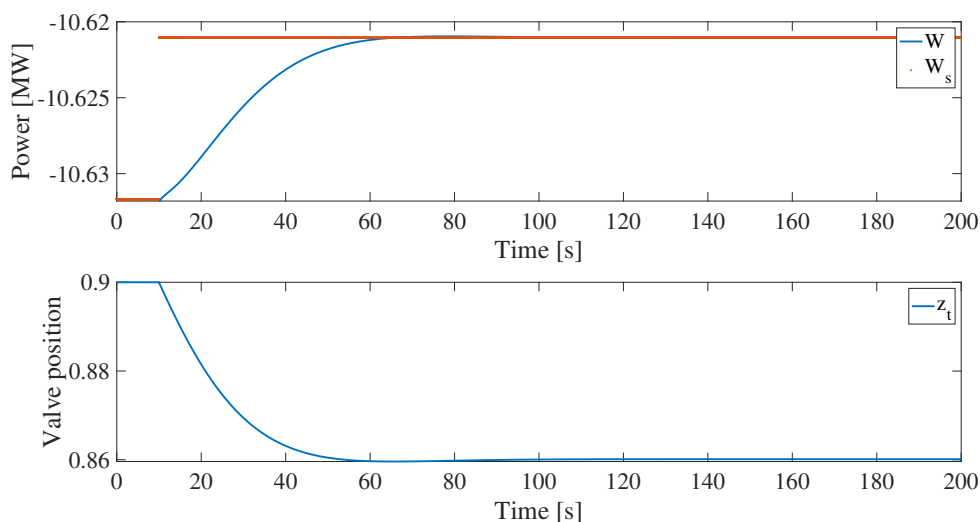**Figure A.26:** Plot of T_a and $\dot{m}_{a,b}$ after a 1% closed loop setpoint change in T_{as}

A.8.5   Condenser temperature controller

Figure A.27: Plot of T_c and $\dot{Q}_c$ after a 1% open loop step response in $\dot{Q}_c$
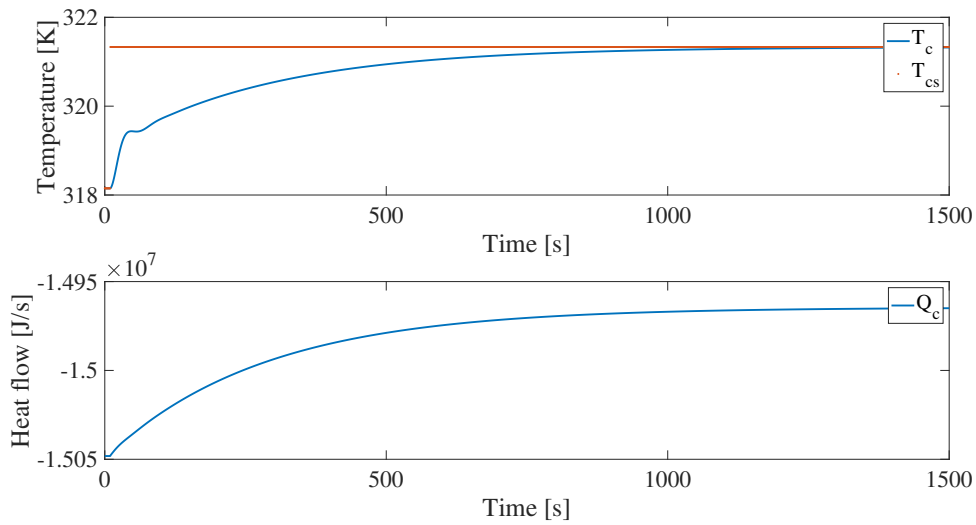
Figure A.28: Plot of T_c and $\dot{Q}_c$ after a 1% closed loop closed loop setpoint change in T_{cs}

A.8.6 Power controller
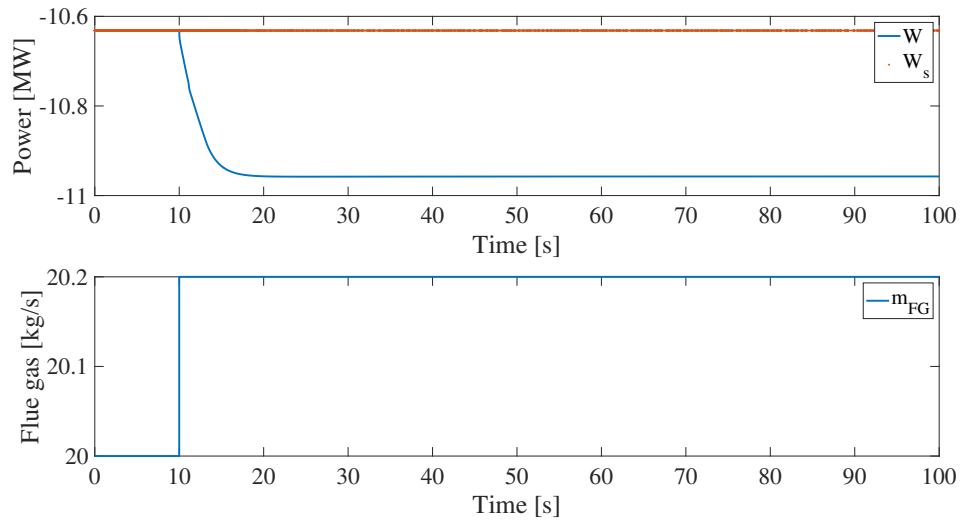
Figure A.29: Plot of W and $\dot{m}_{FG}$ after a 1% open loop step response in $\dot{m}_{FG}$

Figure A.30: Plot of W and $\dot{m}_{FG}$ after a 1% closed loop setpoint change in W_s

A.9 Decentralized τ_1 - sequential controller tuning of the floating pressure control structure

The tunings for the T_r-controller and $T_{FG,eco}$-controller from the boiler-driven τ_1 sequential controller tuning is used for the floating pressure control structure as well. The latter controllers in the sequence are tuned through open loop input step responses and verified through closed loop stepoint responses in Figures A.31- A.36 below.
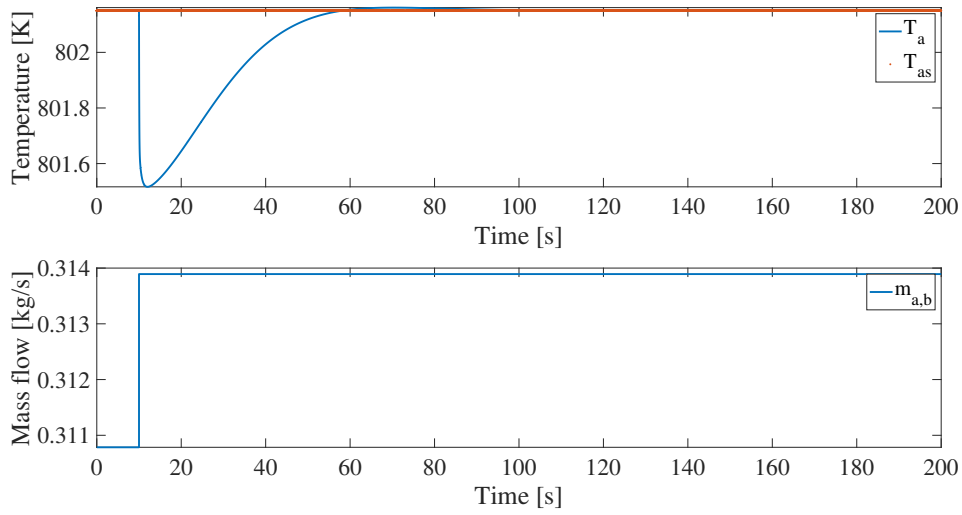
A.9.1 Attemperator temperature controller

Figure A.31: Plot of T_a and $\dot{m}_{a,b}$ after a 1% open loop step response in $\dot{m}_{a,b}$
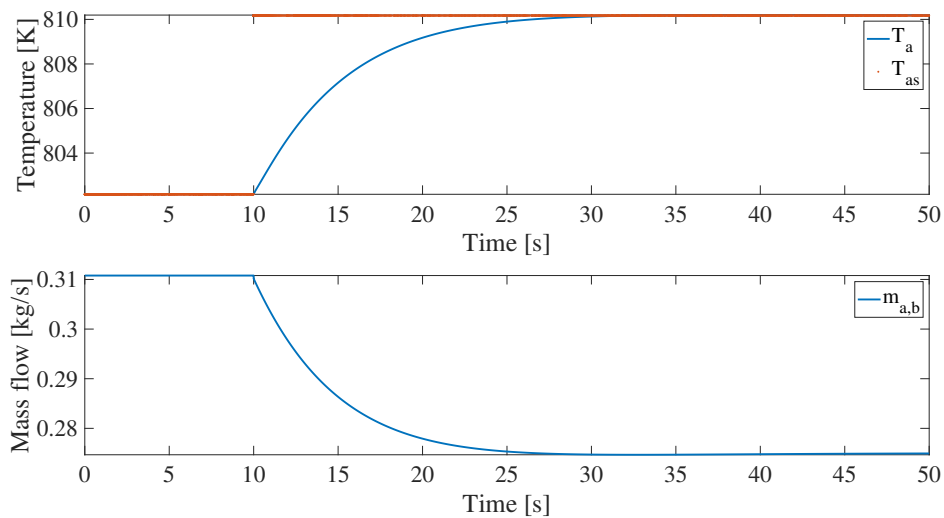
Figure A.32: Plot of T_a and $\dot{m}_{a,b}$ after a 1% closed loop setpoint change in T_{as}

A.9.2   Condenser temperature controller
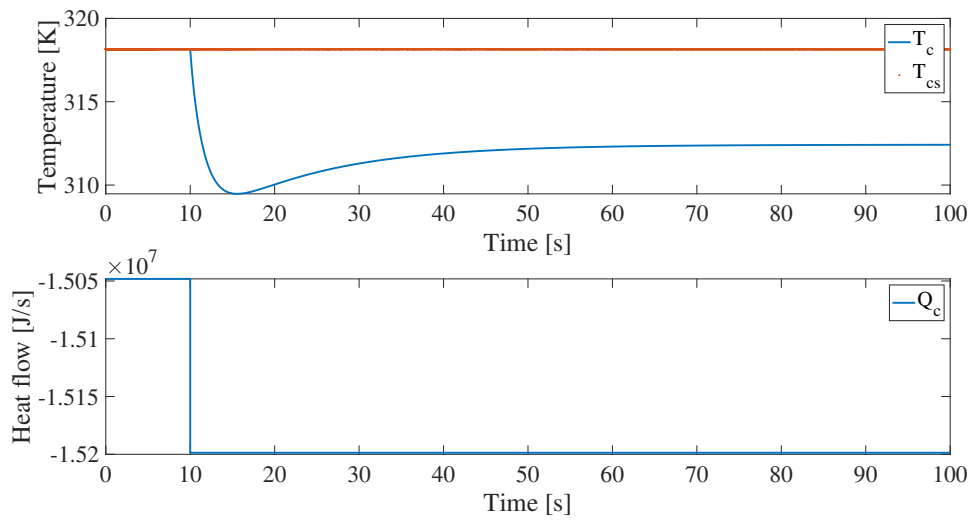
Figure A.33: Plot of T_c and $\dot{Q}_c$ after a 1% open loop step response in $\dot{Q}_c$
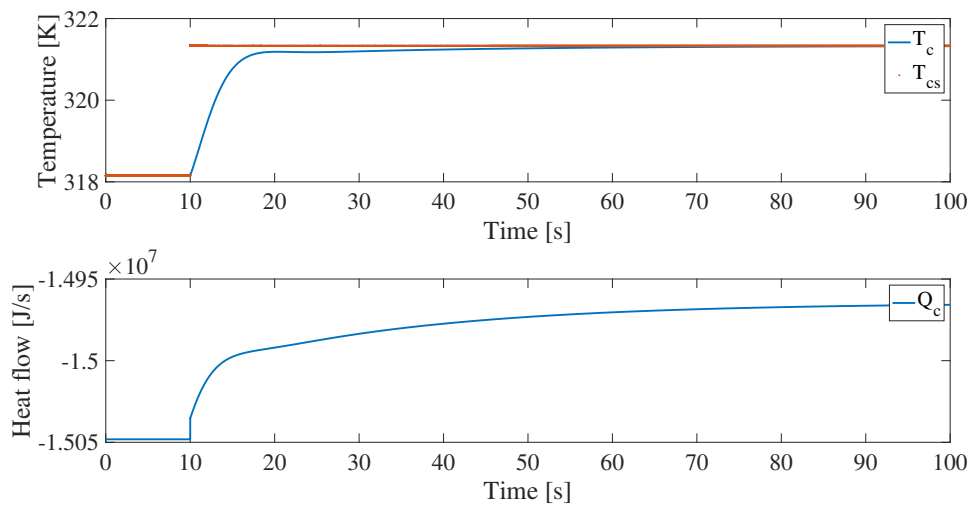
Figure A.34: Plot of T_c and $\dot{Q}_c$ after a 1% closed loop closed loop setpoint change in T_{cs}
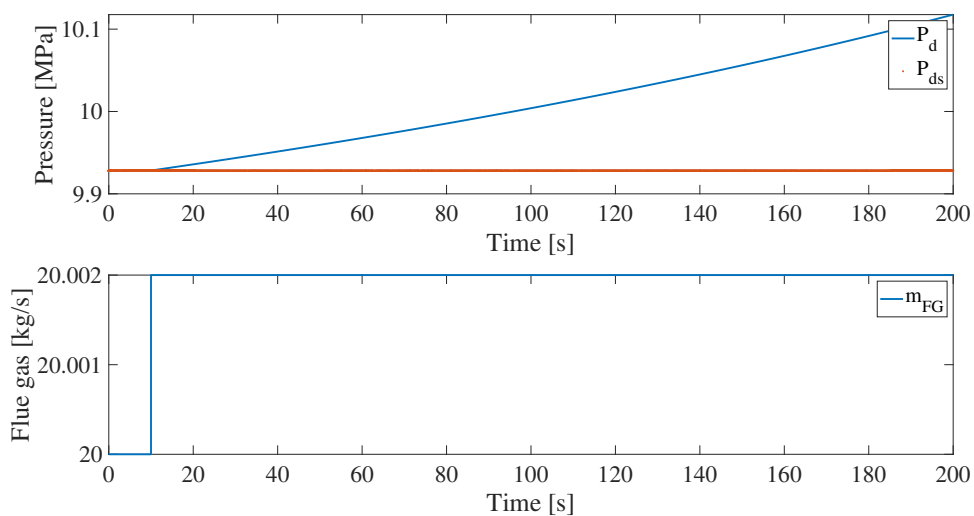
A.9.3 Power controller
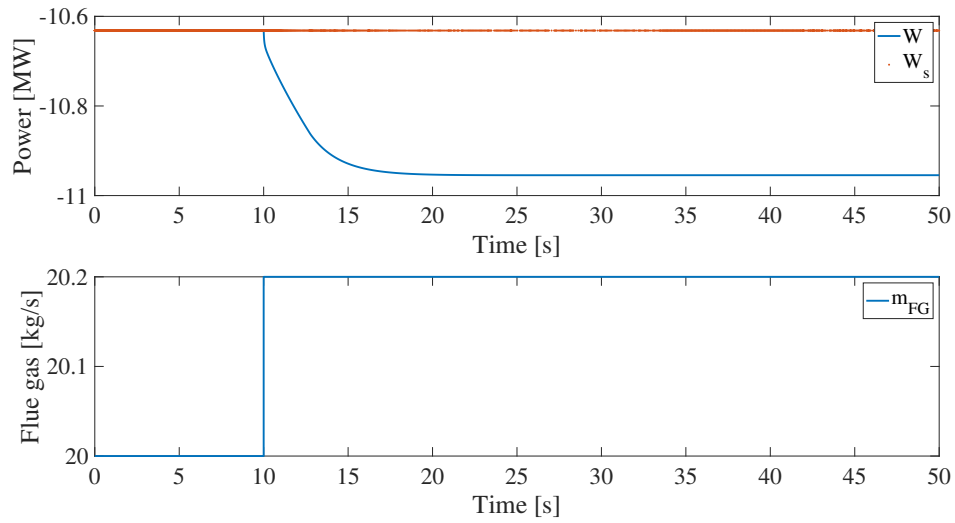
Figure A.35: Plot of W and $\dot{m}_{FG}$ after a 1% open loop step response in $\dot{m}_{FG}$
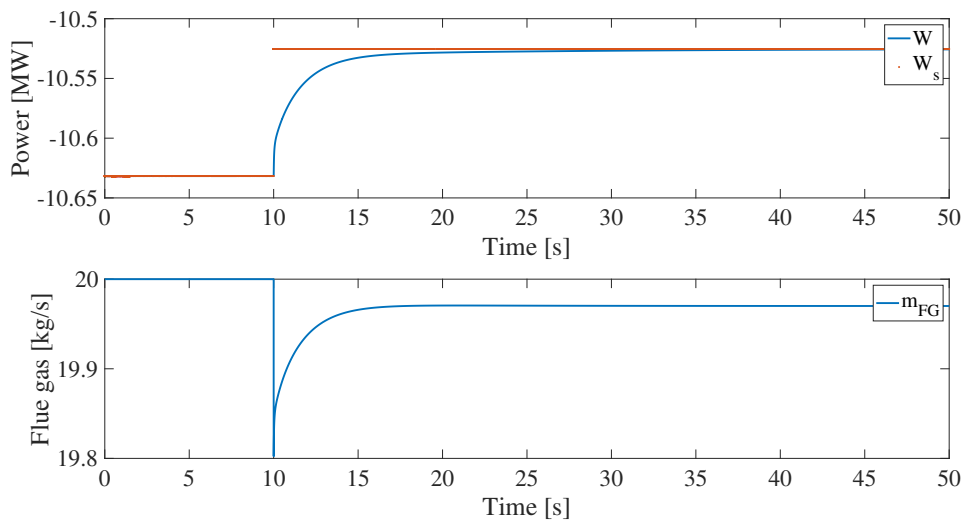
Figure A.36: Plot of W and $\dot{m}_{FG}$ after a 1% closed loop step decrease in W_s

A.10 Decentralized τ_1 - sequential controller tuning of decentralized control for the turbine-driven control structure

The tuning for the T_r-controller and $T_{FG,eco}$-controller from the boiler-driven τ_1 - sequential controller tuning is used for the turbine-driven control structure as well. The latter controllers in the sequence are tuned through open loop input step responses and verified through closed loop stepoint responses in Figures A.37- A.42 below.

A.10.1 Power controller
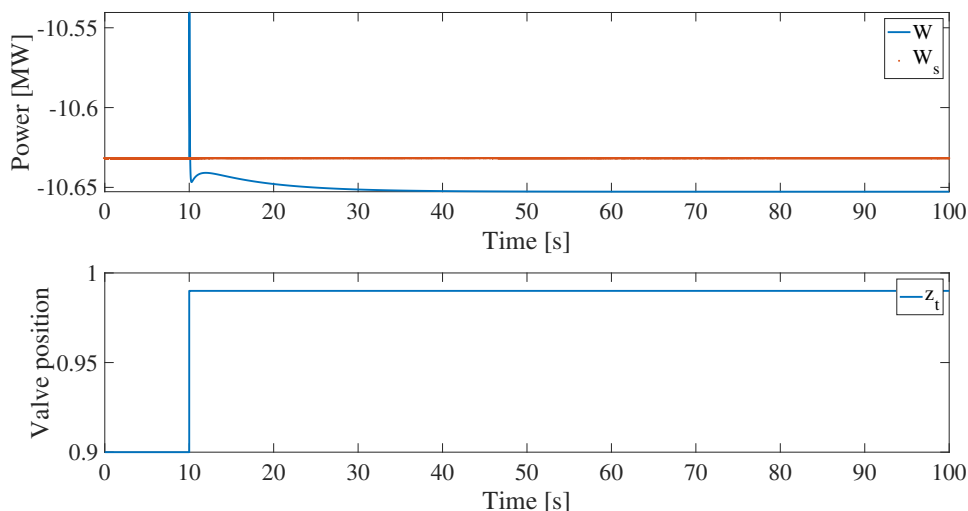
Figure A.37: Plot of W and z_t after a 10% open loop step response in z_t

Figure A.38: Plot of W and z_t after a 0.1% closed loop step decrease in W_s

A.10.2 Attemperator temperature controller

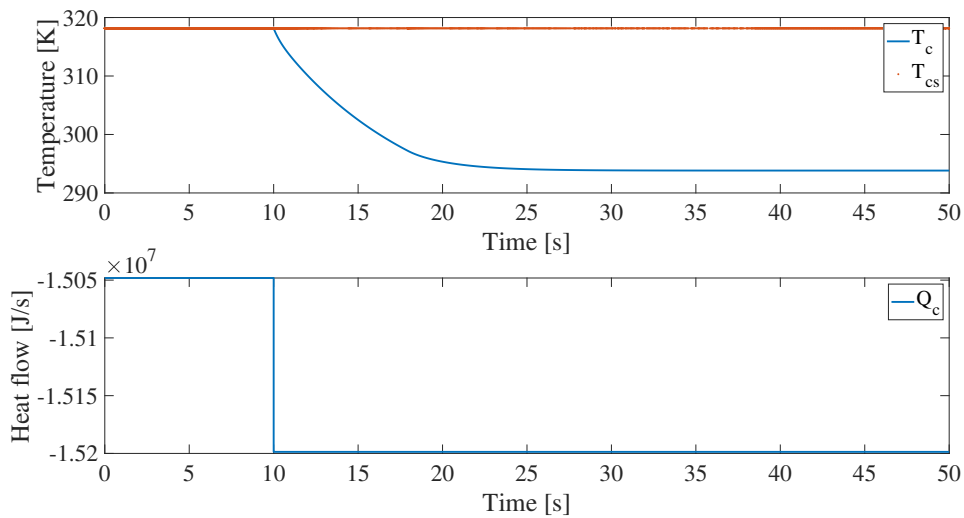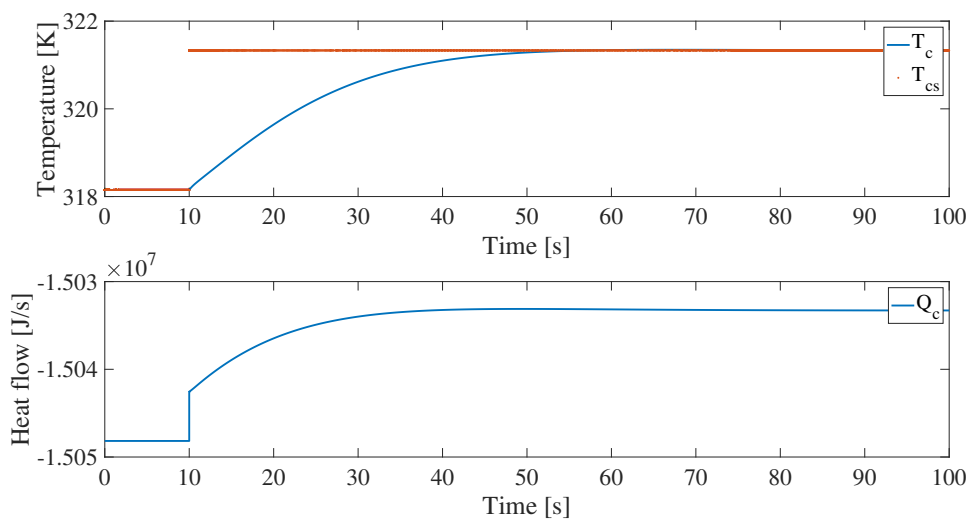**Figure A.39:** Plot of T_a and $\dot{m}_{a,b}$ after a 1% open loop step response in $\dot{m}_{a,b}$
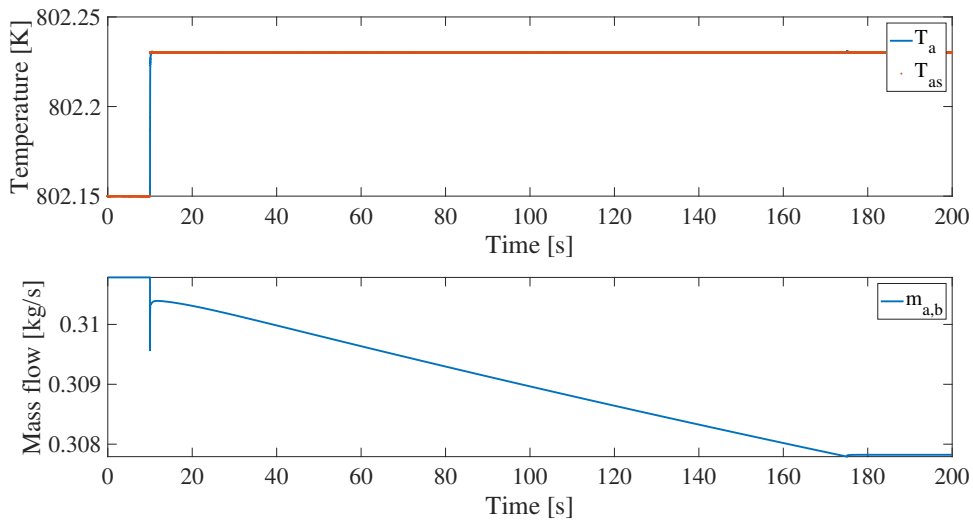
Figure A.40: Plot of T_a and $\dot{m}_{a,b}$ after a 0.01% closed loop setpoint change in T_{as}

A.10.3 Drum pressure controller

Figure A.41: Plot of P_d and $\dot{m}_{FG}$ after a 0.01% open loop step response in $\dot{m}_{FG}$
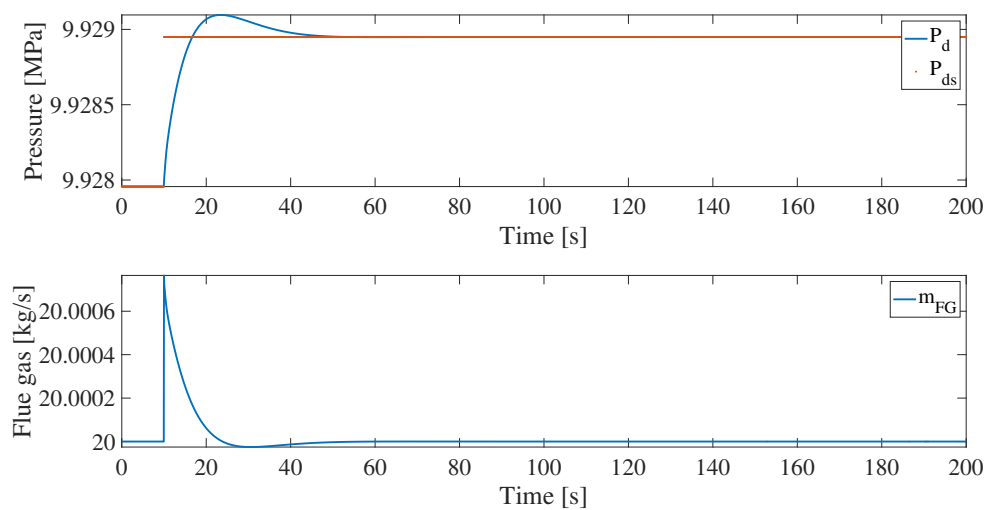
Figure A.42: Plot of P_d and $\dot{m}_{FG}$ after a 0.01% closed loop closed loop setpoint change in P_{ds}

A.10.4 Condenser temperature controller
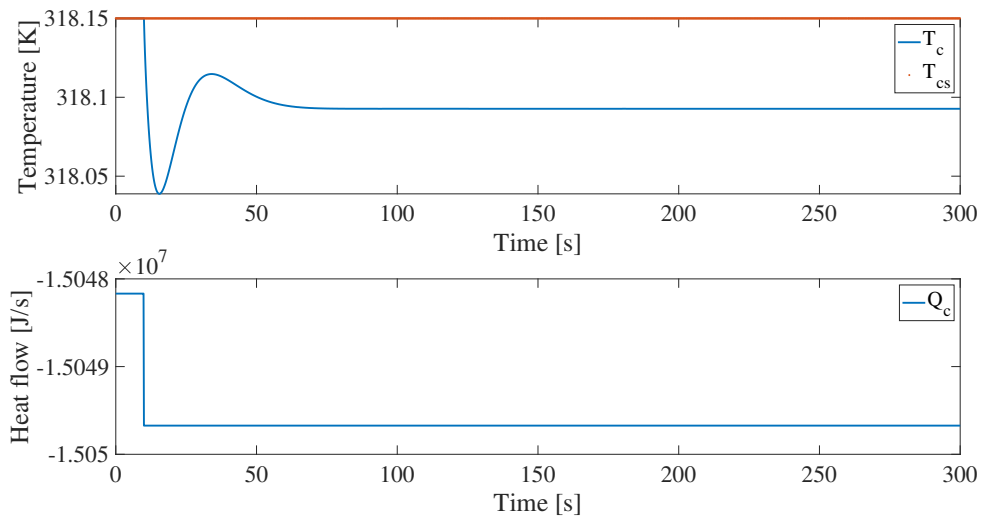
**Figure A.43:** Plot of T_c and $\dot{Q}_c$ after a 0.01% open loop step response in $\dot{Q}_c$
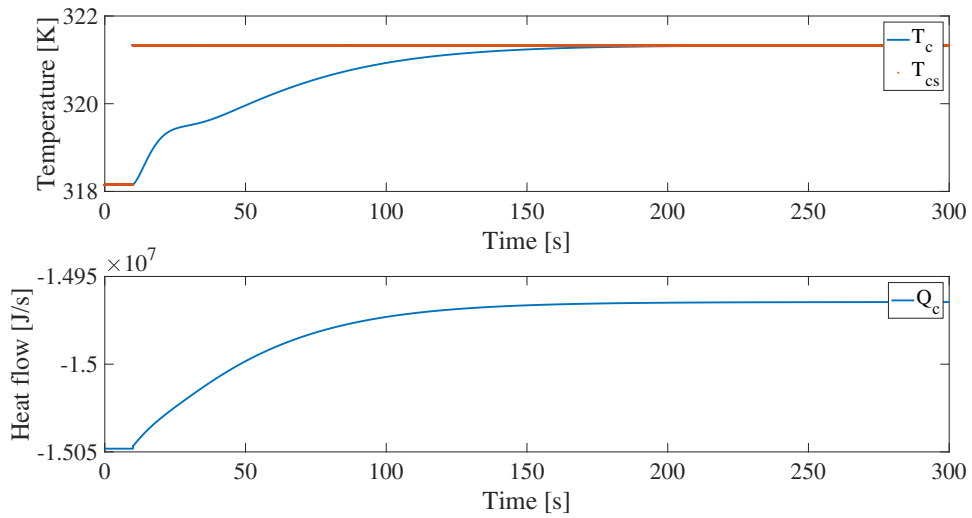
Figure A.44: Plot of T_c and $\dot{Q}_c$ after a 1% closed loop closed loop setpoint change in T_{cs}

A.11 Decentralized τ_C - sequential controller tuning of the boiler-driven control structure

The same tunings were used for T_r and $T_{FG,eco}$-controllers as from the τ_1 - sequential controller tuning. The latter controllers in the τ_c - sequence for the boiler-driven control structure are tuned through open loop input step responses and verified through closed loop stepoint responses in Figures A.45- A.52 below.

A.11.1 Condenser temperature controller

Figure A.45: Plot of T_c and $\dot{Q}_c$ after a 1% open loop step response in $\dot{Q}_c$

Figure A.46: Plot of T_c and $\dot{Q}_c$ after a 1% closed loop closed loop setpoint change in T_{cs}

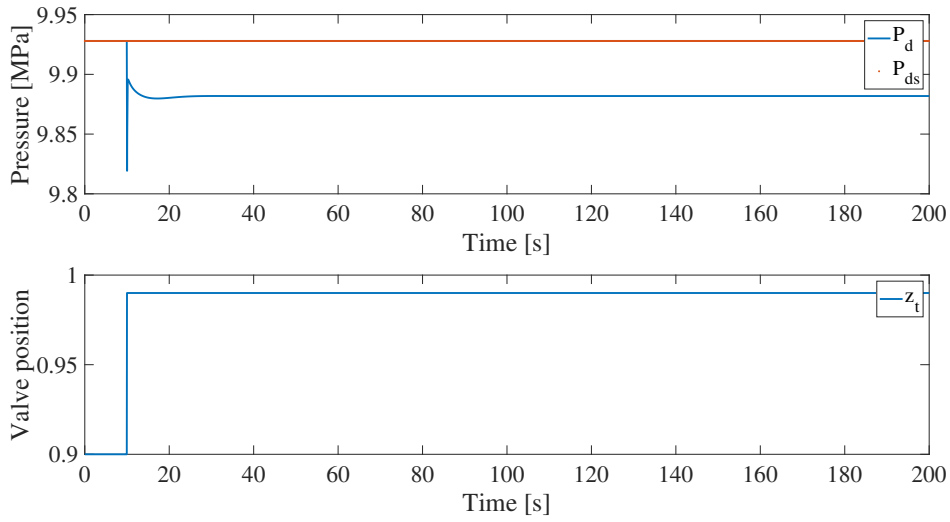## A.11.2 Attemperator temperature controller
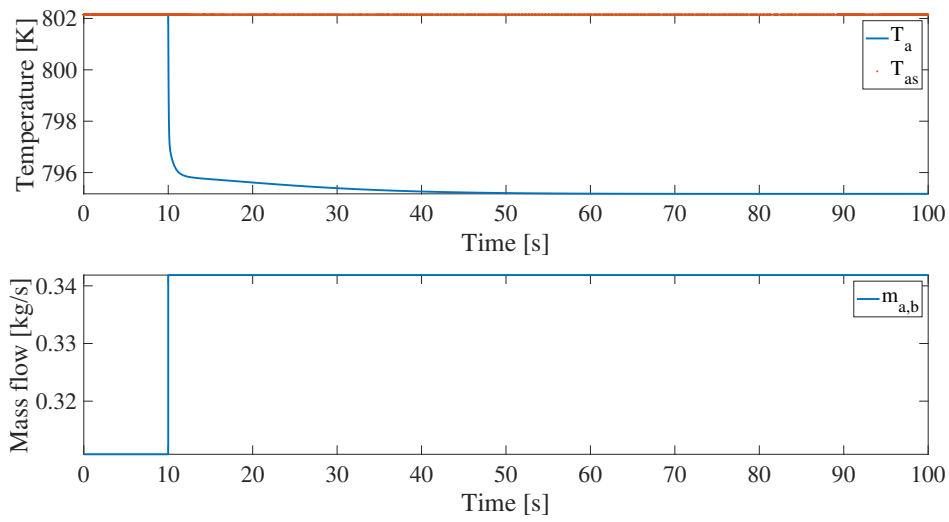
Figure A.47: Plot of T_a and $\dot{m}_{a,b}$ after a 10% open loop step response in $\dot{m}_{a,b}$
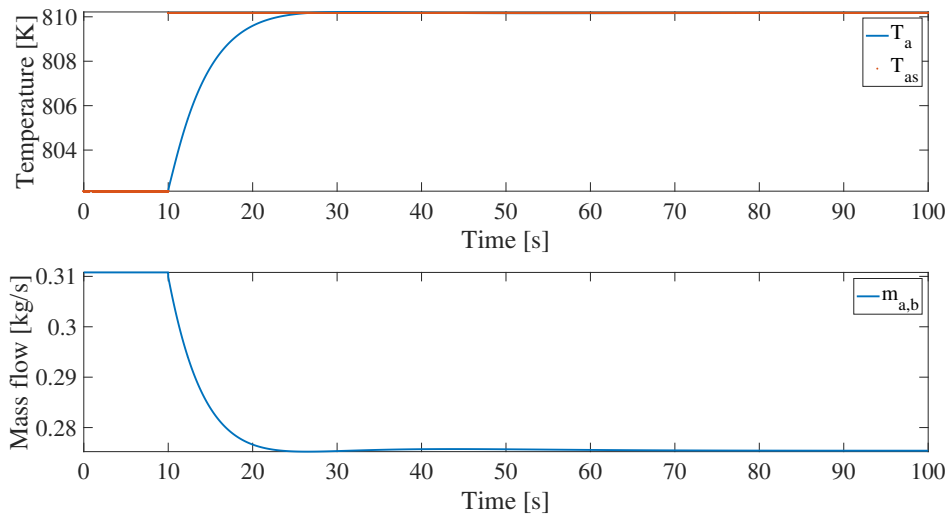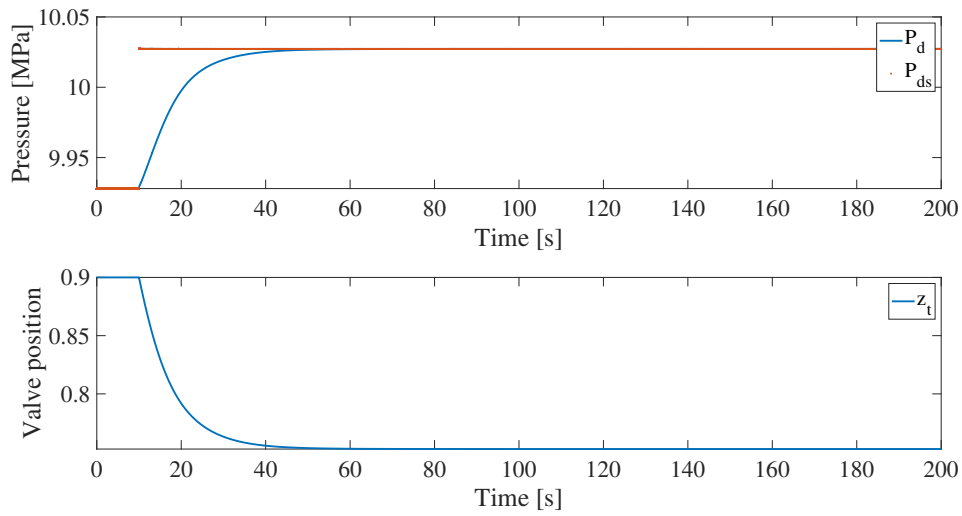

Figure A.48: Plot of T_a and $\dot{m}_{a,b}$ after a 1% closed loop setpoint change in T_{as}

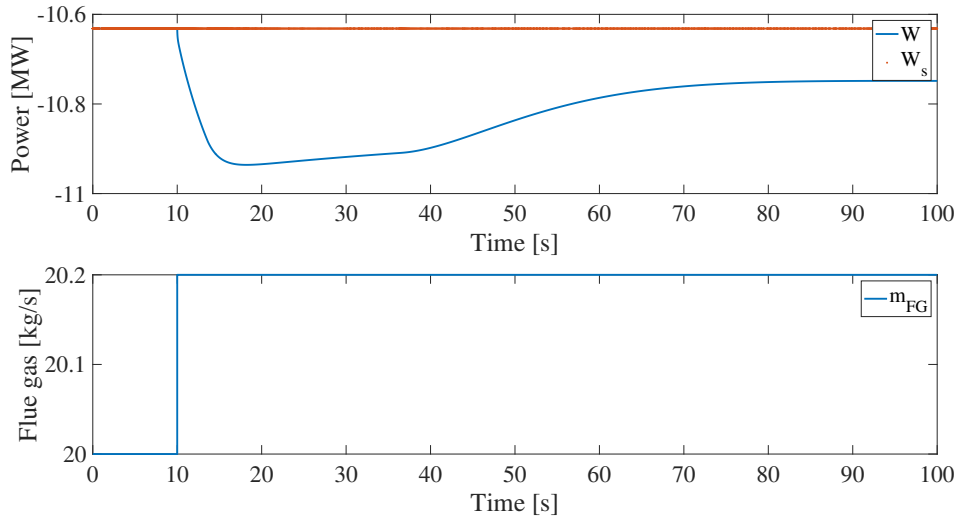### A.11.3   Drum pressure controller

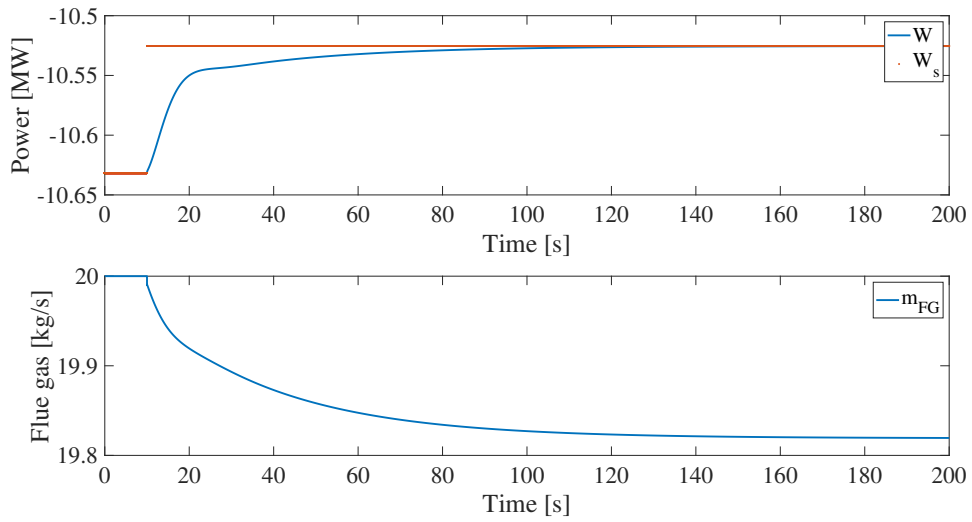**Figure A.49:** Plot of P_d and z_t after a 10% open loop step response in z_t

Figure A.50: Plot of P_d and z_t after a 1% closed loop setpoint change in P_{ds}

A.11.4 Power controller

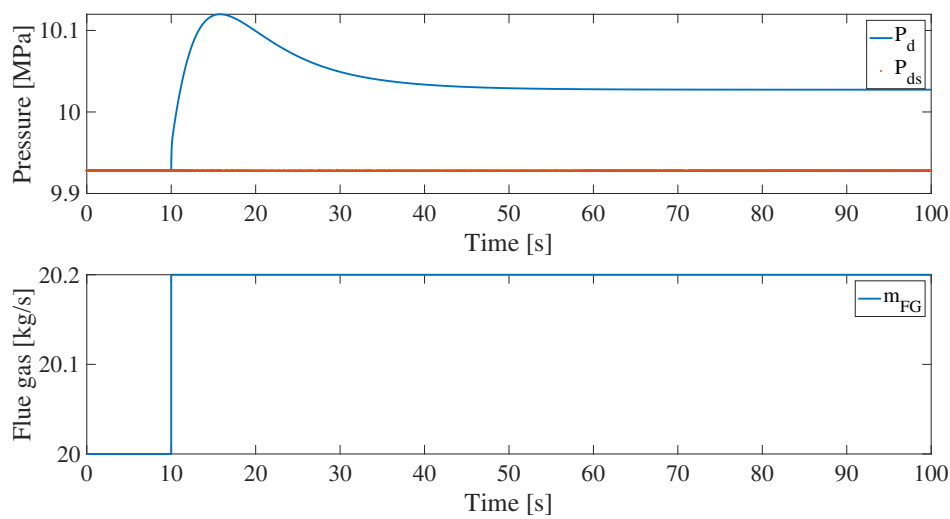**Figure A.51:** Plot of W and $\dot{m}_{FG}$ after a 1% open loop step response in $\dot{m}_{FG}$

Figure A.52: Plot of W and $\dot{m}_{FG}$ after a 1% closed loop setpoint change in W_s
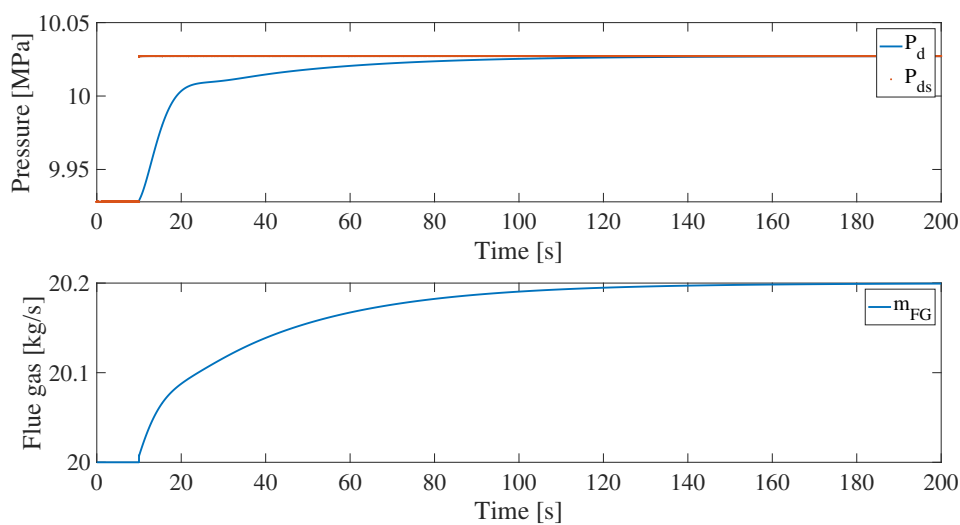
A.12 Decentralized τ_c - sequential controller tuning of the turbine-driven control structure

The same tunings were used for the T_r, $T_{FG,eco}$, T_c and T_a-controllers as the τ_c - sequential controller tuning for the boiler-driven control structure. The only controllers left to tune are the P_d and W controllers. The drum pressure (P_d) and power (W) controllers are tuned through open loop input step responses and verified through closed loop stepoint responses in Figures A.53- A.56 below.
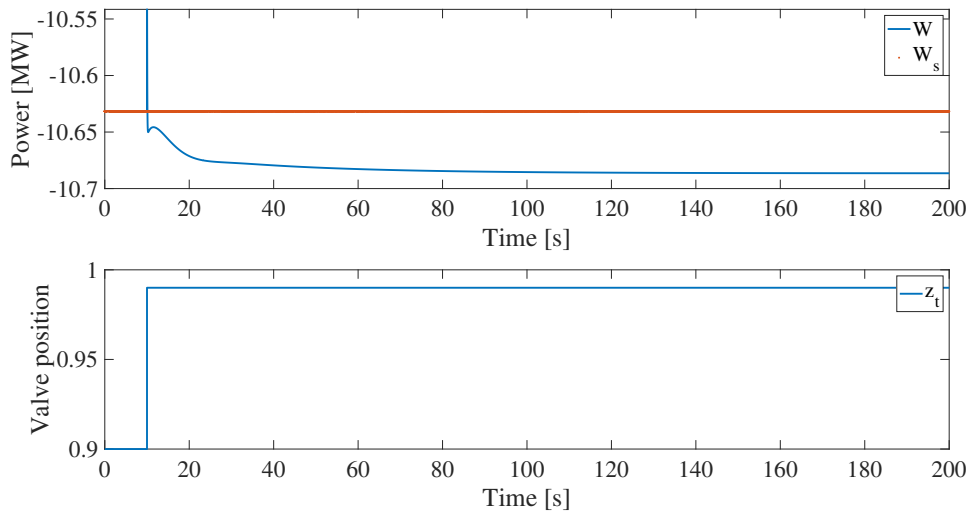
A.12.1 Drum pressure controller

Figure A.53: Plot of W and $\dot{m}_{FG}$ after a 1% open loop step response in $\dot{m}_{FG}$

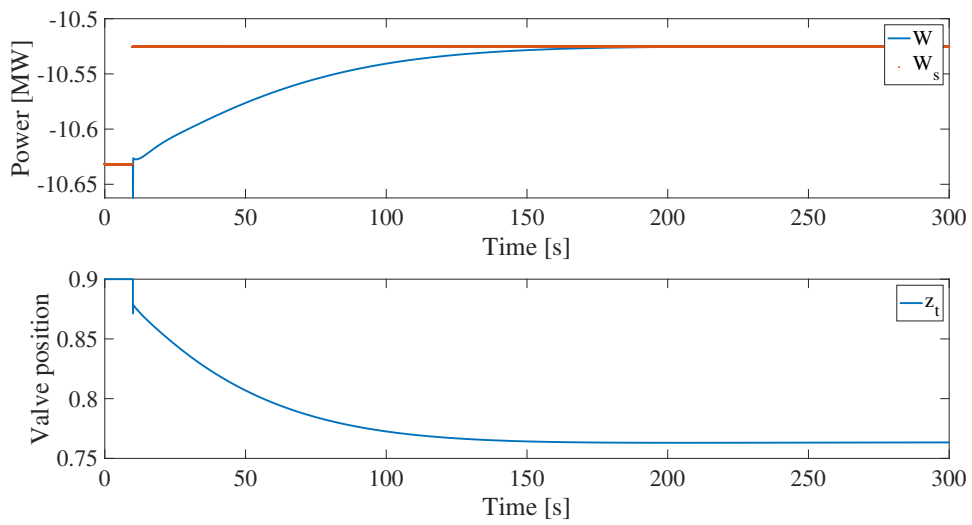**Figure A.54:** Plot of P_d and z_t after a 1% closed loop setpoint change in P_{ds}

A.12.2   Power controller

Figure A.55: Plot of P_d and z_t after a 10% open loop step response in z_t

Figure A.56: Plot of W and $\dot{m}_{FG}$ after a 1% closed loop step decrease in W_s

A.13 Decentralized τ_1 - sequential controller tuning of the parallel power control structure

The same tunings for the T_r, $T_{FG,eco}$ and the fast W-controller were used from the τ_1 - sequential controller tuning of the turbine-driven control structure in Section A.10. The second slower power controller was tuned through an open loop step response in $\dot{m}_{FG}$ in Figure A.57. Both the slow and fast power controllers were closed, tuned and verified at the same time shown in Figure A.58. The attemperature temperature (T_a) controller and condenser temperature controller (T_c) are tuned through open loop input step responses and verified through closed loop stepoint responses in Figures A.59 - A.62 below.

A.13.1 Slow power controller
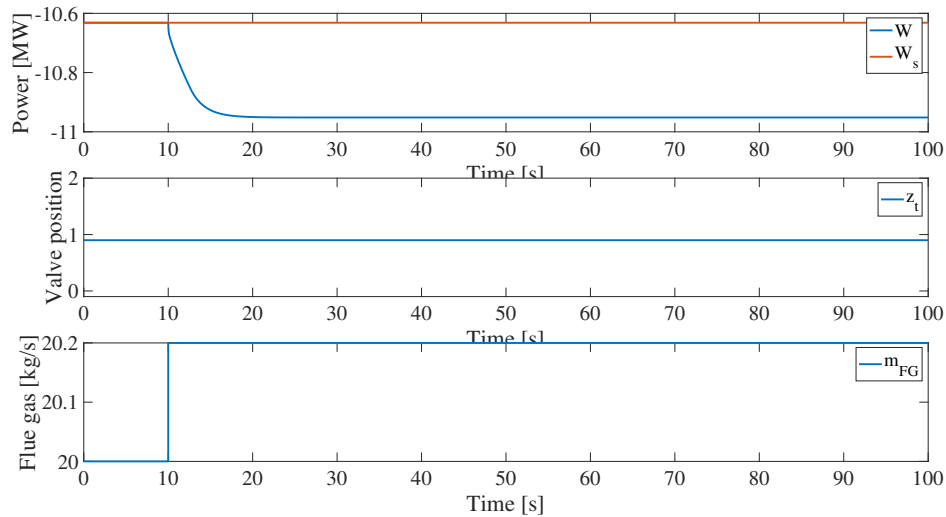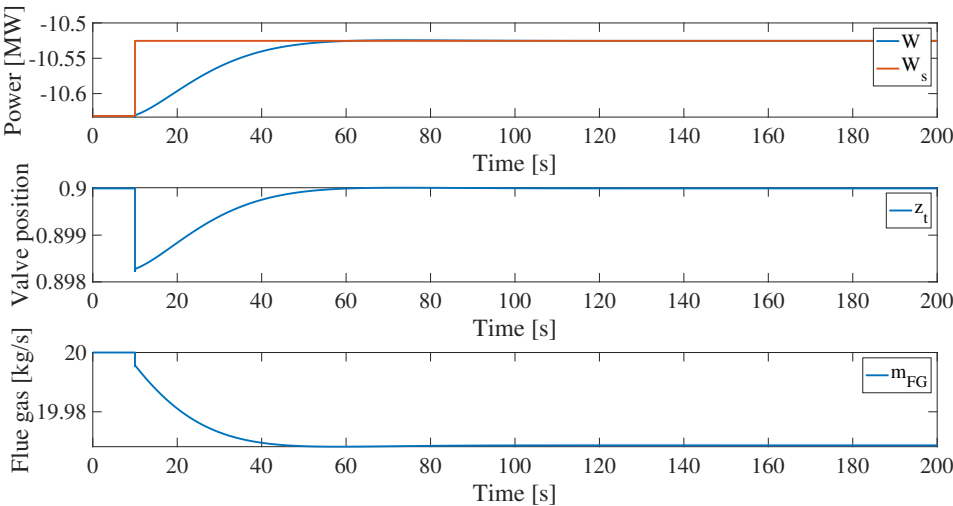

Figure A.57: Plot of W, $\dot{m}_{FG}$ and z_t after a 1% open loop step response in $\dot{m}_{FG}$

Figure A.58: Plot of W, $\dot{m}_{FG}$ and z_t after a 1% closed loop step decrease in W_s with both power controllers on

A.13.2 Attemperator temperature controller
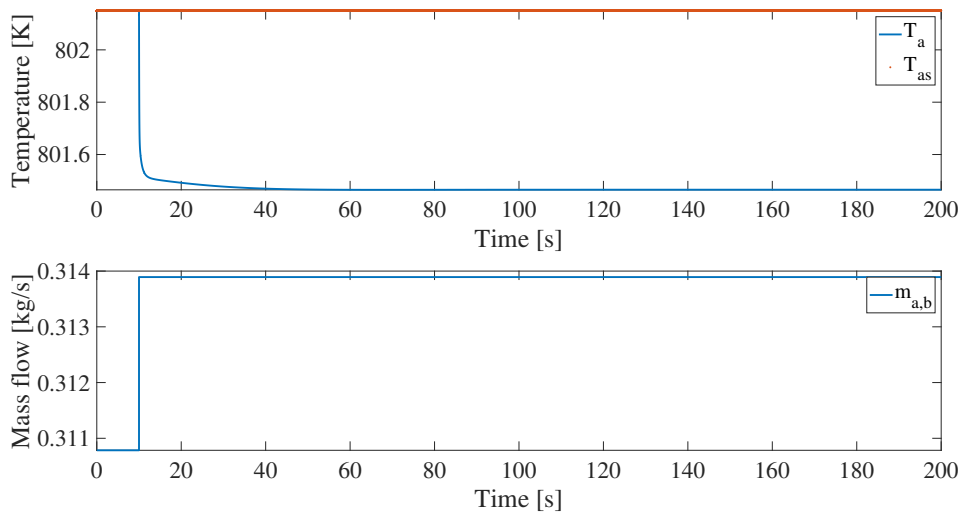
Figure A.59: Plot of T_a and $\dot{m}_{a,b}$ after a 1% open loop step response in $\dot{m}_{a,b}$
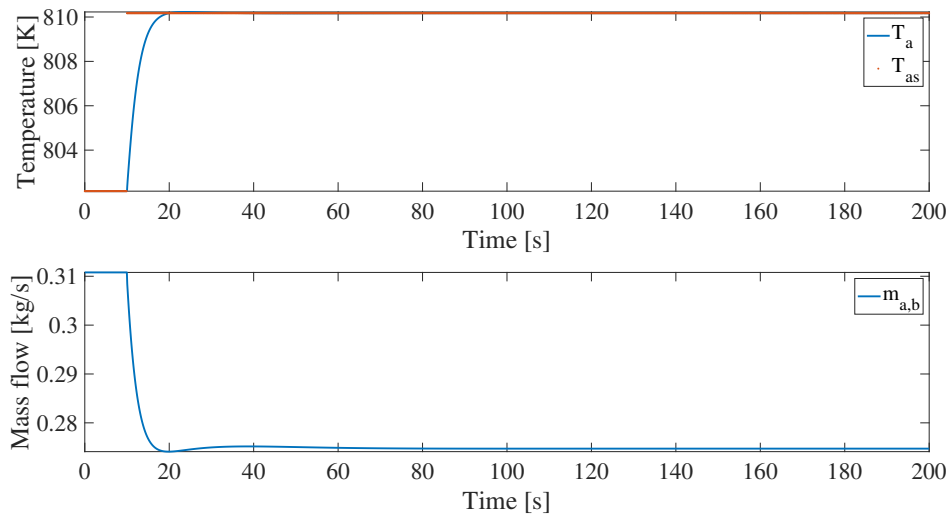
Figure A.60: Plot of T_a and $\dot{m}_{a,b}$ after a 1% closed loop setpoint change in T_{as}

A.13.3   Condenser temperature controller
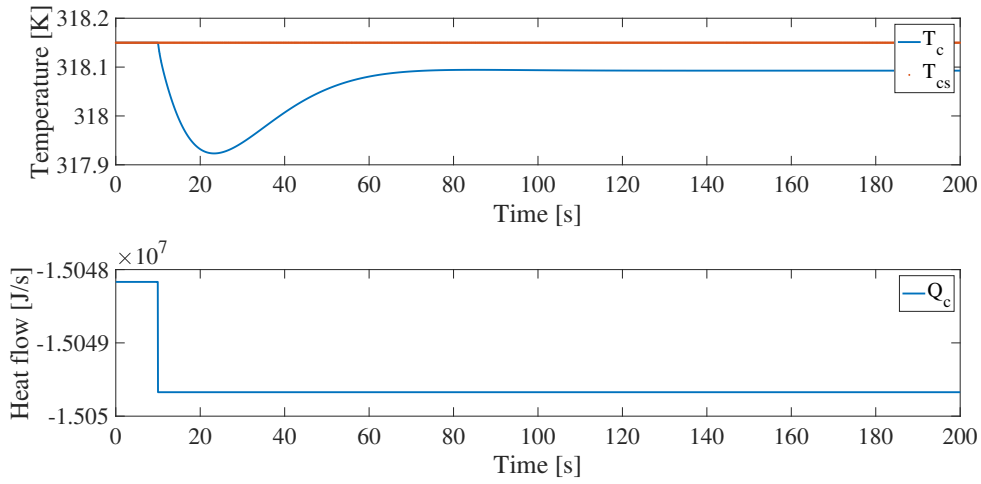
Figure A.61: Plot of T_c and $\dot{Q}_c$ after a 0.01% open loop step response in $\dot{Q}_c$
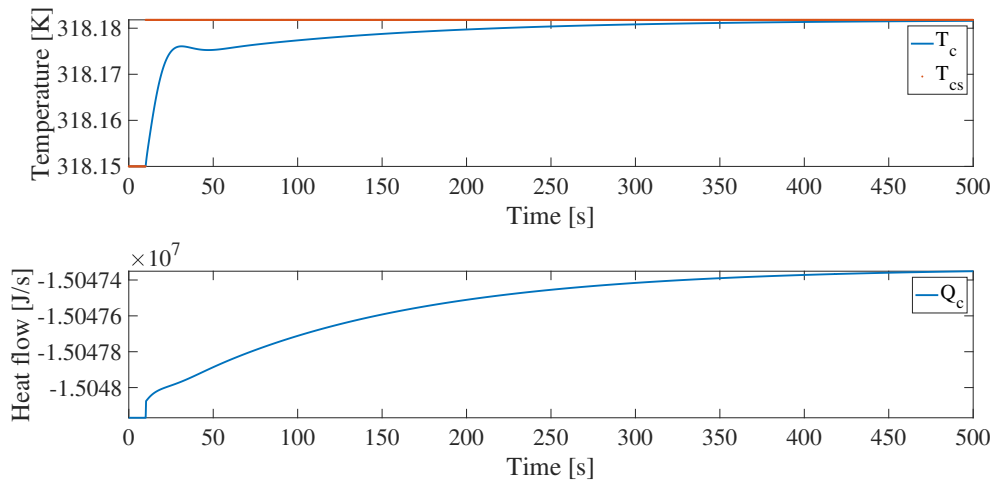
Figure A.62: Plot of T_c and $\dot{Q}_c$ after a 0.001% closed loop closed loop setpoint change in T_{cs}

A.14 Decentralized τ_1 - sequential controller tuning of the valve position control structure

The same tunings for the T_r, $T_{FG,eco}$ and W-controllers were used from the τ_1 - sequential controller tuning of the turbine-driven control structure in Section A.10. The power controller is verified in Figure A.63. The valve position controller (VPC), attemperature temperature (T_a) controller and condenser temperature controller (T_c) are tuned through open loop input step responses and verified through closed loop stepoint responses in Figures A.64- A.69 below.
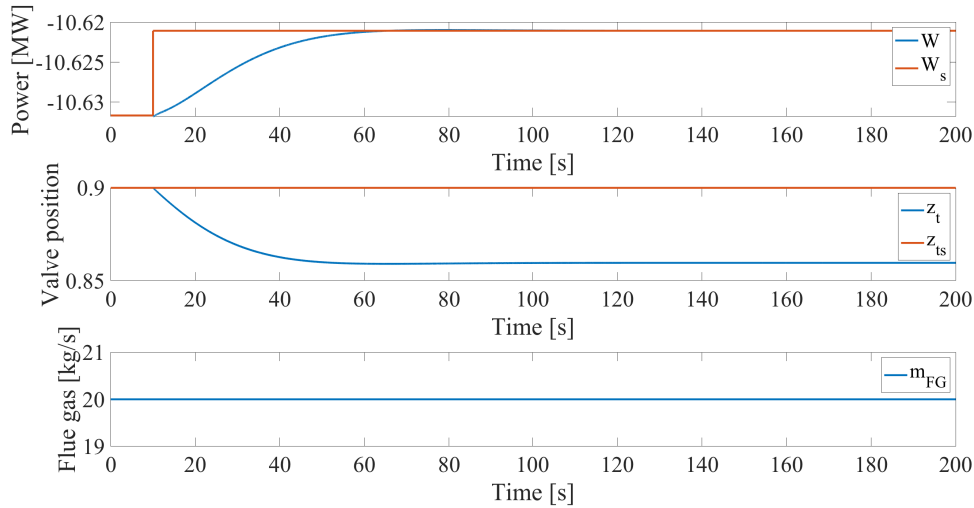
Figure A.63: Plot of W, $\dot{m}_{FG}$ and z_t after a 0.1% closed loop step decrease in W_s

A.14.1   Valve position controller

**Figure A.64:** Plot of W, $\dot{m}_{FG}$ and z_t after a 0.1% open loop step response in $\dot{m}_{FG}$
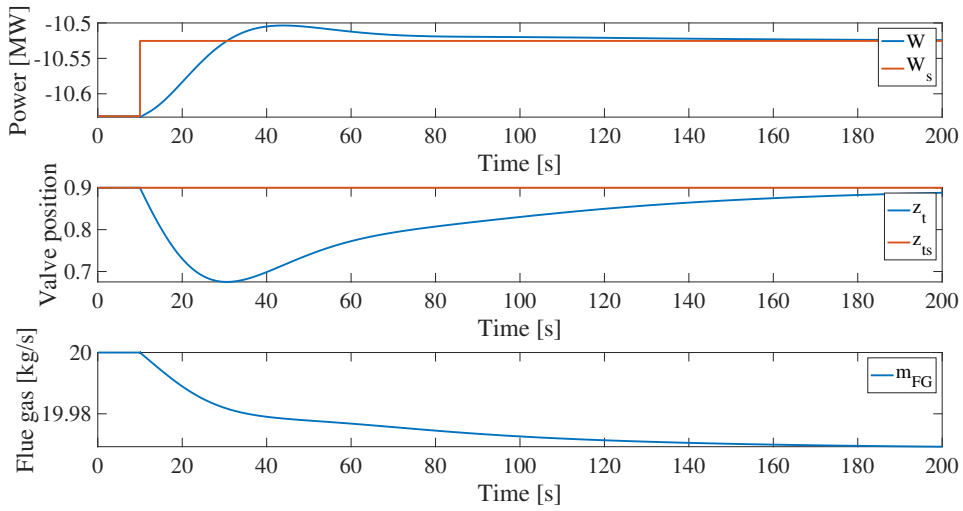
Figure A.65: Plot of W, $\dot{m}_{FG}$ and z_t after a 1% closed loop step decrease in W_s with VPC on

A.14.2 Attemperator temperature controller
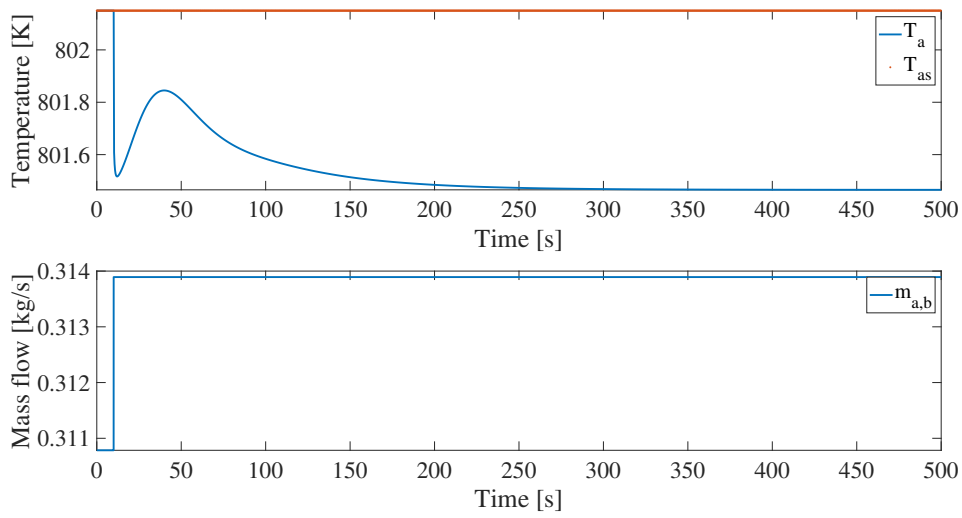
Figure A.66: Plot of T_a and $\dot{m}_{a,b}$ after a 1% open loop step response in $\dot{m}_{a,b}$
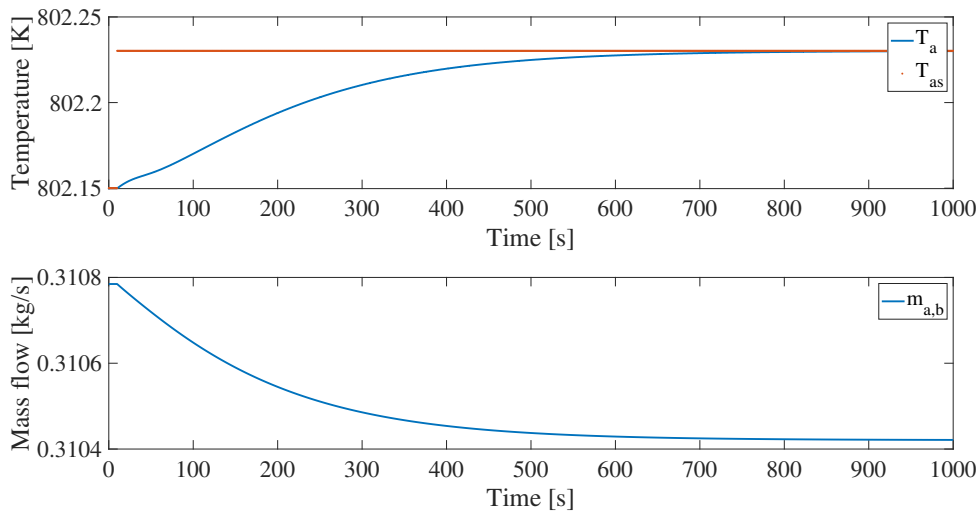
Figure A.67: Plot of T_a and $\dot{m}_{a,b}$ after a 0.01% closed loop setpoint change in T_{as}

A.14.3 Condenser temperature controller

**Figure A.68:** Plot of T_c and $\dot{Q}_c$ after a 0.01% open loop step decrease in $\dot{Q}_c$

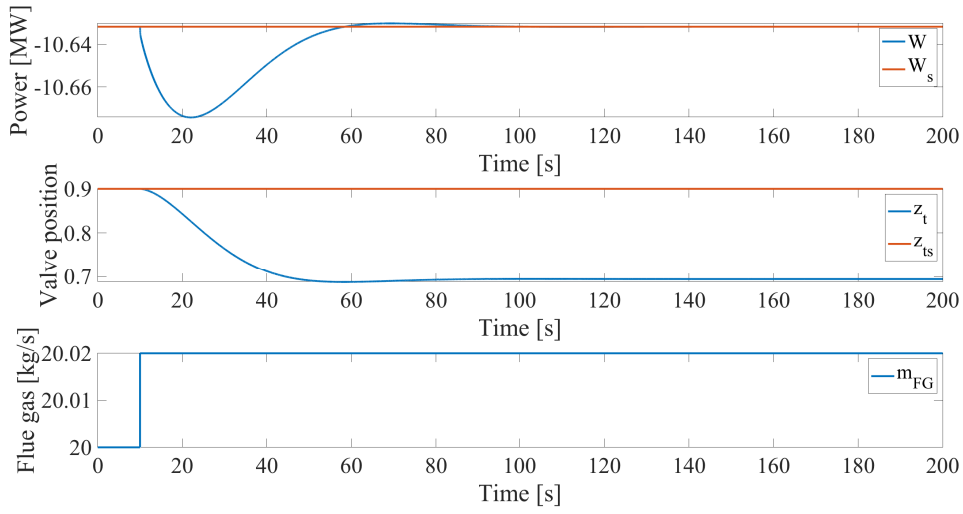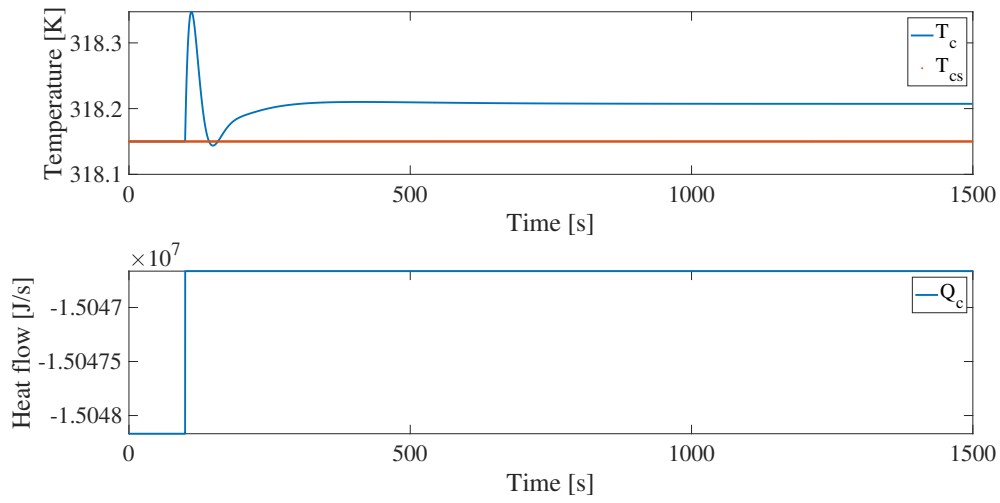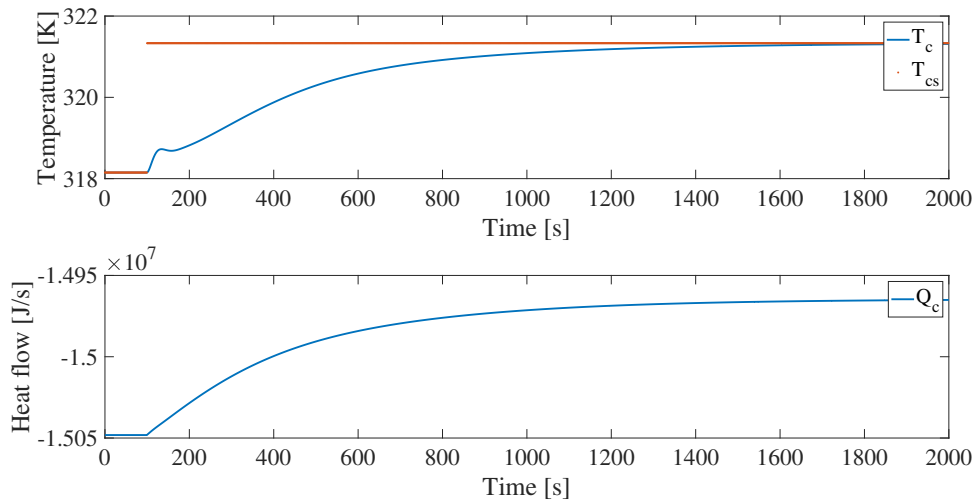**Figure A.69:** Plot of T_c and $\dot{Q}_c$ after a 1% closed loop closed loop setpoint change in T_{cs}

A.15   MATLAB and Simulink files

The *Heat2PowerCycle.zip* file added to the thesis includes several functions and scripts. The functions are found in the function folder and are described within each function script.
There was implemented a total of five Simulink files for the heat-to-power cycle, one for each control structure, described in the list below.

- *H2PBD.slx*: Simulation of the heat-to-power cycle with the boiler-driven control structure.

- *H2PTD.slx*: Simulation of the heat-to-power cycle with the turbine-driven control structure.

- *H2PFD.slx*: Simulation of the heat-to-power cycle with the floating pressure control structure.

- *H2PPWC.slx*: Simulation of the heat-to-power cycle with the parallel power control structure.

- *H2PFD.slx*: Simulation of the heat-to-power cycle with the valve position control structure.

There was also made scripts to increase the efficiency of tuning and plotting of the variables found in the *PlotScripts* and *TuningScripts* folder, respectively. Each simulation can be run independently in *RunCode.m* or from the multiplot scripts found in the *PlotScripts* folder. The controller tunings for each control structure was implemented into their own respective scripts described in the list below.

- *CTBDInd.m*: Independent controller tunings for the boiler-driven control structure.

- *CTBDSeq.m*: τ_1 - sequential controller tunings for the boiler-driven control structure.

- *CTBDSeq2.m*: τ_c - sequential controller tunings for the boiler-driven control structure.

- *CTTDInd.m*: Independent controller tunings for the turbine-driven control structure.

- *CTTDSeq.m*: τ_1 - sequential controller tunings for the turbine-driven control structure.

- *CTTDSeqSelfReg.m*: τ_1 - sequential controller tunings for the turbine-driven control structure assuming T_a is self regulating.

- *CTTDSeq2.m*: τ_c - sequential controller tunings for the turbine-driven control structure.

- *CTFDInd.m*: Independent controller tunings for the floating pressure control structure.

- *CTFDSeq.m*: τ_1 - sequential controller tunings for the floating pressure control structure.

- *CTFDSeq2.m*: τ_c - sequential controller tunings for the floating pressure control structure.

- *CTPWC.m*: Controller tunings for the parallel power control structure.

- *CTVPC.m*: Controller tunings for the valve position control structure.

Other folders included in the *Heat2PowerCycle.zip* are described in the list below.

- *SSModels*: Folder containing the steady state scripts presented in Section A.16.

- *fullfig_v1*: Folder containing the fullfig package from MATLAB to initialize full-screen figures found from [Greene, 2014].

- *PictureIcons*: Folder containing figures used in the simulation subsystem masks.

A.16   Steady state scripts

In this section the steady state scripts used to compute initial guesses, constants and parameters are presented.

A.16.1   Parameters

The *Parameters.m* script computes the initial guesses, constants and parameters for the simulation. It contains two subscripts: *SS_Hex.m* and *SS_Turbine_Condenser.m* which are used to obtain steady state data for the heat exachangers and the condenser, respectively.

```matlab
%% Nominal values
N_nom = 211.92; % [rad/s]
md_nom = 5.9750; % [kg/s] inlet flow of boiler/Evaporator
meco_b_nom = 0.5; % [kg/s] bypass flow Economizer
msh_nom = md_nom; % [kg/s] outlet flow of boiler
ma_b_nom = 0.310784629432208; %0.311;% bypass stream [kg/s]
zt_nom =  0.9;   %  Valve opening
mFG_nom = 20; % flue gas in HEX [kg/s]
mFG_r_nom = 5; % flue gas in reheater [kg/s]

%% Fixed initial conditions

% Holdups
Md_0 = 10; % [kg]1e2 Boiler drum holdup
Ma_0 = 2.645; % [kg]10 Attemperator holdup
Mt_0 = 2.508; % [kg]1e-1 Turbine
Mc_0 = 5; % [kg] 10 Condenser holdup
Meco_0 = 1; % [kh] Economizer holdup

% Temperatures
Tref = 3.1815; % [K]1e2 Reference temperauture
Tc_0 = Tref;
Td_0 = 5.840688; % [K]1e2
Tsh_0 = 8.7678;  % [K]1e2
Tr_0 = 7.516923357850542; %6.074421806784751; %6.139593;  % [K]1e2
Teco_0 = Td_0;  % [K]1e2

% Flows
meco_0 = md_nom - meco_b_nom; % [kg/s]
mmix_0 = meco_0 + meco_b_nom; % [kg/s]

%% Parameters

CpSteam = 2e3; % Heat capacity steam (gas)  [J/kg,K]
CpFG = 1063.1; % Heat capacity methane [J/kg,K]
CpWater = 4.18e3; % Heat capacity liquid water [J/kg,K]

dHvap311 = 1321.9e3; % Heat of vap at 311C [J/kg]
dHvap45 = 2394e3; % Heat of vap at 45C [J/kg]
TFG0 = 1000 + 273.15; % Initial temperature gas [K]
Trefbp = Td_0; % Treference temperature gas boiling point [K]1e2

Antoine.A = 5.11564; % Antoine parameters
Antoine.B = 1687.537;
```

```
Antoine.C = -42.98;

Mmwater = 18e-3; % Mole weight water [kg/mol]
R = 8.3145; % Gas constant [J/mol,K]
V = 1; % Volume in mixer and turbine holdup


%% Heat exchangers

run SS_Hex.m
UAsh = double(sol.UAsh);   % [W/m2K]
UAd = double(sol.UAd);   % [W/m2K]
UAeco = double(sol.UAeco);   % [W/m2K]
UAr = double(sol.UAr); % [W/m2K]
Tmix_0 = double(sol.Tmix)*1e-2;   % [K]1e2
TFG_sh_0 =  double(sol.TFGsh)*1e-3;   % [K]1e3
TFG_d_0 =  double(sol.TFGd)*1e-2;   % [K]1e2
TFG_eco_0 =  double(sol.TFGeco)*1e-2;   % [K]1e2
TFG_r_0 = double(sol.TFGr)*1e-2; % [K]1e2
Hd_0 = Hd*1e-9; % [J]1e9

%% Parameter vector

P = [CpSteam CpFG CpWater Mmwater Tref Trefbp dHvap311 dHvap45 Antoine.A ...
    Antoine.B Antoine.C R V TFG0 UAsh UAd UAeco UAr];

Np = size(P,2);

%% Initial guess

Ta_0 = ((((md_nom*(CpWater*(Td_0-Tref)*1e2 + dHvap311 + ...
    CpSteam*(Tsh_0-Td_0)*1e2)/(md_nom+ma_b_nom))-(CpWater*(Td_0-Tref)*1e2...
    + dHvap311))/CpSteam)...
    + Td_0*1e2)*1e-2; % [K] 1e2

% Pressures
Pa_0 = rhoEqPa([Ma_0; Ta_0],P); % [Pa]1e6
Pt_in_0 = rhoEqPt(Mt_0, Ta_0,P);  % [Pa]1e6
Pt_out_0 = AntoineEq2(Tc_0,P);  % [Pa]1e3
Pt_hp_0 = (Pt_in_0*1e6*(390/(Ta_0*1e2))^(1/0.23))*1e-5; % [Pa]1e5

% Valve coefficient for msh
Kmsh = md_nom/(AntoineEq(Td_0,P)*1e6 - Pa_0*1e6);
% Valve coefficient for ma
Kma = (md_nom+ma_b_nom)/(zt_nom*(Pa_0*1e6-Pt_in_0*1e6));
% Stodola coefficient
Kt = (md_nom+ma_b_nom)/sqrt((Pt_in_0*1e6*Mmwater/...
    (R*Ta_0*1e2))*Pt_in_0*1e6*(1-((Pt_out_0*1e3)/(Pt_in_0*1e6))^2));

% Constant volumetric flow coefficient
%q3s = (md_nom+ma_b_nom)/((Pt_in_0*1e6*Mmwater)/(R*Ta_0*1e2));
%%
run SS_Turbine_Condenser.m
Qc_nom = Qc_r; % [J/s]

%%
```

```
Mdyn = [1 0 0; 0 1 0];
Malg = [0 0 1];
```

A.16.1.1 SS_Hex.m

```
%% SS Script
syms Qsh Qd Qeco UAsh UAd UAeco TFGsh TFGd TFGeco Tmix Qr UAr TFGr

Tt_hp_r = 3.90;

% Economizer
heco_in = meco_0*CpWater*(Tc_0 - Tref)*1e2;
heco_out = meco_0*CpWater*(Teco_0- Tref)*1e2;

% Mixer/ Drum inlet
heco_b = meco_b_nom*CpWater*(Tc_0 - Tref)*1e2;
hmix = md_nom*CpWater*(Tmix - Tref*1e2);

% Drum outlet// Superheater inlet
hd = md_nom*(CpWater*(Td_0-Tref)*1e2 + dHvap311);
Hd = Md_0*1e2*hd/md_nom;

% Superheater outlet
hsh     = md_nom*(CpWater*(Trefbp-Tref)*1e2 + dHvap311 + ...
    CpSteam*(Tsh_0-Trefbp)*1e2);

% Outlet HP Turbine
Hhp    = CpWater*(Trefbp*1e2-Tref*1e2) + dHvap311 + ...
    CpSteam*(Tt_hp_r*1e2-Trefbp*1e2);
hhp    = (md_nom+ma_b_nom)*Hhp;

% Outlet reheater
Hr   = CpWater*(Trefbp*1e2-Tref*1e2) + dHvap311 + ...
    CpSteam*(Tr_0*1e2-Trefbp*1e2);
hr   = (md_nom+ma_b_nom)*Hr;

% Superheater
eqn(1) = hd-hsh+Qsh==0; % Energy balance steam side
eqn(2) = mFG_nom*CpFG*(TFG0-TFGsh)- ...
    UAsh*((TFG0+TFGsh)/2-(Td_0*1e2+Tsh_0*1e2)/2)==0; % Obtain UAsh
eqn(3) = mFG_nom*CpFG*(TFG0-TFGsh)-Qsh==0;   % Energy balance gas side

% Drum
eqn(4) = hmix - hd + Qd == 0; % Energy balance steam side
eqn(5) = mFG_nom*CpFG*(TFGsh-TFGd)-...
    UAd*((TFGsh+TFGd)/2-(Td_0*1e2+Tmix)/2)==0; % Obtain UAd
eqn(6) = mFG_nom*CpFG*(TFGsh-TFGd)-Qd==0; % Energy balance gas side

% Economizer
eqn(7) = heco_in - heco_out + Qeco == 0; % Energy balance steam side
eqn(8) = mFG_nom*CpFG*(TFGd-TFGeco)-...
    UAeco*((TFGd+TFGeco)/2-(Tc_0*1e2+Teco_0*1e2)/2)==0; % Obtain UAeco
eqn(9) = mFG_nom*CpFG*(TFGd-TFGeco) - Qeco == 0; % Energy balance gas side

% Mixer/Drum inlet
eqn(10) = heco_out + heco_b - hmix == 0; %% To find Tmix
```

```
% Reheater

eqn(11) = hhp-hr+Qr == 0; % Energy balance steam side
eqn(12) = mFG_r_nom*CpFG*(TFG0-TFGr)-...
    UAr*((TFG0+TFGr)/2-(Tt_hp_r*1e2+Tr_0*1e2)/2)==0; % Obtain UAr
eqn(13) = mFG_r_nom*CpFG*(TFG0-TFGr) - Qr==0;% Energy balance gas side

sol=solve(eqn,UAsh,UAd,UAeco,Qsh,Qd,Qeco,TFGsh,TFGd,TFGeco,Tmix,UAr,Qr,TFGr);
```

A.16.1.2 SS_Turbine_Condenser.m

```
Tt_in_0_r = Ta_0*1e2;

% Computing mass flow through stodola approximation
rho3 = Pt_in_0*1e6*Mmwater/(R*Tt_in_0_r); % Calculating density
PR = Pt_in_0*1e6/(Pt_out_0*1e3); % Pressure ratio
% Stodola equation for mturbine
mturbine = Kt*sqrt(rho3*Pt_in_0*1e6*(1-(1/PR)^2));
m4 = mturbine; % At nominal conditions

% Equations
Pt_hp_0_r = Pt_hp_0*1e5; % Pressure out of HP turbine [Pa]
% Computing intermediate temperature after HP turbine
Tt_hp_0_r = Tt_in_0_r*(Pt_hp_0_r/(Pt_in_0*1e6))^0.23;
% Computing power output from HP turbine
W_hp_r = (mturbine*CpSteam*(Tt_hp_0_r-Tt_in_0_r));

% Computing temperature out of LP turbine
Tt_lp_0_r = Tr_0*1e2*(Pt_out_0*1e3/Pt_hp_0_r)^0.23;
% Computing power output from LP turbine
W_lp_r = (mturbine*CpSteam*(Tt_lp_0_r-Tr_0*1e2));
W_r = W_hp_r+W_lp_r; % Total power output [W]

% Specific enthalpies [J/kg]
hturbine_r = CpWater*(Tref-Tref)*1e2 + dHvap45 +...
    CpSteam*(Tt_lp_0_r-Tref*1e2); % Into condenser
h4_r = CpWater*(Tc_0-Tref)*1e2; % Out of condenser

% Cooling water heat flow [J/s]
Qc_r = m4*h4_r - mturbine*hturbine_r;
```

A.16.2 Pump

The steady state script for the pump is used to obtain the constants in the pump function block. The pump model is described in Section 4.6.7.

```
% Clearing
clear
close all
clc;

% Locating variables
syms k1 k3 dPs dPq

% Parameters
rho_ref = 974; % Average fluid denisty kg/m^3
N = 211.92; % rad/s Pump speed demand
P_in = 9.614638196694839*1e3; % Pa Inlet pressure
rho = 970; % kg/m^3 Inlet density
m = 6.285784629432207; % Mass flow kg/s
F = m/rho; % Volumetric flow m^3/s
P_out = 100e5; % Outlet pressure [Pa]
dP = P_out - P_in;
k2 = 0;

f(1) = F - N*(k1/(k2+(1/k3)))^(0.5); % Volumetric flow
f(2) = dPq - k3*rho_ref*F^2; % Pressure drop across load
f(3) = dP - (dPs + dPq); % Pressure rise across pump
f(4) = dPs/dP - 0.6766; % Static to total pressure difference ratio

sol = solve(f,k1,k3,dPq,dPs);
k1  = double(sol.k1)  % [m^2]
k3  = double(sol.k3)  % [m^-4]
dPq = double(sol.dPq) % [Pa], static pressure rise across the pump
dPs = double(sol.dPs) % [Pa], Pressure drop across load
```

Ida Andersskog

Modelling and control of a Heat-to-Power cycle

NTNU
Norwegian University of
Science and Technology